DEVELOPMENT AND SYNTHESIS OF MOLECULES TO STUDY ENDOGENOUS PROTEINS: NEW INHIBITORS OF NADPH OXIDASE ISOFORM 2 AND EFFORTS TOWARDS THE DEVELOPMENT OF A TRACELESS AFFINITY MOLECULE

by

Alicia Mercer

B.Sc., University of the Fraser Valley, 2015

A THESIS SUBMITTED IN PARTIAL FULFILLMENT OF
THE REQUIREMENTS FOR THE DEGREE OF

MASTER OF CHEMISTRY

In

THE COLLEGE OF GRADUATE STUDIES

(Chemistry)

THE UNIVERSITY OF BRITISH COLUMBIA

(Okanagan)

July 2019

The following individuals certify that they have read, and recommend to the College of Graduate Studies for acceptance, a thesis entitled:

DEVELOPMENT AND SYNTHESIS OF MOLECULES TO STUDY ENDOGENOUS PROTEINS: NEW INHIBITORS OF NADPH OXIDASE ISOFORM 2 AND EFFORTS TOWARDS THE DEVELOPMENT OF A TRACELESS AFFINITY MOLECULE

Submitted by Alicia Mercer in partial fulfillment of the requirements of the Master's degree.

Dr. Frederic Menard

Supervisor

Dr. Kevin Smith

Supervisory Committee Member

Dr. Paul Shipley

Supervisory Committee Member

Dr. John Klironomos

External Examiner

Abstract

The study of proteins is essential to further our understanding of their functions in both healthy and diseased organisms. While several techniques are available for the study of isolated proteins, far fewer are available to study them in their native environments. The ability to understand how proteins interact with other biological molecules (other proteins, hormones, neurotransmitters, etc.) can allow us to develop specific drugs for specific interactions, potentially lessening side effects. In this thesis, two approaches to studying the function of living cells have been investigated. The first approach involves the design and synthesis of enzyme inhibitors. The second focuses on the design of a universal protein tagging method.

Chapter two of this thesis focuses on the synthesis of novel NADPH oxidase (NOX) inhibitors based on Vasopharm's VAS2870 (which contains a triazolopyrimidine backbone). The reactive oxygen species (ROS) generated by NOX have been implicated in the development of several neurodegenerative diseases (such as Alzheimer's and Parkinson's). The first inhibitor described contains a *p*-azidomethyl substituent for future tagging studies. Initial ROS inhibition experiments show that this modification does not interfere with the inhibitor's activity. The second inhibitor replaces a reactive sulfur-carbon bond of the original inhibitor with a carbon-carbon bond. This compound did not show any inhibitory effects, indicating that the sulfur-carbon bond is necessary for the activity of VAS2870 and the *p*-azidomethyl derivative. This finding may call into question the conclusions of previous neurobiological studies.

Chapter three describes efforts toward the development of a traceless affinity molecule. This molecule is composed of a ligand, cleavable linker, and chemical tag. When the linker is cleaved, the ligand is free of the tag, and can dissociate. Cleavage of the linker, an α-silyl-β-lactone, can be achieved via a Peterson olefination with a lysine residue outside of the ligand binding site. The result is a tag-protein complex, which enables the visualization of the protein in real time. In addition, the location of the tag is such that it should not interfere with the native functions of the protein. This study establishes the pioneering work necessary to design viable cleavable linkers for future protein labelling.

Lay Summary

Chemical probes – small molecules that monitor/modulate a protein's activity – are important tools for studying biology. Studying proteins in their native environment provides insight into how they behave in healthy and diseased organisms. This thesis describes two projects involving novel chemical probes. Chapter two describes the synthesis of analogues to a known enzyme inhibitor to reveal its mode of action and label the affected proteins. These enzymes produce reactive oxygen species (ROS) which are known to be detrimental if over-produced. Chapter three describes efforts toward the development of a traceless affinity molecule. The molecule is engineered to label only the desired protein target to enable visualization of the protein in real-time. These compounds can be used to visualize interactions between the proteins. The information gathered with our probes will expose how the target proteins contribute to various diseases, and help create new drugs.

Preface

Alicia Mercer designed this research project under the guidance of Dr. Frederic Menard. Design of experiments along with specific project objectives for each chapter are independently credited below. Alicia Mercer performed all experiments and characterization of the syntheses described in this dissertation. Appendix B, describing the biological assays in Chapter 2, were written and executed by Wyatt Slattery and Aaron Johnstone.

Table of Contents

List of Tables

List of Figures

List of Schemes

List of Abbreviations

Ar	–	argon
Arg	–	arginine
Asp	–	aspartate; aspartic acid
$CDCl_3$	–	deuterated chloroform
CHL	–	chemiluminescence
CNS	–	central nervous system
Cys	–	cysteine
DBU	–	1,8-Diazabicyclo[5.4.0]undec-7-ene
DCM	–	dichloromethane
DCC	–	*N,N'*-dicyclohexylcarbodiimide
DIPA	–	diisopropylamine
DIPEA	–	diisopropylethylamine
DMSO	–	dimethyl sulfoxide
DMF	–	dimethylformamide
DPI	–	diphenyleneidonium
Duox	–	dual oxidase
E_A	–	activation energy
eq	–	equivalents
FAD	–	flavin adenine dinucleotide
(g)	–	gas
Glu	–	glutamate; glutamic acid
gp91-2	–	NADPH oxidase 1
$gp91^{phox}$	–	NADPH oxidase 2; cytochrome b-245 heavy chain
gp91-3	–	NADPH oxidase 3
GPX	–	glutathione peroxidase
GSH	–	glutathione
g	–	grams
^1H NMR	–	proton nuclear magnetic resonance
h	–	hour
HEK293	–	human embryonic kidney
His	–	histidine

HL-60	–	human leukocyte
HMG-CoA	–	hydroxymethylglutaryl coenzyme A
[^{3}H]NEM	–	N-[2-^{3}H]ethylmaleimide
HTA	–	homoserine transacetylase
HUVEC	–	human umbilical vein endothelial cells
IR	–	infrared
LDA	–	lithium diisopropylamide
LOX	–	5-lipoxygenase
LPS	–	lipopolysaccharide
M	–	molar
MHz	–	megahertz
min	–	minute(s)
mL	–	millilitre
mmol	–	millimoles
MS	–	mass spectrometry
NADP	–	nicotinamide adenine dinucleotide phosphate
NGF	–	nerve growth factor
NOX	–	nicotinamide adenine dinucleotide phosphate oxidase
NOXA2	–	neutrophil cytosolic factor 2 (NCF2)
NOXO1	–	NADPH oxidase organizer 1
$ONOO^-$	–	peroxynitrite
oxLDL	–	oxidized low-density lipoprotein
$p22^{phox}$	–	human neutrophil cytochrome b light chain
$p40^{phox}$	–	neutrophil cytosolic factor 4
$p47^{phox}$	–	neutrophil cytosolic factor 1
$p67^{phox}$	–	neutrophil cytosolic factor 2 (NOXA2, NCF2)
PGDF	–	platelet derived growth factor
PMA	–	propidium monoazide
POI	–	protein of interest
ppm	–	parts per million
PS	–	phosphatidylserine
Rac	–	Ras-related C3 botulinum toxin substrate
RENOX	–	NADPH oxidase 4

Rh	–	rhodamine
ROS	–	reactive oxygen species
rt	–	room temperature
RyR1	–	ryanodine receptor
Sat. NaCl	–	saturated sodium chloride
Ser	–	serine
SDS	–	sodium dodecyl sulfate
SDS-PAGE	–	sodium dodecyl sulfate polyacrylamide gel electrophoresis
SOD	–	superoxide dismutase
TCEP	–	tris(2-carboxyethyl)phosphine
TEA	–	triethylamine
TLC	–	thin layer chromatography
TLR	–	toll-like receptor
TMSCl	–	trimethylsilyl chloride
TNF-α	–	tumor necrosis factor alpha
$[TS]^{‡}$	–	transition state
VMSC	–	vascular smooth muscle cells

Acknowledgements

I am eternally grateful to so many people who made this work possible. First and foremost, my supervisor, Dr. Fred Menard, for his endless patience & encouragement. He always pushes me to become the best possible scientist, and for that I am so thankful. Secondly, my lab mate, Dr. Vojtěch Kapras. He was an invaluable resource during both experimentation and the writing process. I would also like to thank my fellow lab mate, Wyatt Slattery, for his time developing and executing the respiratory burst assays in chapter 2. Lastly, I would like to thank my other two committee members, Dr. Paul Shipley and Dr. Kevin Smith. Throughout my degree they have taught me so much. I would not be here today if it were not for all of you.

Dedication

To my husband, Matt. Without his patience (which I envy), love and support, obtaining my master's degree would not have been possible.

Chapter 1: General Introduction

Proteins are polypeptides essential to the structure and function of organisms. Their interactions with other biomolecules (i.e., small molecules or other proteins), functions, and cellular localization are critical to an organism's survival. It is therefore important to understand how their activity helps to maintain a healthy organism. If a protein's activity is disrupted, it may lead to disease and/or death of the organism. Having the tools to study proteins' native interactions, functions, and localization can provide insight in a larger biological context. Small molecules are an important tool for these studies, as they can be used to modulate a protein of interest's (POI's) activity.

Small molecules are critical to several biological processes.[1] They include ligands for signal transduction cascades (i.e., neurotransmitters), secondary messengers (for protein-protein interactions), and many other processes. Through the use of chemical synthesis, we are able to synthesize these small molecules. In addition, we are also able to design analogues to provide insights in to the composition of amino acid residues of the ligand binding sites. This can lead to compounds with increased selectivity and potency for protein targets. For the purposes of chemical biology, we call these small molecules chemical probes.[2]

By using a chemical probe, we can answer questions regarding mechanistic and phenotypic effects of the POI's activity. Moreover, the probe can be used without genetic modification, making it a desirable tool in the study of whole organisms. This thesis presents two individual projects, both based on the synthesis of novel chemical probes: the first for inhibition of a specific protein type, the NOX enzymes; the latter for universal protein labelling.

1.1 CHEMICAL PROBES

Chemical probes may be used to elucidate a protein's role in a biological system. These probes can have a range of functions, including inhibition of biological activity and visualizing the protein.[1] In addition to studying the POI's activity, the use of probes can extend to other areas of study. A probe may also be designed to determine a molecule's mechanism of action on a protein. This is the basis of the work presented in chapter two, which describes the design and synthesis of analogues to a known enzymatic inhibitor.

If a probe has a specific receptor target on the POI, it can be synthetically modified to deliver a chemical tag. This process is known as affinity labelling and is the basis of the work in chapter three.[3]

The probe is attached to the tag via a linker. While the probe and POI are bound, the linker undergoes a reaction with an amino acid residue on the surface of the protein. This initiates a reaction cascade that results in a protein being covalently attached to the tag.

1.2 INHIBITION OF NADPH OXIDASE ENZYMES

Enzymes belong to a class of proteins that catalyse biochemical reactions, via active sites for specific types of transformations such as methylation, phosphorylation.[4] An active site typically contains amino acid residues that form intermolecular bonding interactions with the substrate.[5] Upon binding, the enzyme can change shape to transform the substrate to its product (Figure 1.1). Once the product is formed, the initial binding interaction is less favorable, and the product dissociates, freeing the enzyme for the next substrate.

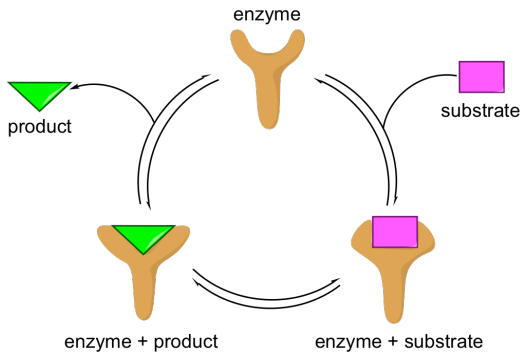

Figure 1.1 Schematic representation of the enzymatic transformation of a substrate.

To ensure that the enzyme is not constantly active, biomolecules such as proteins or small molecules can inhibit transformations competitively, noncompetitively, uncompetitively, or by mixed-type inhibition (Figure 1.2).[6] Competitive inhibition occurs when a molecule and substrate both have affinity for the enzymatic active site (Figure 1.2, **A**). For noncompetitive inhibition, the inhibitor and substrate bind to different sites on the enzyme (Figure 1.2, **B**). The inhibitor binds to an allosteric site, resulting in a change in conformation of the enzyme (which can activate or inhibit the enzyme).[5] Uncompetitive inhibition involves the inhibitor binding to the enzyme-substrate complex, preventing the transformation from taking place (Figure 1.2, **C**). Mixed-type inhibition can involve any combination of these.

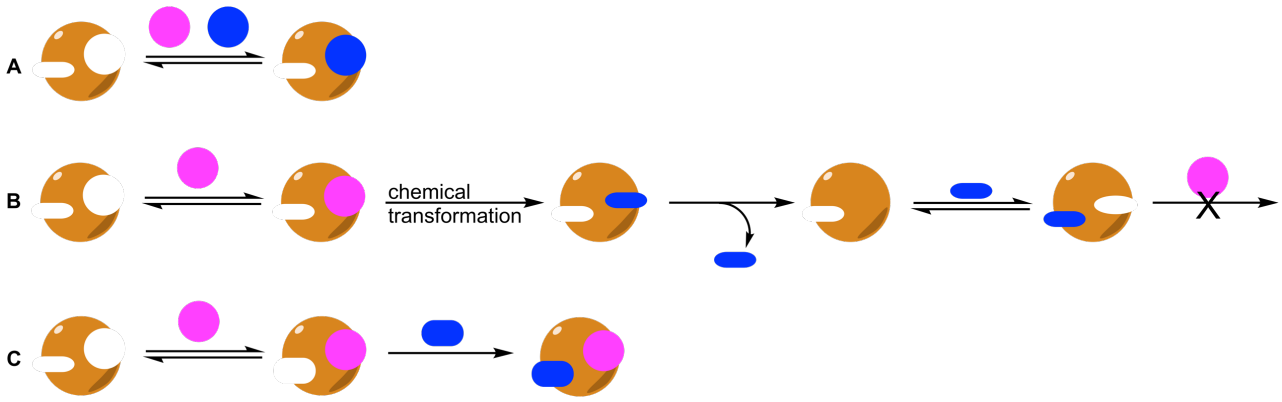

Figure 1.2 The three modes of enzyme inhibition: **A** competitive, **B** noncompetitive, and **C** uncompetitive. The product/inhibitor is shown in blue, the substrate in fuschsia, and the enzyme in tan.

Disruption of enzyme activity is known to contribute to the onset and progression of diseases.[5] Over the past several decades, methods in chemical genetics have been developed to study how disruption in regulation of enzymes (and other proteins) is related to the progression of diseases. If the mechanisms of regulation are known, this may provide insights towards preventing and treating diseases. A tool used to probe enzymatic function is an inhibitor – a small molecule (i.e., a drug, peptide, enzyme product) which can be used to reduce or stop the enzyme's catalytic activity.

1.2.1 NOX Inhibitor VAS2870 Has an Unknown Mode of Inhibition

The inhibitors described in chapter two were developed for the enzymatic complex NOX2 which is found in phagocytic cells (such as microglia in the central nervous system (CNS)).[7] NOX2 produces reactive oxygen species (ROS) used by phagocytes to breakdown foreign bodies (e.g., bacteria) and debris (e.g., damaged/dead cells).[8–10] Prolonged, uncontrolled ROS production has been implicated in the progression of several types of diseases (e.g., neurodegenerative diseases, such as Alzheimer's Disease).[11] In light of this, there is active research into methods of regulating the production of ROS produced by NOX2.

In 2004, Vasopharm created a series of triazolopyrimidine compounds as inhibitors of NOX2 in cardiac tissue.[12] One of these, VAS2870 (**1**, Figure 1.3) has been found to be active against NOX2 and other NOX isozymes, but how it inhibits the enzyme is still not understood.[13–17] Currently, it is not known if **1** inhibits NOX2 by non-covalent or covalent binding.

1.2.2 Research Objective

To investigate its mechanism of inhibition, I propose the synthesis of two analogues (**2** and **3**, Figure 1.3). The first analogue, **2**, retains all features of **1** but has an azidomethyl substituent on the benzyl moiety. Maintaining the mercaptobenzoxazole moiety may still allow reactions with thiols in the cell. If **2** successfully inhibits NOX2, the azidomethyl substituent can then be used for the addition of a chemical tag *in situ.* If cysteine thiols of NOX2 have reacted with **1**, this method could enable visualization of the thiols that have reacted with **1**. The second analogue **3** retains the structure of **1**, but substitutes a carbon for the sulfur. This compound should not be susceptible to nucleophilic attack by thiols. If **3** successfully inhibits NOX2, it would indicate that **1** can act as a NOX inhibitor through a ligand-binding interaction.

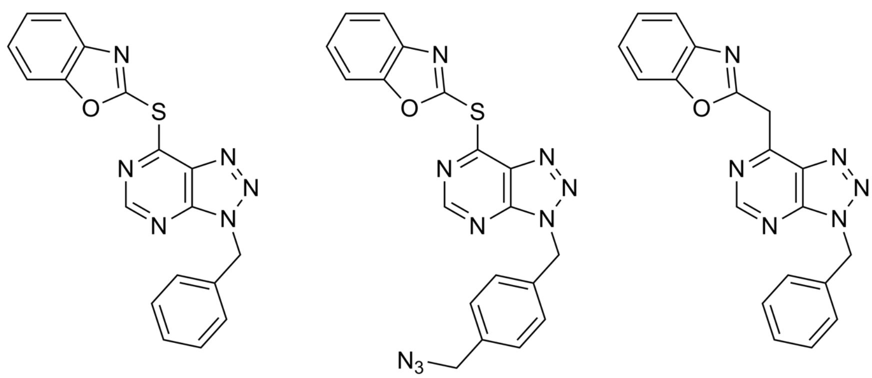

1 **2** **3**

Figure 1.3 The structures of VAS2870 (**1**), azidomethyl analogue **2**, and methylene analogue **3**.

1.3 TRACELESS-AFFINITY LABELLING OF PROTEINS FOR REAL-TIME MONITORING

The use of inhibitors is effective for probing the activity of an enzyme, but a different method is required if we wish to retain the POI's activity. Two such methods are bioorthogonal chemistry and traceless-affinity labelling.[3,18] Bioorthogonal chemistry uses genetic incorporation of a non-native chemical group into a protein. The ideal group is unreactive towards other cellular components, and selectively reacts with a chemical probe to label the protein (e.g., click chemistry, Figure 1.4). This method is highly selective but has limited applications in living systems.

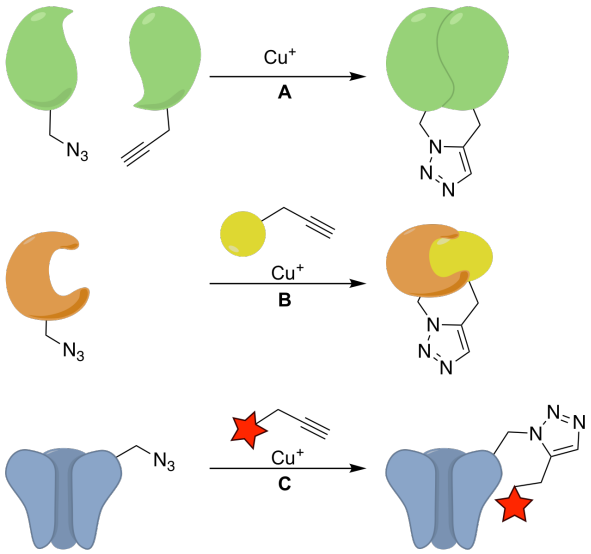

Figure 1.4 Click chemistry can be used to covalently link (A) two proteins; (B) a protein binding site and ligand; or (C) a receptor and a chemical tag. The azide is a small functional group, so it is not likely to perturb the POI's functions or interactions. It is added to the POI through genetic modification or metabolic uptake and is nonreactive towards other components of the protein. In the presence of a Cu^{+} catalyst, it undergoes a [2+2] cycloaddition to an alkyne, which can be coupled to another protein, chemical tag, or probe.[19,20]

A recent development in chemical genetics, traceless affinity labelling, uses ligand-directed delivery of a probe to proteins in their native environment, in real-time (Figure 1.5).[3] The ligand and tag are connected by a cleavable linker. When the ligand binds to the protein, the linker reacts with a nucleophilic residue on the exterior of the active site, cleaving the ligand from the (now covalently bound) tag. Once the ligand dissociates, the tag remains bound, and the protein can retain its native structure and function. This system is advantageous because no genetic modification is required to tag the POI, allowing it to be used *in vivo*.[3]

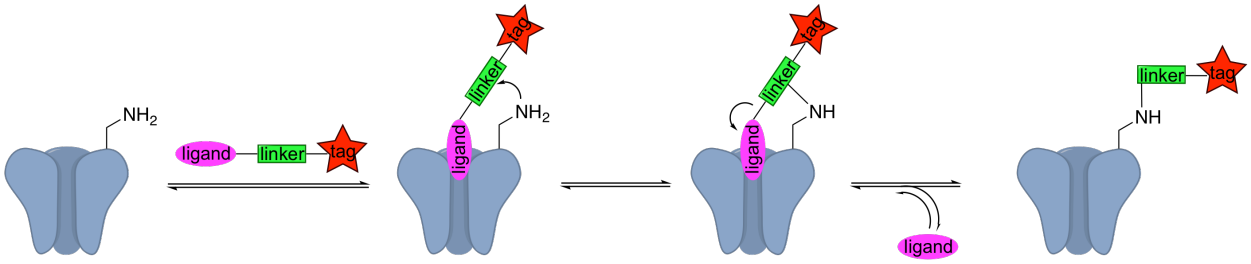

Figure 1.5 Ligand-directed delivery of a chemical tag to the POI. The linker reacts with a nucleophilic residue (e.g., lysine or serine) on the exterior of the binding site to covalently bind a chemical tag.

1.3.1 Towards the Development of a Silicon-Based Traceless-Affinity Linker

The third chapter of this thesis describes the efforts towards the development of a traceless affinity linker to covalently deliver a chemical tag to the surface of the POI (Figure 1.6) The proposed linker, **4**, contains an α-silyl-β-lactone, with a ligand bound to the silicon atom and a tag bound to the lactone. The α-silyl-β-lactone may undergo a reaction cascade with a lysine residue to simultaneously cleave the ligand from the tag, and covalently bind the tag to the POI.

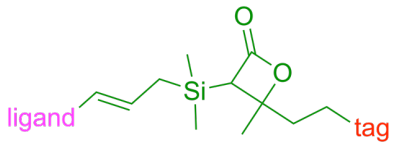

4

Figure 1.6 Structure of the proposed traceless-affinity molecule **4**.

1.4 OVERVIEW OF THIS THESIS

Given that this thesis addresses two topics, a more in-depth introduction is presented in each chapter. Chapter two of this thesis focuses on the synthesis of novel NADPH oxidase (NOX) inhibitors based on Vasopharm's VAS2870 (which contains a triazolopyrimidine backbone). The reactive oxygen species (ROS) generated by NOX have been implicated in the development of several neurodegenerative diseases (such as Alzheimer's and Parkinson's). The first inhibitor described contains a *p*-azidomethyl substituent for future tagging studies. The second inhibitor replaces a reactive sulfur-carbon bond of the original inhibitor with a carbon-carbon bond.

Chapter three describes efforts toward the development of a traceless affinity molecule. This molecule is composed of a ligand, cleavable linker, and chemical tag. When the linker is cleaved, the ligand is free of the tag, and can dissociate. The result is a tag-protein complex, which enables the visualization of the protein in real time. In addition, the location of the tag is such that it should not interfere with the native funtions of the protein. This study establishes the pioneering work necessary to design viable cleavable linkers for future protein labelling.

Chapter 2: Microglial NADPH Oxidase Activity and Inhibition

Recently, substantial evidence has emerged to suggest that prolonged, uncontrolled inflammation is a driving force in the progression of neurodegenerative diseases.[11,15,21–23] The brain's immune system is mediated by microglia, specialized phagocytic cells that are responsible for removing debris and pathogens in the central nervous system (CNS) (i.e., damaged neurons, microbes, and microbial products), which are further described in the beginning of this chapter.[11,21] When they recognize debris or pathogens, they produce inflammatory factors such as cytokines (e.g., interleukin-6) that recruit microglia to the affected area.[7] The microglia then engulf debris and break them down with reactive oxygen species (ROS).

The primary source of ROS in microglia is the NAD(P)H oxidase 2 (NOX2) enzymatic complex.[10,17,24,25] Its precise role in inflammatory neurodegenerative diseases is currently under active investigation.[9,22] Several studies have been aimed at inhibiting NOX2 through the use of genetic modification (e.g., knocking out the gene for NOX2) and chemical inhibitors.[6,21,29,38] The following section surveys the known probes for NOX inhibition, focusing on a triazolopyrimidine compound VAS2870. As the mode of inhibition of this compound is still unknown,[13,16,17,27,28] this chapter describes the development of two new triazolopyrimidine compounds designed to provide insight on the inhibitory effect of VAS2870.

2.1 MICROGLIA AND THEIR ROLE IN CNS INFLAMMATION

Under normal physiological conditions, microglia are in a "resting" state, but not dormant.[29,30] Protrusions of their cell body enable them to move and to monitor their environment using surface proteins.[30,31] At their surface, they present two main classes of receptors:[9] Toll-like receptors (TLRs) are monomeric membrane-spanning receptors that recognize microbes; and phosphatidylserine (PS) receptors that recognize apoptotic cellular substances.[30,31] When either of these receptors bind their respective targets, microglia become activated. Microglial activation results in enhanced proliferation, migration, phagocytosis, and production of bioactive compounds. [21,23,30,31] These bioactive compounds range from cytotoxic mediators to trophic factors, which can be beneficial or destructive to the CNS.[32]

One type of such compounds produced as a result of activation are reactive oxygen species (ROS, Figure 2.1).[23]

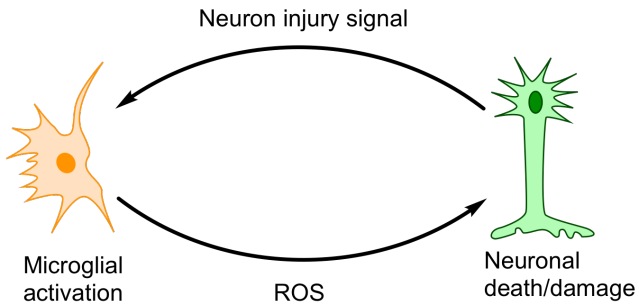

Figure 2.1 Microglia-mediated neuronal damage results from reactive oxygen species (ROS) produced by microglia.[23]

2.1.1 Reactive Oxygen Species Production in Microglia

Microglial activation in response to damage or foreign bodies result in the formation of ROS. The concentration of ROS in microglia (and other phagocytic cells) is approximately 1000-fold higher than that of non-phagocytic cells.[33] These ROS are generated from molecular oxygen via electron transfer reactions within the enzymatic complex NAD(P)H Oxidase 2 (NOX2) to form superoxide (eq. 1) .[26,34]

$$NOX2 + O_2 \rightarrow O_2^{\bullet -} + H^+ \qquad \text{(eq. 1)}$$

Superoxide has a short half-life and is readily converted to hydrogen peroxide (H_2O_2) or peroxynitrite ($ONOO^-$, Figure 2.2).[32] H_2O_2 may react with an iron (II) hemoglobin/myoglobin complex to form the hydroxyl radical or get neutralized to H_2O by glutathione peroxidase (GPX). $ONOO^-$ reacts with CO_2 to generate both hydroxyl and nitrite radicals.[32,35]

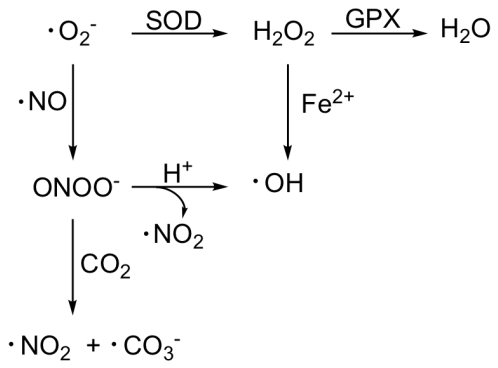

Figure 2.2 Conversion of superoxide to other reactive oxygen species (ROS). Conversion to H_2O_2 is achieved by superoxide dismutase (SOD). H_2O_2 is quenched by glutathione peroxidases (GPX) to H_2O, or by an Fe^{2+}hemoglobin/myoglobin complex to a hydroxyl radical. Superoxide can also react with nitric oxide to form peroxynitrite. In the presence of acid, this leads to the hydroxyl and nitrite radicals. It may also react with aqueous CO_2 to yield nitrite and carbonate radicals.[32,35]

In healthy systems, microglial ROS participate in cell signalling and degradation of pathogens and cell debris, contributing to normal CNS functions.[26] There are also structures in place to monitor ROS levels, such as superoxide dismutase (SOD) and glutathione peroxidases.[33] However, excessive uncontrolled ROS production no longer has a positive immune function, but begins destroying healthy neurons.[21] At these levels, the cells can no longer regulate ROS levels and the oxidative damage leads to cellular death. Neurons have limited cell renewal and regenerative capacities; therefore, these effects are often detrimental – physically and cognitively.

2.1.2 Microglial Enzyme NOX2 Generates Reactive Oxygen Species

ROS in microglia are generated by enzymes present in the mitochondria, 5-lipoxygenases (LOX), and nicotinamide adenine dinucleotide phosphate (NAD(P)H) oxidases (herein referred to as NOX) (Table 2.1), which can be found throughout the body. All NOX family members (NOX1-5 and Duox1-2) have the sole purpose of generating ROS in a variety of cell types.[25] A common motif amongst NOX1-5 members is a transmembrane protein, the NOX isozyme, while the cytosolic components vary (Table 2.1, Figure 2.3).[25] All of the components must combine upon microglial activation to produce ROS.

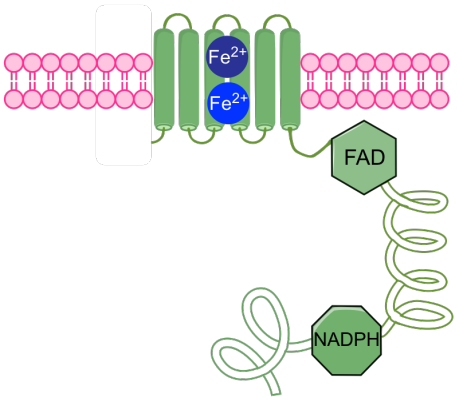

Figure 2.3 Schematic representation of the main protein composing the NOX2 enzyme complex. Conserved amongst NOX isozymes are a six transmembrane helical domain, four highly conserved heme-binding histidines within the transmembrane domain, and binding sites for NADPH and flavin adenine dinucleotide (FAD) at the distal and proximal ends of the C-terminal cytosolic dehydrogenase domain, respectively;.[25]

This transmembrane protein is the catalytic subunit responsible for the generation of ROS. It facilitates electron transport across biological membranes to convert oxygen to superoxide. Each NOX isozyme type requires a unique assembly of smaller subunits, which results in different cellular functions.

Table 2.1 The known compositions of the NOX family members.[25]

Membrane-bound		**Cytosolic Co-proteins**					
NOX isozyme (alt name)	**p22*phox***	**NOXO1**	**NOXA1**	**p40*phox***	**p47*phox***	**p67*phox***	**Rac1 / Rac2**
NOX1 (gp91-2)	✓	✓	✓		✓		✓
NOX2 (gp91*phox*)	✓			✓	✓	✓	✓
NOX3 (gp91-3)	✓	✓	✓				
NOX4 (RENOX)	✓						
NOX5							

There is a general consensus that the majority of ROS in microglia are produced by NOX2 (Table 2.1, Figure 2.4).[23,34] In the resting state of NOX2, the co-proteins are not bound to the transmembrane isozyme gp91*phox*. It is important to note that there are contradicting theories surrounding the composition of the cytosolic cofactors. This is likely due to the use of isolated domains of each co-proteins for binding studies.[36] Yet a widely accepted resting state suggests that the p47*phox* co-protein separated from the cytosolic dimer (p40*phox* and p67*phox*).[13,36–38]

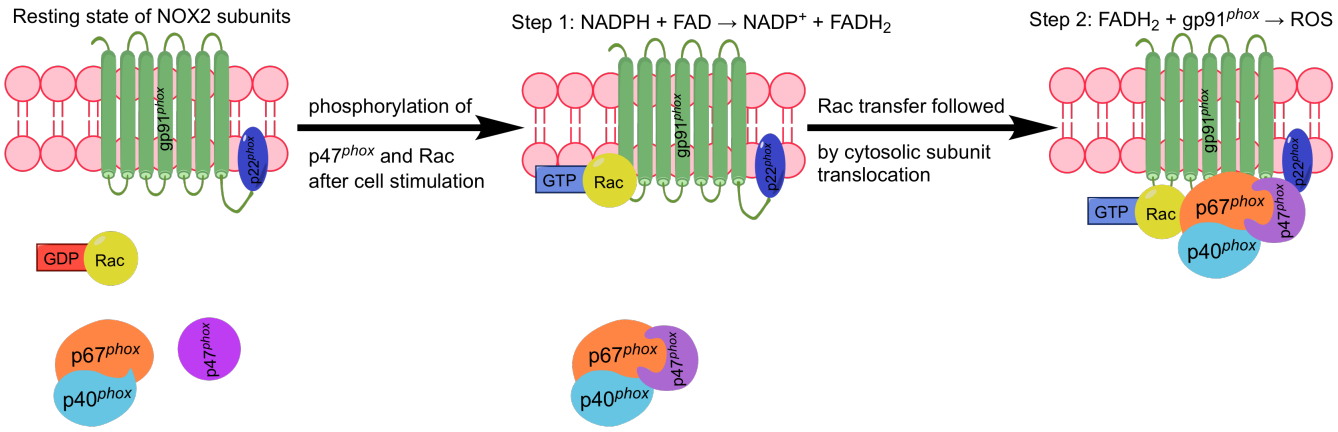

Figure 2.4 Assembly and activation of NOX2. Upon cellular stimulation, ROS production begins in a two-step process.[36] In the first step, guanosine diphosphate (GDP-Rac (1 or 2)) and p47 *phox* are phosphorylated (primarily by protein kinase C).[13,37–40] Then, the activated GTP-Rac migrates to the transmembrane isozyme gp91^{phox} to initiate electron transfer.[13,37,38] At the same time, phosphorylation of p47^{phox} serine residues cause a conformational change, enabling activation of the remaining cytosolic subunits, p40^{phox} and p67^{phox}. These proteins can exist as a trimer at the resting state, but do not exhibit activity until phosphorylation occurs. Secondly, GTP-Rac translocates to p67^{phox}, and subsequent migration of the cytosolic complex to the membrane completes the active NOX2 assembly.[38,39] Finally, association of p67^{phox} and gp91^{phox} makes the electron transfer possible, thereby producing ROS.[38,39]

ROS production is achieved by transporting electrons from the cytosolic portion of gp91^{phox} to the extracellular surface, in a two-step process.[41,42] The first step involves electron transfer from NADPH to FAD, reducing FAD to $FADH_2$. This is followed by electron transfer from $FADH_2$ to the inner gp91^{phox} - associated heme groups, by reduction of Fe^{3+}. The electrons then move to the outer heme groups where they reduce molecular oxygen to superoxide.

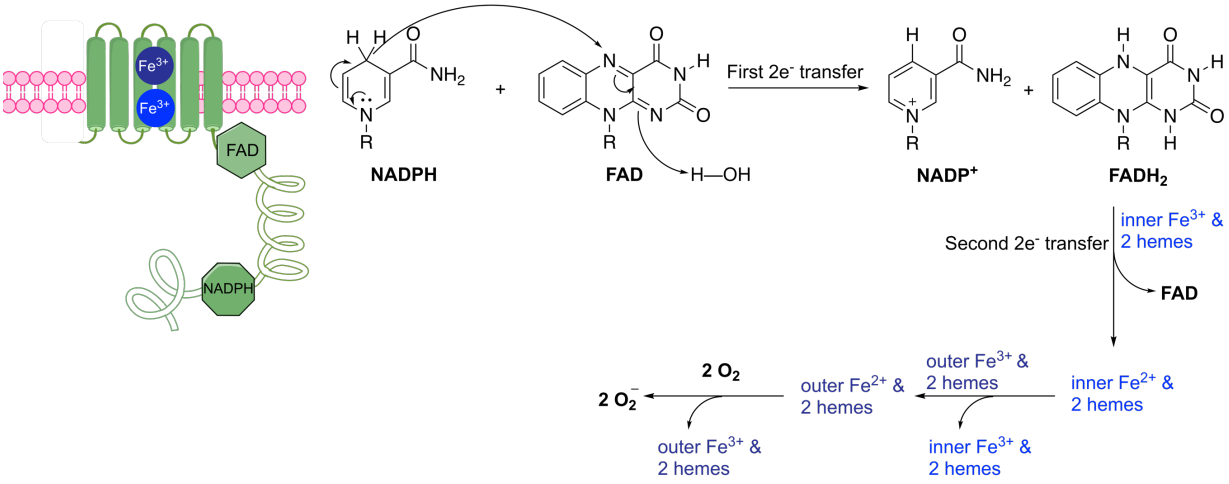

Figure 2.5 Electron transport across the transmembrane gp91*phox* isozyme (NOX2) is responsible for ROS production in microglia.

Several NOX inhibitors have been developed to prevent ROS production by disrupting/preventing electron transport across cellular membranes. Having the ability to prevent specific steps in the electron transport chain may provide insights into how to slow down or stop excessive ROS production.

2.2 A SURVEY OF NOX INHIBITORS

Over the past several decades, a series of NOX inhibitors have been identified (Table 2.2). Despite the range of chemical structures, the quest is still ongoing for isozyme-selective inhibitors that present no side reactions. Apocynin (entry 2) binds to p47*phox*'s N-terminal binding domain and has been commonly used in NOX inhibition assays until 2008, when it was reported that it also acted as a ROS scavenger.[39] While a wide range of compounds have been reported as NOX inhibitors since then, there is still a need for new inhibitors. This is due to lack of selectivity, unknown mechanisms of action, and/or undesirable side effects. VAS2870 (entry 3) is now one of the most commonly used NOX2 inhibitor. While its mechanism of inhibition is still unclear, it is known that it does not act a ROS scavenger like Apocynin.

Table 2.2 Examples of reported NOX inhibitors.[26,43]

Traditional Inhibitors of NOX					
Entry	**Name**	**Structure**	**Isozyme Selectivity**	**Mode of action**	**Off-target effects**
1	DPI (1972, Holland & Sherratt)	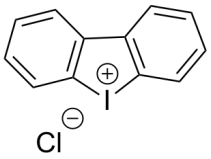	None	Forms adduct with FAD to inhibit ROS production	Irreversible, nonselective inhibitor of Flavin-dependent enzymes (including NO synthase & xanthine oxidase)
2	Apocynin (1990, Simons *et al*)	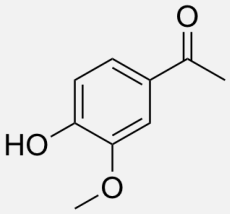	None	Inhibits translocation of p47^{phox} to plasma membranes; requires activation by myeloperoxidase	Antioxidant: nonspecific scavenger of nonradical oxidant species
Triazolo pyrimidines					
Entry	**Name**	**Structure**	**Isozyme Selectivity**	**Mode of action**	**Off-target effects**
3	VAS2870 (**1**) (2004, Vasopharm)	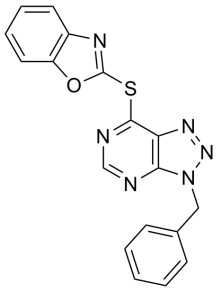	NOX1, 2, and 4	unknown	Thioalkylation of RyR1 and GSH
4	VAS3947 (**5**) (2005, Vasopharm)	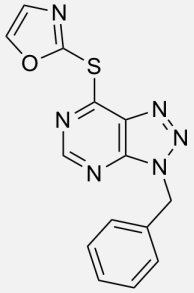	None	unknown	Thioalkylation
Other NOX inhibiting compounds					
Entry	**Name**	**Structure**	**Isozyme Selectivity**	**Mode of action**	**Off-target effects**

5	Fulvene-5 (2010, Bhandarkat *et al*)	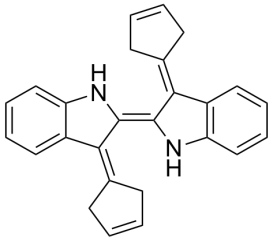	NOX2 & 4	unknown	
6	Naloxone (2012, Wang *et al*)	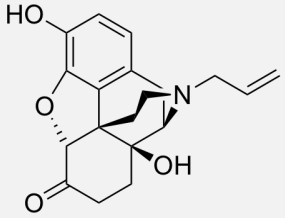	Unknown, only NOX2 studied	Binds to NOX2 & blocks translocation of p47^{phox} to plasma membrane	Antagonist of opioid receptors
7	Celastrol (2011, Jaquet)	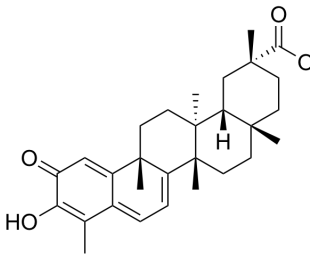	NOX 1, 2, and 4	unknown	Acts on several distinct stress response pathways, sometimes stimulating ROS production
8	Ebselen (2012, Smith)	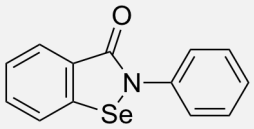	NOX2	Blocks translocation of p47^{phox} to neutrophil membranes; a glutathione peroxidase mimic.	H_2O_2 scavenger
		Bridged Tetrahydroquinolines			
Entry	**Name**	**Structure**	**Selectivity**	**Mode of action**	**Off-target effects**
9	(±)-(*1S*,*4R*,*9S*)-5-bromo-3,3-dimethyl-9-(2-methylallyl)-10-pentyl-1,2,3,4-tetrahydro-1,4-(epiminomethano)naphthalene (2010, Borbely *et al*)	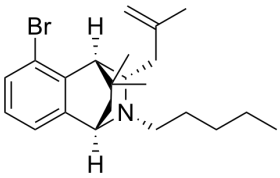	NOX2	unknown	unknown
10	(±)-(*1S*,*4R*,*9S*)-5-bromo-3,3-dimethyl-9-(2-methylallyl)-10-(thiophen-2-ylmethyl)-1,2,3,4-tetrahydro-1,4-(epiminomethano)naphthalene (2010, Borbely *et al*)	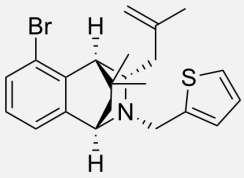	NOX2	unknown	unknown

2.2.1 NOX2 Inhibitor VAS2870

In 2004, a patent for the NOX inhibitor 7-(benzo[*d*]oxazol-2-ylthio)-3-benzyl-3*H*-[1,2,3]triazolo[4,5-*d*]pyrimidine, referred to as VAS2870, was published for cardiac tissue (Table 2.2, entry 3; **1**, Figure 2.6).[26,43,44] The primary NOX isozyme in cardiac tissue is NOX2 (Table 2.1), which is also the predominant isozyme in microglia (and other phagocytic cells). As shown in Figure 1.2, ROS consume nitric oxide (NO), and loss of NO is a known link to pathogenesis of cardiovascular disease.[12]

Literature reports show that VAS2870 can inhibit NOX1, NOX2 NOX4, and NOX5, but the mechanism has yet to be determined.[16,26,28] While it does not act as a ROS scavenger, it was recently found to react with thiols in Ryanodine receptors (cystine residues) and glutathione.[16,40] As it is actively used as a NOX2 inhibitor, I am developing two analogues to determine its mode of action. If this can be elucidated, it may aid in the development of novel, isozyme selective NOX inhibitors.

2.3 POTENTIAL MECHANISM(S) OF INHIBITION OF NOX2 BY VAS2870

Two kinds of assays have been used to study NOX2 inhibition by **1** *in vitro*: whole cell and semi-recombinant assays. These studies showed that **1** will only inhibit ROS production when added to whole cells, prior to stimulation. Platelet-derived growth factor with two B subunits (PDGF-BB) was used in whole cell assays and 12-myristate-13-acetate (PMA) was used in the semi-recombinant assays.[13,27] No inhibition was observed when **1** was added after stimulation,[25] or when semi-recombinant techniques were used (in which the cytosolic subunits p47^{phox}, p67^{phox}, and Rac are pre-assembled).[13] This indicated that **1** may prevent the cytosolic triad from forming, which would prevent ROS production. Two possibilities are that **1** may prevent the triad from forming by a ligand binding interaction with one of the co-proteins, or it may covalently modify a co-protein. Either of these may prevent formation of the cytosolic triad, and therefore prevent ROS production.

VAS2870 (**1**) has a triazolopyrimidine moiety that is similar to the purine moiety of FAD and NADP (Figure 2.6). Both FAD and NADP bind to the C-terminal cytosolic dehydrogenase domain of NOX2, which is highly conserved amongst all five isozymes. Since **1** is not capable of redox

reactions like the flavin and nicotinamide components of FAD and NADPH, respectively, if it occupies one of their boinding sites, this could account for its inhibitory effect.

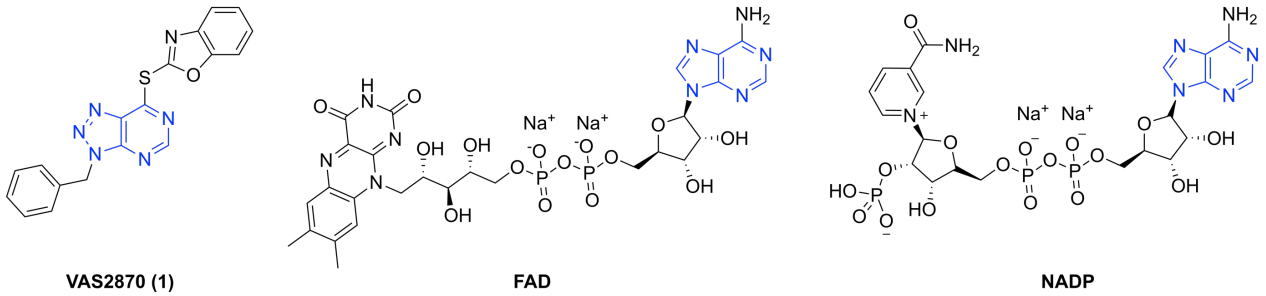

Figure 2.6 The structures of VAS2870 (**1**), FAD, and NADP. Their respective triazolopyrimidine and purine moieties are shown in blue.

A possible mode of inhibition of **1** is that it covalently modifies a cysteine's thiol present on a NOX2 component via alkylation by the triazolopyrimidine moiety. In fact, the demonstrated reaction between **1** and glutathione (GSH) suggests that alkylation of the GSH thiol with the triazolopyrimidine moiety (Figure 2.6).[40] VAS2870 has also been shown to react with cysteine thiols in Ryanodine receptors (RyR1).[28] This ability of **1** to react with thiols indicates a potential mechanism of action for **1**.[16,26,28]

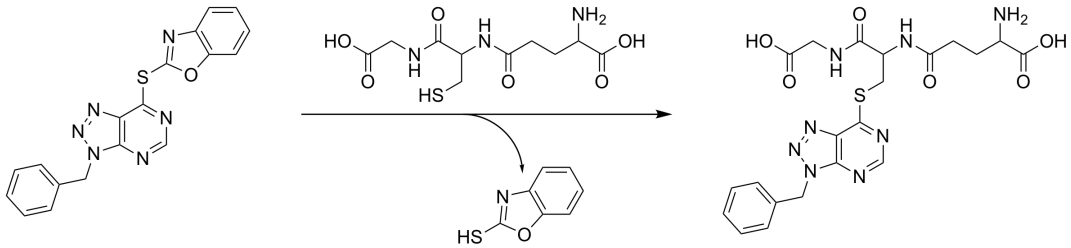

Figure 2.7 The nucleophilic aromatic substitution of VAS2870 by GSH, resulting in thioalkylation of GSH by the triazolopyrimidine moiety of **1**.[28]

With the knowledge that **1** is able to react with cysteine thiols and that **1** is ineffective when the p47 ^{phox}/p40 ^{phox}-p67^{phox} cytosolic triad is preassembled, I propose the following mechanism of inhibition: **1** inhibits formation of the cytosolic complex via covalent modification of one or more cysteine thiols. In the following section, I will examine each cytosolic co-protein for cysteines that may react with **1**.

2.3.1 Cysteines of the NOX2 Isozyme are Possible Sites of Thioalkylation by VAS2870

Intracellular soluble proteins p67^{phox}, Rac, gp91^{phox}, and p47^{phox} all contain cysteine residues which may react with **1**. p67^{phox} does not present cysteines at the binding interface with Rac or p47^{phox}, so alkylating the cysteine residues likely would not account for the effect of **1**. Rac possesses a cysteine (Cys18) in proximity to the binding site with p67^{phox} (Figure 2.8). However, it has been shown that disulfide formation between Cys18 and glutathione increases its activity, so this would likely not account for the effect of **1**.[45]

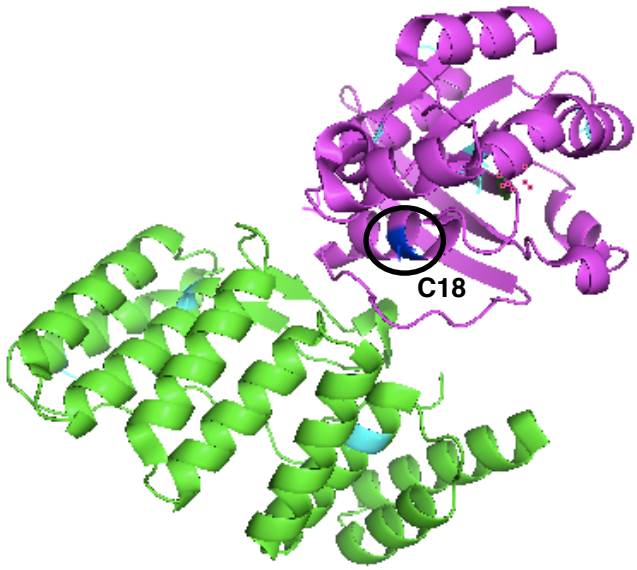

Figure 2.8 The crystal structure of GTP-Rac (purple) bound to p67 ^{phox} (green) (PDB: 1E96). Cys18 is shown in blue and the other Cys residues present are in cyan. GTP-Rac's C-terminus extension and p67^{phox}'s tetratricopeptide repeat domain assemble upon cellular stimulation.[38] The contact interface occurs between Rac's switch 1 and the β hairpin insertion of p67^{phox} via direct hydrogen bonding (Gly-30$_{Rac}$ with Asp-67$_{p67}$ and Glu-31$_{Rac}$ with Ser-37$_{p67}$). [38]

NOX2 (gp91^{phox}) has two cysteines that are critical to its function: Cys369 and Cys537 (Figure 2.9).[46,47] Cys369 is unique to NOX2 and is proposed to be exposed to cytosolic factors during assembly of the complex. Although Cys369 is not part of the binding site of FAD, the mutation Cys369Arg prevented FAD binding and formation of the active enzymatic complex.[46] A second mutation,

Cys537Arg, prevented NADPH from binding and ROS production, but did not inhibit formation of the complex.[46,47]

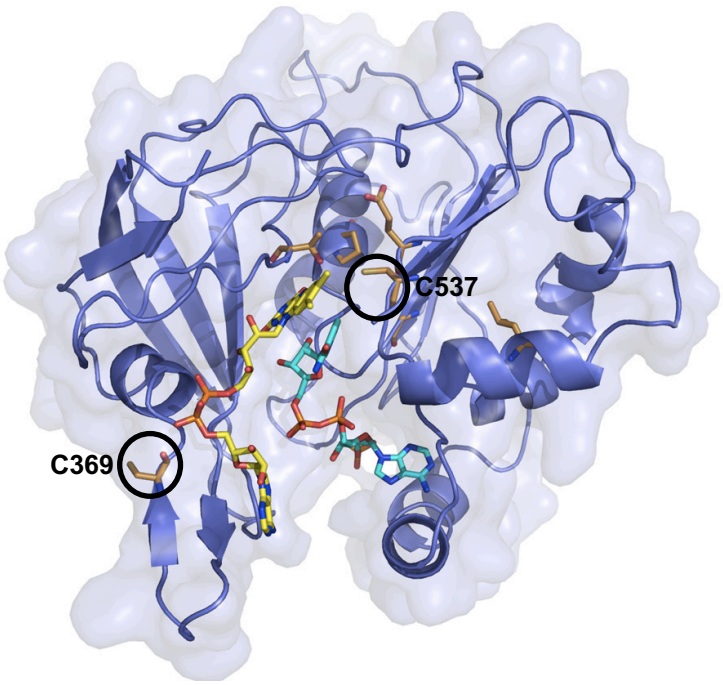

Figure 2.9 A computational homology model of the DH (double-homologous) domain of gp91^{phox}.[34] The carbons of FAD and NADPH are yellow and cyan, respectively. This shows the relative positions of Cys369, exposed to the intracellular environment, and Cys537, part of the sequence for binding the ribose portion of NADPH.

p47^{phox} possesses four cysteine residues: Cys98, Cys111, Cys196, and Cys378. Of the four, only mutations of Cys111 and Cys378 were found to prevent ROS production.[48] Cys111 (along with C98 and C196) was found to be easily labeled with [^{3}H]NEM (N-[2-^{3}H]ethylmaleimide) after exposure to SDS (sodium dodecyl sulfate), but Cys378 is not. These findings suggest that Cys378 is buried in the binding interface of p47^{phox} and p67^{phox} (Figure 2.10).[27,48,49] Thioalkylation of this Cys by **1** may prevent binding of p47^{phox} and p67^{phox}.

Upon activation of NOX2, p47^{phox} binds to the p67^{phox}/p40^{phox} dimer, and the complex translocates to the membrane (Figure 2.10). p47^{phox} then binds to the membrane bound p22^{phox}, bringing p67^{phox} and gp91^{phox} together, completing superoxide production. As the p47^{phox} subunit is critical to NOX2 ROS production, thioalkylation of its Cys378 residue by **1** may account for the observed inhibition.

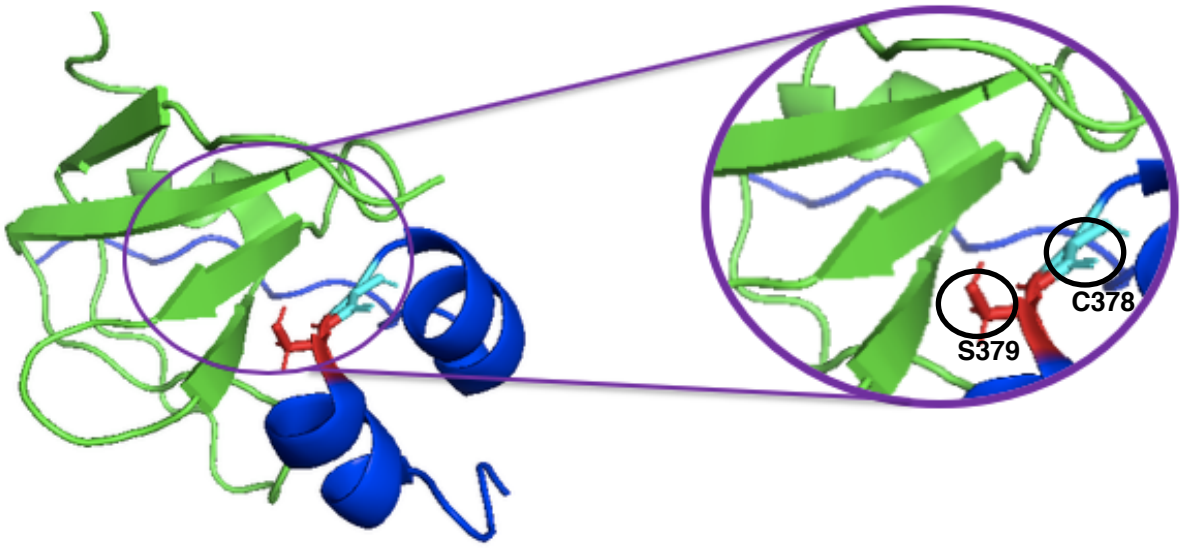

Figure 2.10 The crystal structure of the contact interface between p47*phox* and p67*phox* (PDB 1K4U). p47*phox* is shown in blue, p67*phox*, in green, Cys378 residue in cyan, and Ser379 in red. p47 *phox* binds to p67 *phox* through the C-terminal region.[45] Only p47*phox* has a cysteine residue within the binding site.[27,48] This Cys H-bonds to its Ser379 neighbour, both before and after phosphorylation.[50] Ser379 phosphorylation has been shown to be critical to p47*phox*'s activity by inducing a conformational change which enables translocation to p22*phox*.[51] Upon phosphorylation, the C-terminal tail breaks away from the polybasic auto-inhibited region (AIR) and the SH3 groove is partially exposed for binding to p22*phox*.[51] Cys378 is buried in the C-terminus upon phosphorylation, and this site is necessary to bind to p67*phox*.[51] Thioalkylation of Cys378 could prevent phosphorylation of Ser379, binding to p22*phox*, or p67*phox*. Any combination of these effects could result in the observed inhibition of NOX2 by **1**.

2.4 PROPOSED DESIGN OF VAS2870 ANALOGUES TO PROBE ITS MODE OF INHIBITION

VAS2870 may inhibit NOX2 via thioalkylation of its cysteine thiols and/or a ligand-binding interaction. To determine how VAS2870 (**1**, Figure 2.6) inhibits ROS production in NOX2, I propose the synthesis of two VAS2870 analogues: 4-(azidomethyl)benzyl-7-(benzo[d]oxazol-2-ylthio)-3-benzyl-3*H*-[1,2,3]triazolo[4,5-d]pyrimidine (**2**) and 7-(benzo[d]oxazol-2-ylmethylene)-3-benzyl-3*H*-[1,2,3]triazolo[4,5-d]pyrimidine (**3**).

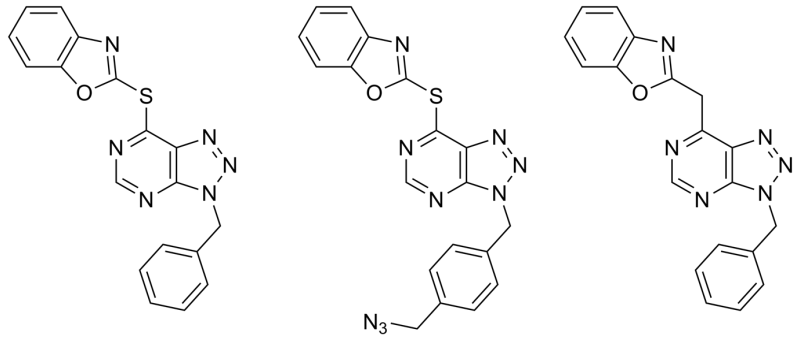

1 **2** **3**

Figure 2.11 The structures of VAS2870 (**1**) and the two target analogues: N_3-VAS2870 (**2**) and CH_2-VAS2870 (**3**).

To determine if a thioalkylation reaction occurs with NOX2, I will synthesize the *p*-azidomethyl analogue **2**. This structure retains all components of VAS2870, with the addition of the *p*-azidomethyl group. The patent for **1** (Table 2.3) reports retention of NOX inhibition with a *p*-methoxy substituent, so **2** should still fit into the putative binding site of **1**. Should a thioalkylation take place with the triazolopyrimidine moiety, the azide would then be permanently attached to the protein. After incubation of NOX2 with **2**, the azide can be reacted with a chemical tag (e.g., click chemistry, Figure 1.4). Cell lysis followed by separation of proteins via an SDS-PAGE will show if any proteins were covalently modified by **1**.

Alternatively, to determine if **1** can inhibit NOX2 through a ligand-binding interaction, a VAS analogue must be used that cannot undergo thioakylation with cysteines. For this, methylene analogue **3** will be used. This compound retains the size and shape of **1** but replaces the thiobenzoxazole with a methylenebenzoxazole. Replacing the sulfur prevents **3** from thioalkylating cysteines by eliminating the electrophilicity of the pyrimidine's C-7 position (Figure 2.12). If **3** successfully inhibits ROS production, it would indicate that VAS2870 and NOX2 may interact through a non-covalent ligand-binding interaction.

2.5 SYNTHESIS OF VAS2870, *p*-AZIDOMETHYL- AND METHYLENE ANALOGUES

In the patent for VAS2870, changes were made to the 1,2,3-triazolo[4,5-*d*]pyrimidine moiety to optimize the inhibition of platelet activation (Table 2.3). With the presence of 2-(oxazolyl)thio substituents increased the inhibition levels of **1** and **5**; as did the addition of a *p*-methoxybenzyl or *o*-chorobenzyl group (**11** and **12**) significantly increased inhibition (over the benzyl moiety of **1** and **1**,

5, **9**, and **10**). Yet, interestingly only **1** and **5** (VAS3947) have been used as NOX inhibitors. Compound **5** displays better solubility than **1**, it was found to be less selective for individual NOX isozymes.[16]

Table 2.3 Reported activity of a series of VAS compounds toward inhibition of platelet activation.[12]

VAS analogs for inhibition of platelet activation	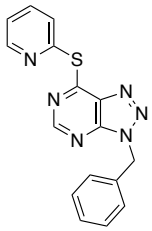 **9**	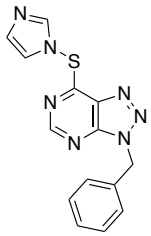 **10**	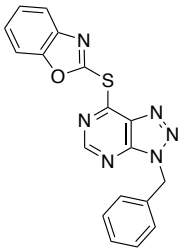 **1**	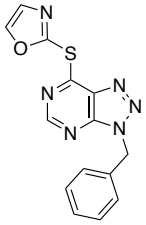 **5**	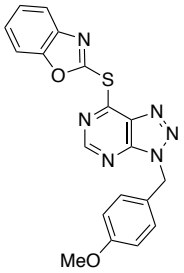 **11**	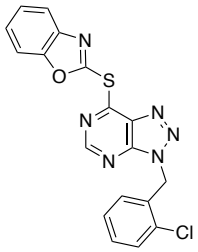 **12**
IC_{50} (μM)	13	12	2	2	2	2
% Inhibition	34	21	49	55	60	80

When designing probes to find the binding mode of **1** and NOX2, it was important to retain as much of **1**'s structure as possible. The proposed carbon analogue **3** maintains the phenyl and 2-(benzoxazolyl)thiol substituents found in **1** (Scheme 2.1). It is therefore expected to sterically occupy the same binding site as **1**. Stamler *et al.* reported the triazolopyrimidine moiety of **1** thiol alkylates GSH and cystines in RyR1 receptors, eliminating the 2-mercaptobenzoxazole group (Figure 2.7).[28] It is possible that **1** may inhibit NOX2 in a similar manner, specifically by thioalkylating a cysteine residue (C378) on $p47^{phox}$ (Figure 2.13). Substituting the sulfur for a carbon on the R_1 position of **3** will prevent such an alkylation. Therefore, if NOX2 is inhibited by **3**, it would indicate that VAS2870 non-covalently occupies a binding site in NOX2. Conveniently, both **1** and **3** have the same chloropyrimidine precursor **4**.

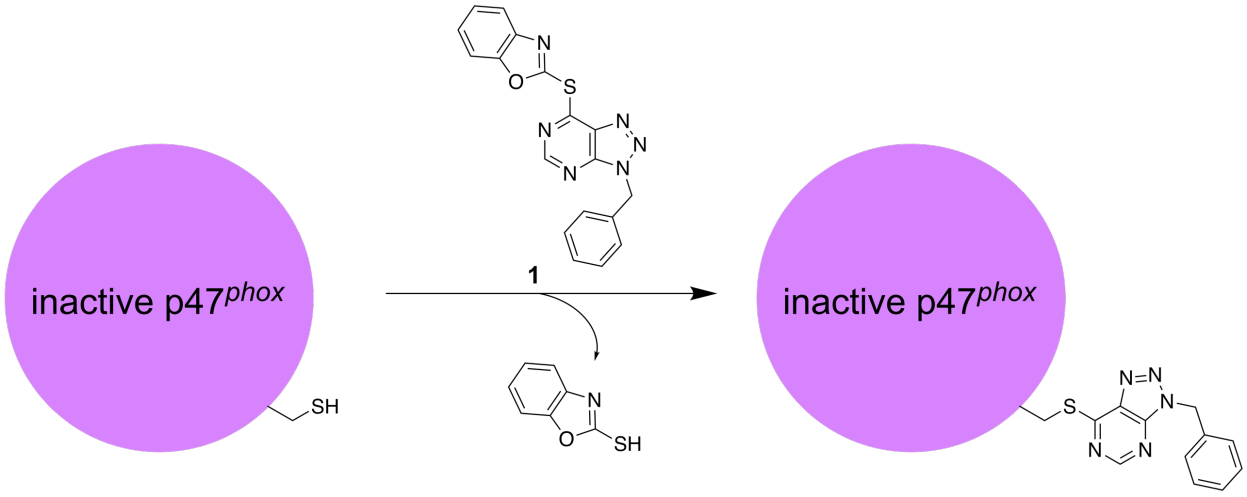

Figure 2.12 Putative reaction between **1** and a cysteine residue on p47*phox*.

To investigate whether or not **1** inhibits NOX2 by alkylating cysteine residues, the *p*-azidomethyl derivative **2** was proposed (Scheme 2.1). It maintains the 2-(benzoxazolyl)thiol substituent of **1**, but adds an *o*-azidomethyl group to the benzyl substituent. The addition of the azidomethyl group is not expected to interfere with binding (based on the % inhibition of **11**). Compounds **1**, **2**, and **3** can be synthesized using two different routes.

In the first sequence, **1** and **3** can be synthesized from the same chloropyrimidine precursor **13** by addition of their respective benzoxazole moieties (Scheme 2.1). Simiarly, **2** may be synthesized from chloropyrimidine **14**. Chloropyrimidines **13** and **14** should be both obtained from the chlorination of the respective pyrimidinones **15** and **16**. Both of which are the result of a cycloaddition between acetamide **17** and azides **18** and **19**, respectively.

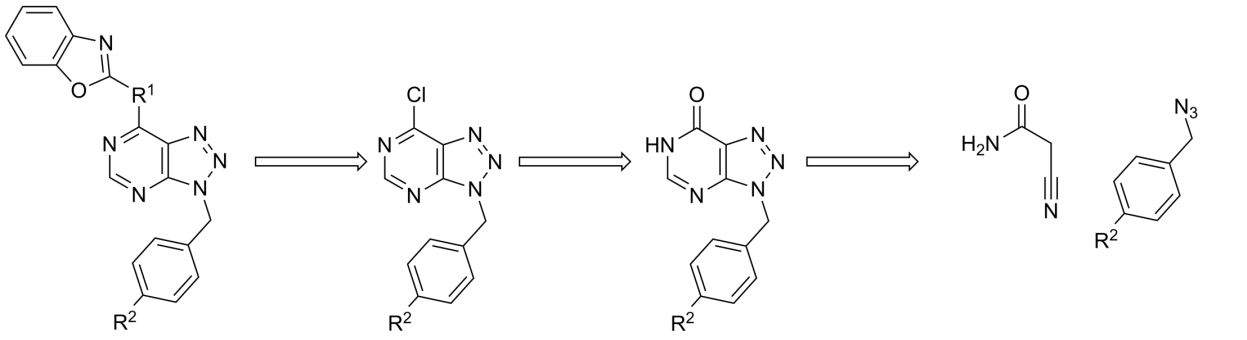

Scheme 2.1 Retrosyntheses one of VAS2870 (**1**) and analogues **2** and **3**, starting from cyanoacetamide (**17**).

For the second route, the last step of the synthesis is the same as above (Scheme 2.2). The triazole ring of **13** and **14** should be formed by first coupling pyrimidine **20** with the appropriate amine (**21** and **22** respectively), then cyclizing the resulting diamine. Both routes were explored to optimize the syntheses of **1** – **3** and are described in the following section.

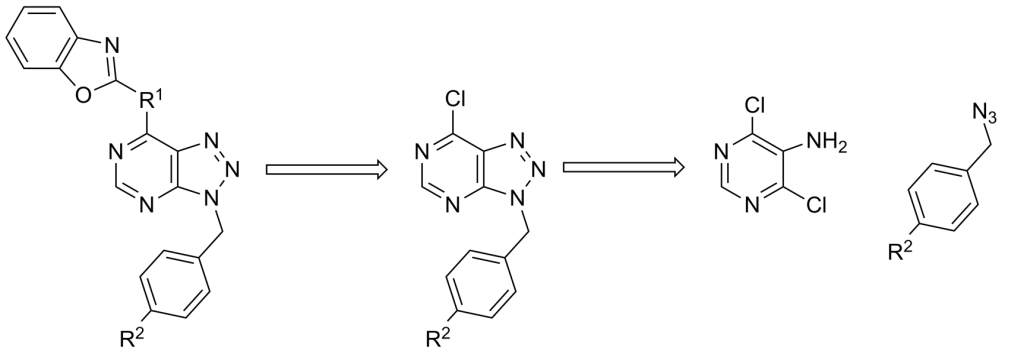

Scheme 2.2 Alternate retrosyntheses of VAS2870 (**1**), carbon analogue **3**, and azidomethyl analogue **2** from chloropyrimidine **20**.

2.6 SYNTHESES OF VAS2870 (1) & CARBON ANALOGUE 3: A FIRST-GENERATION APPROACH

Two synthetic routes were explored to synthesize the key chloropyrimidine precursor **13**. Both were inspired by the original patent for VAS2870 (**1**).[12] In the first route, the triazolopyrimidine core was constructed, followed by chlorination of pyrimidinone **15** to yield **13**.[27] This proved difficult, due to the stability of the pyrimidinone.[52] I then tried to convert the carbonyl oxygen to a triflate or a bromide, to generate a better leaving group. The conversion to a triflate and bromination were unsuccessful, so a second route was explored. It involved functionalizing the pyrimidine core first, then forming the triazole in the final step.

2.6.1 Synthesis of Chloropyrimidine 13 from Pyrimidinone 15

The initial synthesis of the benzyltriazolopyrimidine core began with formation of benzyl azide (**18**, Scheme 2.3). It was prepared by refluxing bromide **23** and sodium azide in a cosolvent of THF and water to obtain the azide in a quantitative yield.[12] Cyclization of the azide with cyanoacetate **17** was achieved by refluxing them under basic conditions. Cooling the reaction mixture allowed triazole intermediate **24** to precipitate out, and it was collected by vacuum filtration in a high yield (92%).[12] The benzyltriazolopyrimidine backbone **15** was assembled by refluxing **24** with formate **25** under basic conditions, in a good yield (87%).[12] Initial attempts (entry 19, Table 2.3) of chlorinating the pyrimidinone produced poor yields and were not reproducible, so other chlorinating conditions were explored.

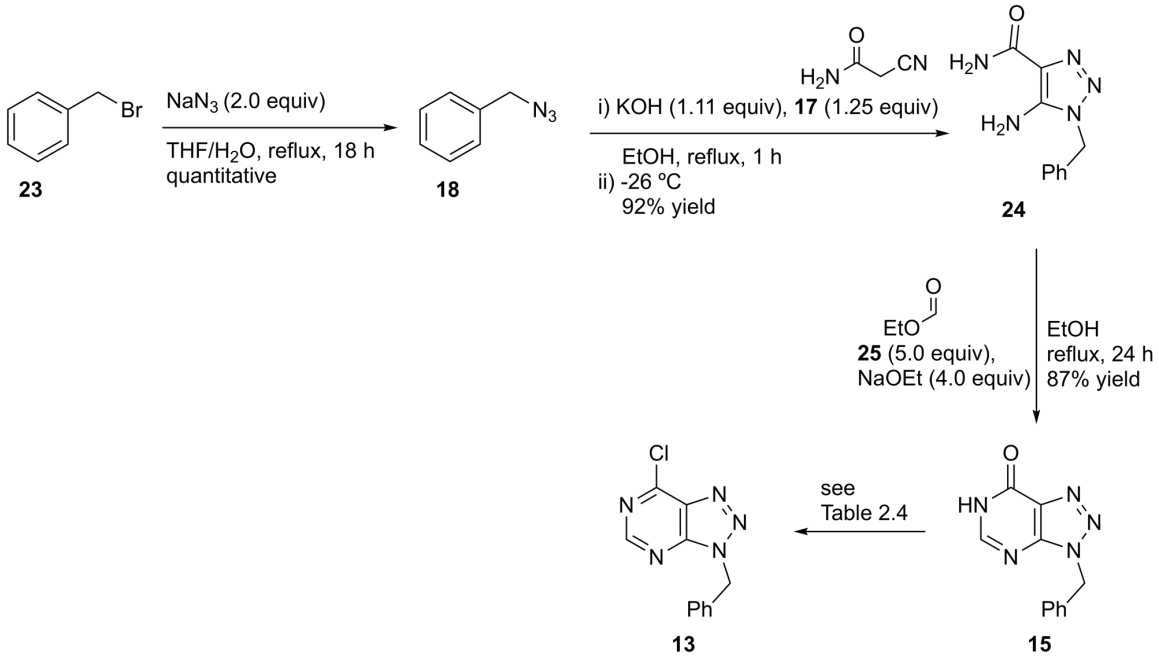

Scheme 2.3 Synthetic route to 7-chloro-triazolopyramidine **13** from pyrimidinone **15.**[12]

2.6.2 Optimizing the Chlorination of Pyrimidinone

In my hands, the chlorination conditions of pyrimidone **15** described in the patent gave inconsistent, low yields. This led me to exploring a variety of conditions to increase yield of chloropyrimidine **13** (Table 2.4). In nearly all cases, **15** was only sparingly soluble (entries marked

with * indicate full solubility of **15**). The apparent lack of reactivity of **15** may have been due to its lack of solubility in the solvents used and the various intermediates generated.[52]

Table 2.4 Attempted chlorination of hydroxypyrimidine (**15**).

.

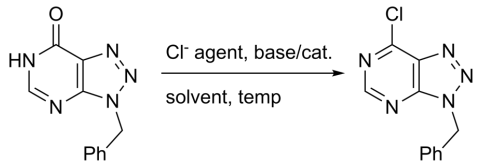

15 **13**

Entry	Cl^- agent (equiv.)	Base/Cat (equiv.)	Solvent	Temp (°C)	Yield (%)	Comments
1	TMSCl (8.5)	n/a	n/a	rt-80	0	TLC showed only **15**
2[53]	TMSCl (5.0)	DMSO (13)	n/a	rt	0	NMR showed **15**
3[53]	TMSCl (8.5)	DMSO (0.26)	THF	rt-	0	TLC showed only **15**
4	TMSCl (5.0)	NaHMDS (1.0)	THF	0-rt	0	TLC showed only **15**
5	TMSCl (5.0)	DIPEA	THF	rt-65	0	TLC showed only **15**
6[53]	TMSCl (5.0)	DMSO (0.3)/NaI (0.1)	THF	rt	0	TLC showed only **15**
7	TMSCl (5.0)	NaI (0.1)	THF	rt-65	0	TLC showed only **15**
8	TMSCl (5.0)	NaI (0.1)	DCM	rt	0	TLC showed only **15**
9	TMSCl (5.0)	NaI (0.1)	MeCN	rt	0	TLC showed only **15**
10[54]	PCl_5 (1.0)	n/a	n/a	rt-105	0	TLC showed only **15**
11[54]	PCl_5 (1.0)	n/a	DCM	0-rt	0	TLC showed only **15**
12[54]	PCl_5 (1.0)	DIPEA	DCM	0-rt	0	TLC showed new faint spot
13[54]	PCl_5 (1.2)	Pyridine (1.2)	DCM	0-rt	0	TLC showed new faint spot
14[54]	PCl_5 (1.2)	Pyridine (1.2)	toluene	0-rt	0	TLC showed only **15**
15*[52,55]	$POCl_3$ (1.2)	DIPEA (1.3)	anisole	95	unk	No **15**; could not isolate **13**
16[52]	$POCl_3$ (9.3)	n/a	n/a	100	61%	2:1 **13/15**
17*[27]	$SOCl_2$ (16)	DMF (1.6)	n/a	reflux	68%	4:1 **13/15**
18[52,55]	$POCl_3$ (1.2)	DIPEA (1.3)	toluene	95	85%	Unable to replicate
19*[52,55]	$POCl_3$ (10)	*N,N*-dimethylaniline	n/a	reflux	55%	Incomplete conversion
20[52]	$POCl_3$ (25)	n/a	n/a	reflux	78%	Incomplete conversion; inconsistent yields.

Chlorination via TMSCl/DMSO was explored to convert oxygen into better leaving group (Scheme 2.4).[53] In the presence of TMSCl, the electrophilicity of DMSO was increased, and the steric bulk may prevent the amide nitrogen from attacking before the oxygen. No conversion of **15** was achieved, so sodium iodide, various bases, and solvents were tested. The sodium iodide was used to form a transient iodopyrimidine *in situ*, so the chloride could displace iodide instead of an oxygen. Bases were used to activate the pyrimidinone towards TMSCl, and solvents were screened for solubility and a larger range of temperatures. None of these modifications showed any evidence of successful conversion, so other chlorinating conditions were explored.

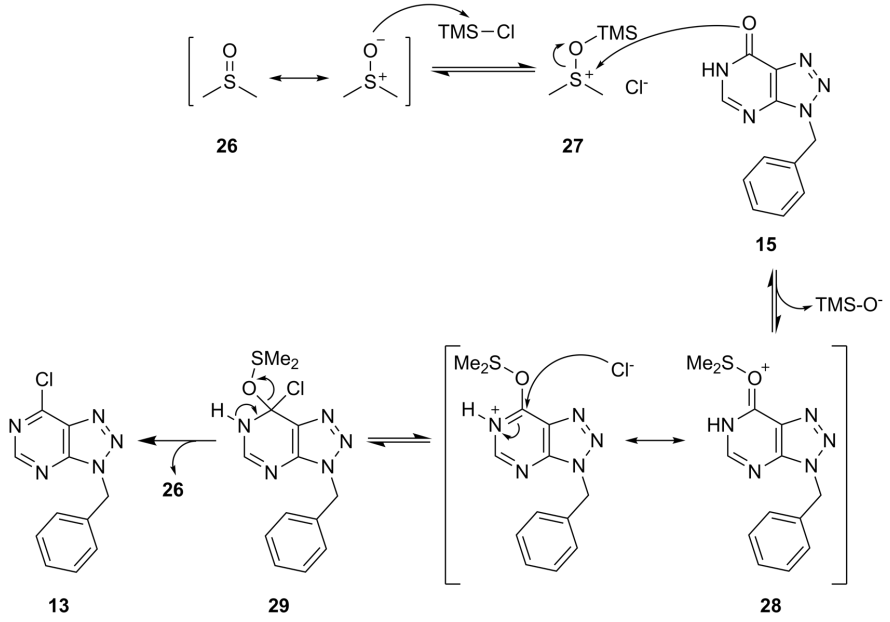

Scheme 2.4 Proposed mechanism for the chlorination of pyrimidinone **15** by activated DMSO.

Conditions using PCl_5, both neat and in the presence of bases, were also attempted, but were unsuccessful.[54] Several reasons may explain why this chlorinating agent did not successfully convert pyrimidinone **15**. First, the low ratio of PCl_5 to **15** may have resulted in the formation of dimers, trimers (**32**), etc., resulting in too much steric bulk for the chloride to attack (Scheme 2.5).[52] It is also possible that the intermediates (**31** and **32**) formed were not soluble in the chosen solvents and temperatures used. I chose to move on to other chlorinating agents instead of screening more bases and equivalents.

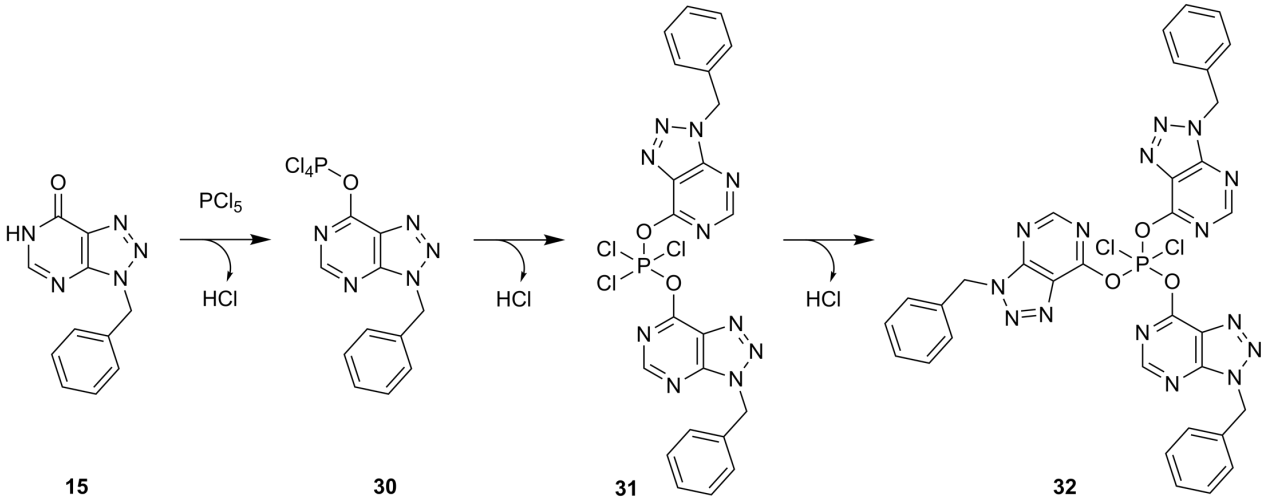

Scheme 2.5 The possible trimer formation of pyrimidinone **15** and PCl_5.[54]

While initial chlorination attempts using $POCl_3$ gave poor yields, I decided to focus on optimizing those conditions. First, refluxing in neat $POCl_3$ gave partial conversion to the desired chloropyrimidine (**13**, 61%). ^{1}H NMR of the reaction mixture did not show any pyrimidinone **15**, indicating full conversion to phosphorous intermediates (e.g., **34**). Next, different bases were screened to convert the intermediate species to chloropyrimidine **13**. The best results came from entry 20, refluxing with excess $POCl_3$ and *N,N*-dimethylaniline (**33**). Use of a large excess of $POCl_3$ prevented the formation of di- and tri- substituted phosphorus intermediates.[52] In the absence of aniline **33**, the intermediate **34** had low solubility. When the aniline is added the solubility of both pyrimidinone **15** and the phosphorous intermediate **34** is greatly increased, allowing a chloride to attack in an addition-elimination mechanism, ejecting PO_2Cl (Scheme 2.6). These conditions were ultimately discarded, because chloropyrimidine **13** reacted with the aniline. The resulting fluorescent byproduct **35** was removed by flash chromatography, but the yield of **13** was still inconsistent. This led to the exploration of a different synthetic route.

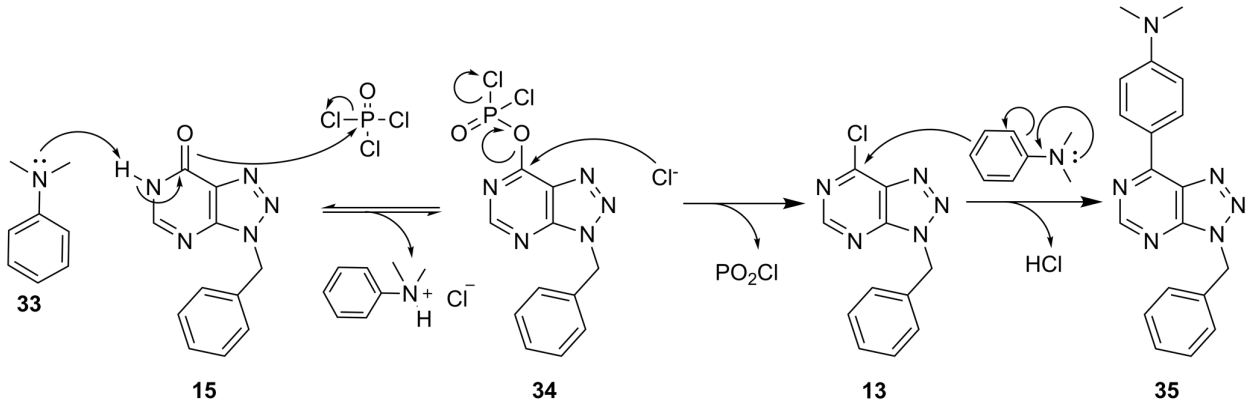

Scheme 2.6 Proposed mechanism for the chlorination of pyrimdinione **15** and subsequent reaction of chloride **13** and *N,N*-dimethylaniline (**33**).

Chloropyrimidine **13** is a commonly used intermediate to functionalize the triazolopyrimidine moiety, so the results in Table 2.2 led me to explore some alternatives (Scheme 2.7). First, the conversion of the carbonyl oxygen of pyrimidinone **15** to triflate **36**. This transformation would make the oxygen-carbon bond weaker, thus making the oxygen a better leaving group. Next, the conversion of pyrimidinone **15** to bromopyrimidine **37**. As bromide is a better nucleophile than chloride, this may favor elimination of the oxygen in the tetrahedral intermediate better than the chlorinated intermediate.

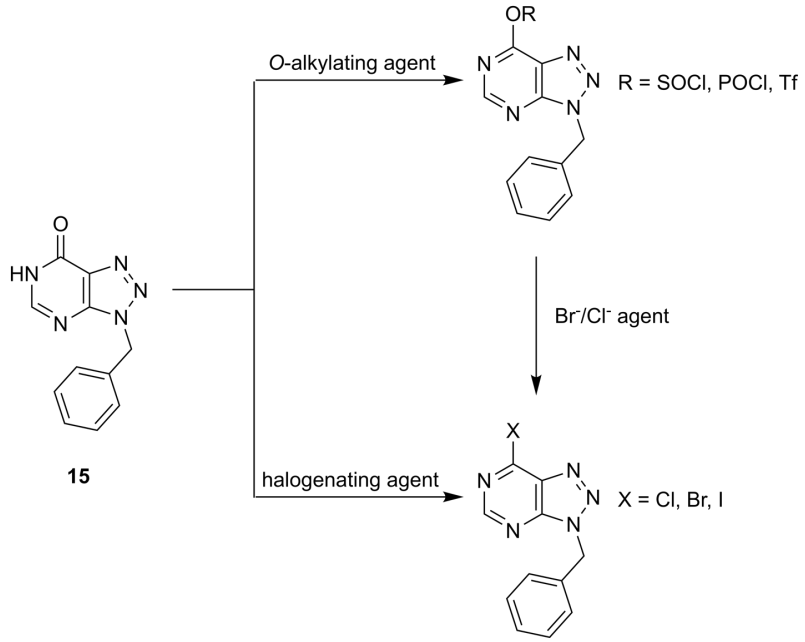

Scheme 2.7 General scheme for the conversion of pyrimidinone **15**.

2.6.3 Attempted Conversion of Pyrimidinone 15 to Pyrimidin-7-yl Triflate

The attempts to convert the carbonyl oxygen of **15** to a triflate leaving group were unsuccessful (Table 2.5). All trials used a base for the initial deprotonation of **15** and triflic anhydride as the electrophile.

Table 2.5 Attempted triflate addition to pyrimidinone **15.**

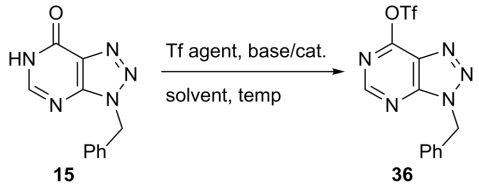

15 **36**

Entry	Tf agent (eq)	Base/Cat (eq)	Solvent	Temp (°C)	Yield (%)	Comments
1[56]	Tf_2O (1.1)	Et_3N (1.0)	DCM	-78-rt	0	NMR showed **15**
2[56]	Tf_2O (1.1)	Et_3N/DMAP (1.0/0.1)	DCM	0-rt	0	NMR showed **15**
3	Tf_2O (2.0)	Et_3N (1.1)	DMF	0-rt	0	NMR showed **15**

Recovery of the starting material suggested a lack of reactivity and/or solubility of pyrimidinone **15** or the intermediates. By changing the solvent to DMF, the goal was to increase solubility, but it too was unsuccessful. Given these unsatisfactory results, this avenue was discarded.

2.6.4 Attempted Conversion of Pyrimidinone to Bromopyrimidine

Conversion to the bromopyrimidine **37** was explored next (Table 2.6). Since conversion of the oxygen to a better leaving group was unsuccessful, I instead looked for a better nucleophile to displace it. Bromide is a more nucleophilic halide than chloride, so it was thought that it should be more adept at substitution.

Table 2.6 Attempted bromination of pyrimidinone **15**.

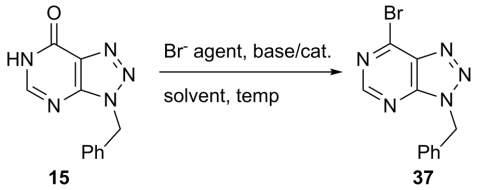

15 **37**

Entry	Br^- agent (eq)	Base/Cat (eq)	Solvent	Temp (°C)	Yield (%)	Comments
1[57]	TMSBr (17)	n/a	$CHCl_3$	rt	0	TLC showed **15**
2	TBAB (4.0)	Swern reagent (1.1)	DCM	-78-rt	0	TLC showed **15**

This route was also fruitless, likely due to the aforementioned stability of pyrimidinone **15** and/or solubility of the possible intermediates generated. Since no conversion was observed, optimization of chlorinating conditions seemed to be the most reasonable route, as I have achieved partial conversion to chloropyrimidine **13**.

2.7 SYNTHESES OF CHLOROPYRIMIDINES FROM DIHYDROXYPYRIMIDINE

With the conversion of pyrimidinone **15** to a chloro- or bromopyrimidine (**13** or **37** respectively) yielding unsatisfactory results, an alternate synthesis of **13** was required. This synthesis used the same number of steps, but chlorinated the pyrimidine in the first step (Scheme 2.8). 4,6-Dihydroxy-5-nitropyrimidine (**38**) and *N,N*-dimethylaniline were refluxed in $POCl_3$, producing dichloropyrimidine **39** in a high yield.[58] Unlike the chlorination of pyrimidinone **15** using these conditions (Scheme 2.6), dichloropyrimidine **39** was less reactive towards the aniline than chloropyrimidine **13**, resulting in less than 4% of the chloride reacting with the aniline. Next, the nitro group of pyrimidine **39** was reduced to amine **20** by refluxing with excess $SnCl_2$, in EtOH, in good yield.[58] The benzylamine then monosubstituted dichloropyrimidine **20** in the presence of a triethylamine (TEA), while refluxing in *n*-butanol, in good yield.[59] Cyclization of diamine **40** using sodium nitrite in a biphasic mixture of DCM and acetic acid (AcOH) produced the desired chloropyrimidine precursor **13** in good yield.[60]

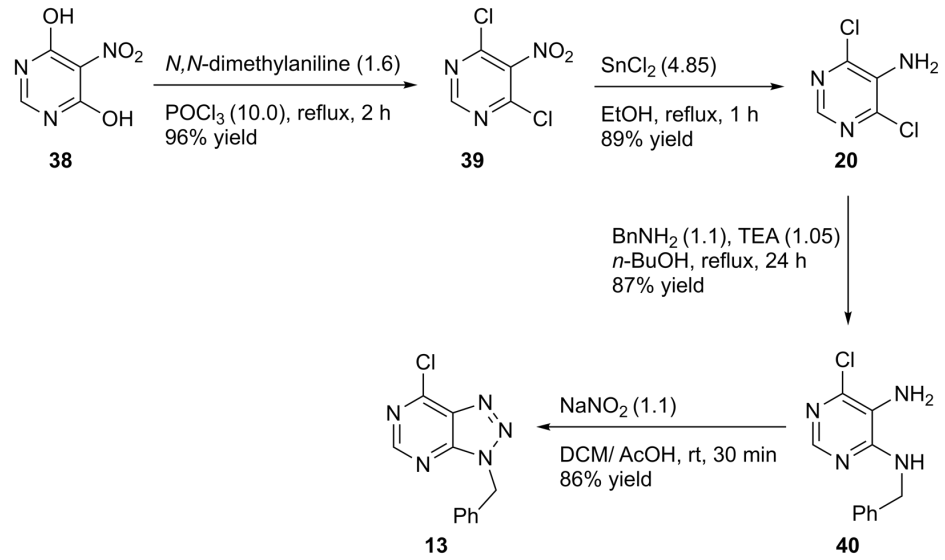

Scheme 2.8 Synthesis of chloropyrimidine **13** from dihydroxypyrimidine **38.**[58–60]

This synthesis was also used to generate azidomethyl derivative **14** (Figure 2.9). The dibromo-*p*-xylene **41** was refluxed with sodium azide in a cosolvent of THF and water to produce bisazide **19** in a quantitative yield.[27] The mono-reduction of an azide on **19** was achieved via a Staudinger reaction to give benzylamine **22** in a 55% yield, with bisreduction of **19** as a major side product.[61] Amine **22** was coupled with chloride **20** in the presence of TEA, while refluxing in *n*-butanol, giving diamine **42** in a 67% yield. Cyclization of diamine **42** to triazole **14** using sodium nitrite in a cosolvent of DCM and AcOH was achieved in a 68% yield.

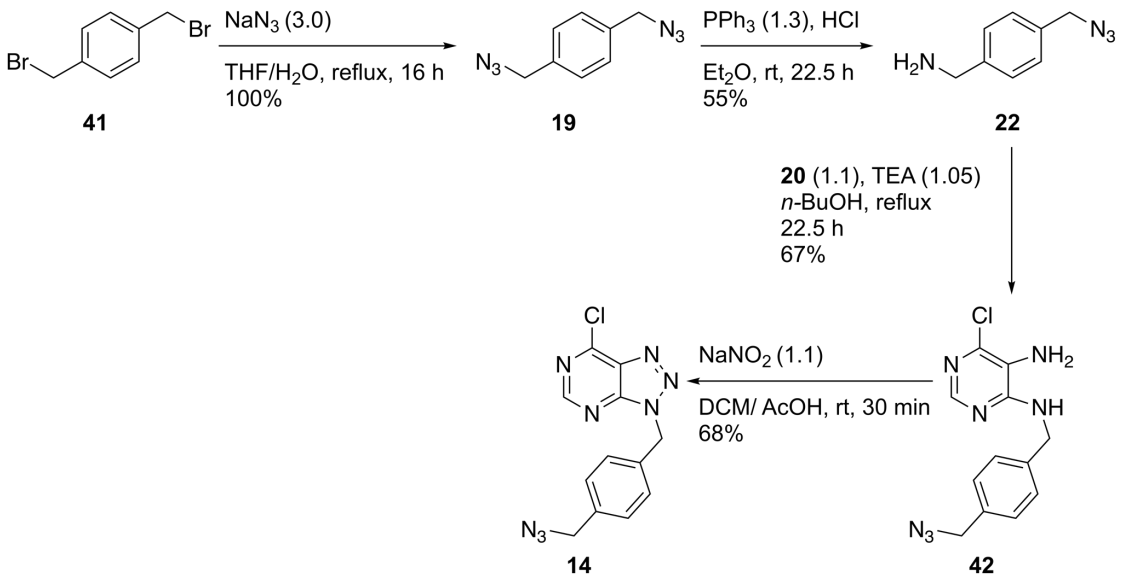

Scheme 2.9 Synthesis of chloropyrimidine **14** from 4-(azidomethyl)benzylamine (**22**).[58–61]

Sodium nitrite has been shown to react with azides in the presence of acid to form hydrazoic acid and nitrous oxide (N_2O, Scheme 2.10) or triazoles (Scheme 2.11). Initial attempts at triazole cyclization of diamine **42** were executed with extreme caution and on a small scale, in case N_2O was produced. The reaction was monitored by TLC and after half an hour, the starting material was completely consumed and only a single spot was visible.

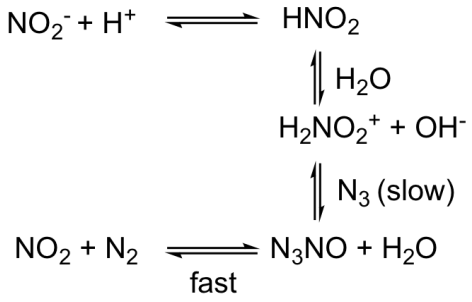

Scheme 2.10 The reaction between hydroxy(oxo)azanium and azide, in the presence of acid, to produce nitrous oxide and nitrogen gas.

Analysis of the ^1H NMR and IR spectra of the crude reaction mixture only showed evidence of chloropyrimidine **14** and acetic acid (which was easily removed by a bicarbonate wash during workup). These results indicated that the cyclization between the diamine **42** and nitrite was faster than the reaction between the azide and nitrite under the conditions used. However, to err on the side of caution, this reaction was only carried out on a small scale (~100 mg).

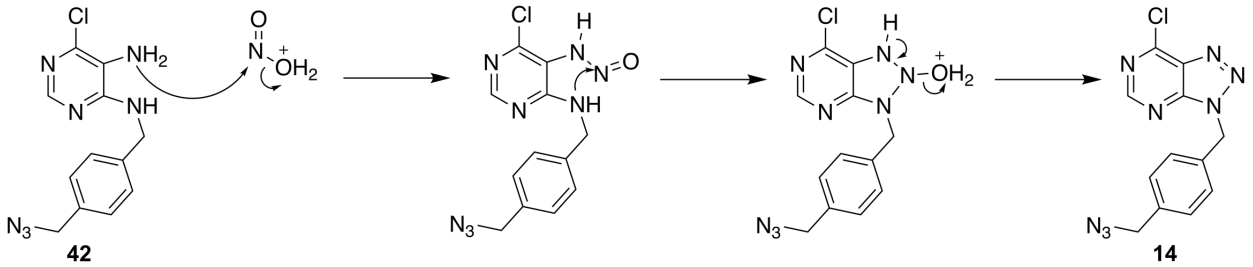

Scheme 2.11 Proposed mechanism for the cyclization of triazole **14** from diamine **42** and nitrite, in an acidic medium.

2.8 ADDITION OF BENZOXAZOLE DERIVATIVES

With the desired chloropyrimidines **13** and **14** in hand, only the addition of the 2-substituted benzoxazole moieties remained in the synthesis of VAS2870 and its derivatives, **2** and **3**. The initial synthetic method for **1**, **2**, and **3** was to substitute the desired benzoxazole for the chloride on the pyrimidine backbone. However, this could only be applied to **1** and **2**. For **3**, the 2-methylbenzoxazole anion was too unstable to generate and couple to **13** in a single step. Instead, it was added as an acetate and decarboxylated.

2.8.1 Syntheses of VAS2870 and 7-(1,3-Benzoxazol-2-ylsulfanyl)-[3-(4-(azidomethyl)benzyl)]-3*H*-[1,2,3]triazolo[4,5-*d*]pyrimidine

The final step in the synthesis of **1**, chloropyrimidine **13** was coupled to 2-mercaptobenzoxazole (**43**) under basic conditions (Scheme 2.12).[27] The poor yield (33%) may be attributed to loss during column chromatography. Time constraints prevented optimization of these conditions, but enough of the compound was collected for the characterization and biological assays. The azide derivative **2** was synthesized using the same conditions to couple chloropyrimidine **14** to benzoxazole **43** in a good yield (70%) (Scheme 2.10).

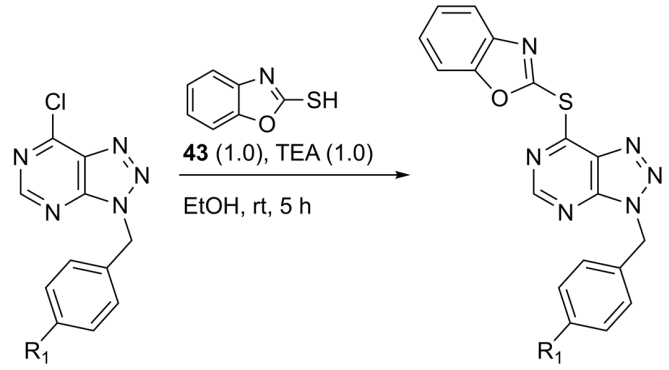

Scheme 2.12 Synthesis of VAS2870 (**1**) and N_3-VAS2870 (**2**).[27]

2.8.2 Attempted Synthesis of 2-((3-benzyl-3*H*-[1,2,3]triazolo[4,5-*d*]pyrimidin-7-yl)methyl)benzo[*d*]oxazole by Direct Coupling of 2-methyl benzoxazole

In the case of the CH_2 derivative **3**, the addition of the benzoxazole moiety proved challenging. Several attempts were made to directly couple 2-methylbenzoxazole (**44**) and chloropyrimidine **13** via nucleophilic addition (S_NAr). A variety of conditions were screened for the deprotonation of benzoxazole **44**, but in all conditions the desired product was not obtained, and the chloride was often quantitatively recovered (Table 2.7). Most conditions began with cold temperatures (-78 to -20°C), to prevent decomposition of the benzoxazole anion of **44**. If no conversion was observed (by TLC), the reaction mixtures were allowed to warm to room temperature, but any higher would quickly result in decomposition of the benzoxazole anion. Polar solvents were typically used in an attempt to stabilize the anion of **44**, but these reactions were still unsuccessful. The equivalents of bases were also varied, with no successful generation of methylene derivative **3**.

Table 2.7 Attempted coupling of 2-methyl benzoxazole (**44**) and chloropyrimidine **13**.

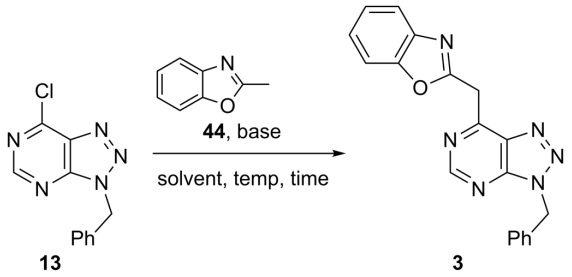

Entry	Base (eq)	44 eq	Solvent	Temp (°C)	Time (h)	Yield (%)	Comments
1	MeLi (1.1)	1.1	THF	-78	0.25	0	TLC showed **13**
2	*n*BuLi (1.0)	1.0	THF	-78	1.0	0	TLC showed **13**
3	NaHMDS (1.1)	1.1	THF	0	0.5	0	TLC showed **13**
4	NaHMDS (1.05)	5.0	DCM	-78	1.0	0	TLC showed **13**
5	NaOH (1.2)	1.2	DMF	rt	1.5	0	TLC showed **15**
6	NaOEt (1.2)	1.2	THF/ EtOH (10:1)	-20	1.5	0	NMR showed **45**
7	NaOEt (1.2)	5.0	THF/ EtOH (10:1)	-20 to rt	4.0	0	NMR showed **45**
8	NaOEt (1.1)	1.2	THF	-20	0.5	0	NMR showed **45**
9	*i*-PrONa (1.2)	1.2	THF/ *i*-PrOH (10:1)	-20 to rt	3.0	0	TLC showed **13**

10	*i*-PrONa (1.2)	5	THF/ *i*-PrOH (10:1)	-20 to rt	2.0	0	TLC showed **13**
11	*i*-PrONa (1.2)	1.2	THF/ *i*-PrOH (10:1)	-20 - rt	5.0	0	TLC showed **13**
12	*i*-PrONa (1.2)	5.0	THF/ *i*-PrOH (10:1)	-20 - rt	5.0	0	TLC showed **13**
13	*i*-PrONa (5.0)	5.0	THF/ *i*-PrOH (10:1)	-20-rt	5.0	0	TLC showed **13**
14[62,63]	*t*-BuOK (1.3)	1.2	THF/ *t*-BuOK(5:1)	-50 to rt	22.0	0	TLC showed **13**
15[62,63]	*t*-BuOK (1.3)	1.2	THF/ *t*-BuOK(5:1)	-50 to rt	22.0	0	TLC showed **13**
16[62,63]	*t*-BuONa (1.2)	1.2	THF/ *t*-BuOH(5:1)	-78	0.5	0	TLC showed **13**
17[62,63]	*t*-BuONa (1.1)	1.2	THF/ *t*-BuOH (10:1)	-20 to rt	18.0	0	TLC showed **13**
18[62,63]	*t*-BuONa (1.1)	1.2	THF/ *t*-BuOH (10:1)	-20 - rt	5.0	0	TLC showed **13**

Several of the bases screened consumed most of the benzoxazole **44** without reacting with chloride **13**, which was quantitatively recovered. The two exceptions were sodium hydroxide (entry 5) and sodium ethoxide (entries 6-8). These reactions produced pyrimidinone **15** and 7-ethoxy pyrimidine **45**, respectively, due to the nucleophilic nature of the ethoxide (Scheme 2.13). The bulkier oxide bases, sodium isopropoxide (entries 9-13), potassium tertbutoxide (entries 14 and 15), and sodium tertbutoxide (entries 16-18) did not react with chloride **1.4**.

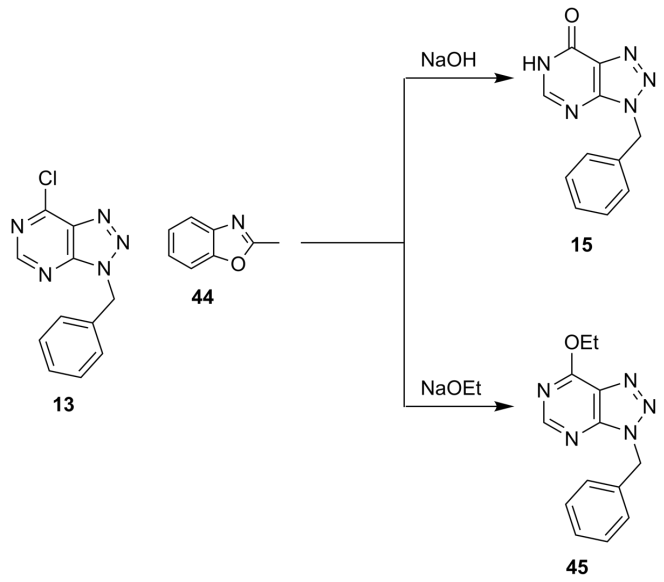

Scheme 2.13 The nucleophilic substitutions of NaOH and NaOEt on chloropyrimidine **13**.

It has been shown that 2-methyl benzoxazole decomposes in the presence of strong bases.[62,63] Since weak bases did not appear to achieve any conversion to methylene derivative **3** and strong bases result in decomposition of benzoxazole **44**, a different route was explored.

2.8.3 Synthesis of 2-((3-benzyl-3*H*-[1,2,3]triazolo[4,5-*d*]pyrimidin-7-yl)methyl)benzo[*d*]oxazole by a Late Assembly of the Benzoxazole Moiety

To circumvent the issue of decomposition of the benzoxazole **44** in the presence of strong bases, the next route was to build the oxazole moiety on to chloride **13**. Various acetates were used to find which would give the best yields (Table 2.8). Each acetate was chosen for its ability to be functionalized into a benzoxazole moiety.

Table 2.8 Addition of acetates to chloropyrimidine **13.**

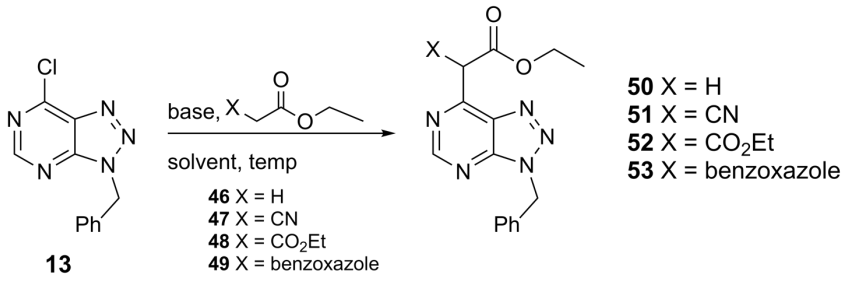

Entry	Acetate (eq)	Base (eq)	Solvent	Temp (°C)	Yield	Comments
1	**46** (2)	NaHMDS (3)	THF	0	Unknown	Crude NMR showed **13** & **50**
2	**46** (2)	NaHMDS (1)	THF	0	0	Crude NMR showed **13** & **46**
3	**46** (2)	LDA (1.1)	THF	-78	0	Crude NMR showed **13** & **46**
4	**46** (2)	*n*-BuLi (1.1)	THF	-78	0	Crude NMR showed **13** & **46**
5[64]	**47** (2)	K_2CO_3 (2)	DMF	120	31	Crude NMR showed **13, 47** & **51**
6[65]	**47** (2)	NaH (2.1)	DMF	rt	0	Crude NMR showed **13** & **47**
7[64]	**48** (2)	Na_2CO_3 (2)	DMF	120	19	Crude NMR showed **13, 48**, & **52**
8	**48** (2)	DBU (2)	DMF	120	17	Crude NMR showed **48** & **52**
9[65]	**48** (2)	NaH (2.1)	DMF	rt	Unknown	Crude NMR showed **13**, **48**, & **52**
10[65]	**49** (2)	NaH (2.1)	DMF	rt	20	Crude NMR showed **49** & **53**

The acetate's substituents provide various degrees of stability to the enolates generated after exposure to a base. The ^{1}H NMR spectrum of the crude NMR for the attempted reaction between ethyl acetate (**46**) (entry 1) and chloropyrimidine **13** only showed a small amount of desired product **50**. There was no attempt to isolate **50**. Cyanoacetate **47** reacted with chloropyrimidine **13** to give cyano intermediate **51** in the best yield (entry 5, 31% yield). To get to CH_2 derivative **3** from **51**, an additional three steps would be required (Scheme 2.14). Decarboxylation of the ethyl ester **51**, followed by hydrolysis and chlorination of the cyano intermediate **54** would yield acetyl chloride **55**. The acetyl chloride moiety could undergo cyclization with 2-aminophenol (**56**) to give CH_2 derivative **3**.

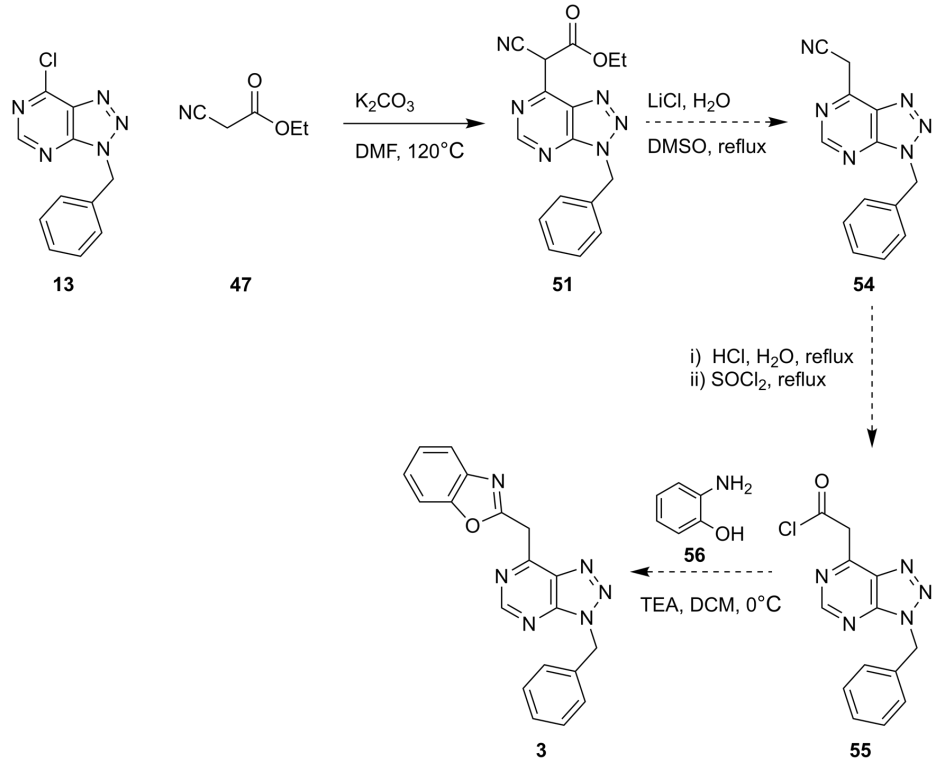

Scheme 2.14 Synthesis of CH_2 derivative **3** via cyanoacetate intermediate **51**.

Ethyl malonate (**48**) successfully reacted with chloropyrimidine **13**, but in lower yields than cyanoacetate (entries 7-9). To obtain CH_2 derivative **3** from diethyl intermediate **52**, three steps would be required. This does not provide a more direct route than cyanoacetate **51** and has a lower yield, so another acetate was explored. The final acetate screened was oxazolylacetate **49**. The oxazolyl intermediate **53** was obtained in a smaller yield than with cyanoacetate (entry 10, 20% yield).

Although the yield was 10% lower, oxazolyl intermediate **53** is only one step away from the CH_2 derivative **3**. No further optimization of **53** was attempted.

The oxazolylacetate derivative **53** was synthesized according to literature procedures from cyanoacetate **47** (Scheme 2.15).[66,67] The cyano group of **47** was converted to iminopropionate **57** by thionyl chloride and aqueous ethanol in a low yield (34%). The iminopropionate **57** and aminophenol **56** were refluxed in ethanol to cyclize to oxazolylacetate **49** in a good yield (75%). The anion of oxazolylacetate **49** was generated using sodium hydride and was then coupled to chloride **13** to give benzoxazole intermediate **53** in a poor yield (20%). Subsequent Krapcho decarboxylation of **53** gave a mixture of unreacted ester **53** and the final product, exclusively as the pyrimidin-7-ylidene tautomer, **3'**, albeit in a low yield (32%).[68] Optimization of these conditions should be explored in future studies, but enough of the was obtained for full characterization and future assays.

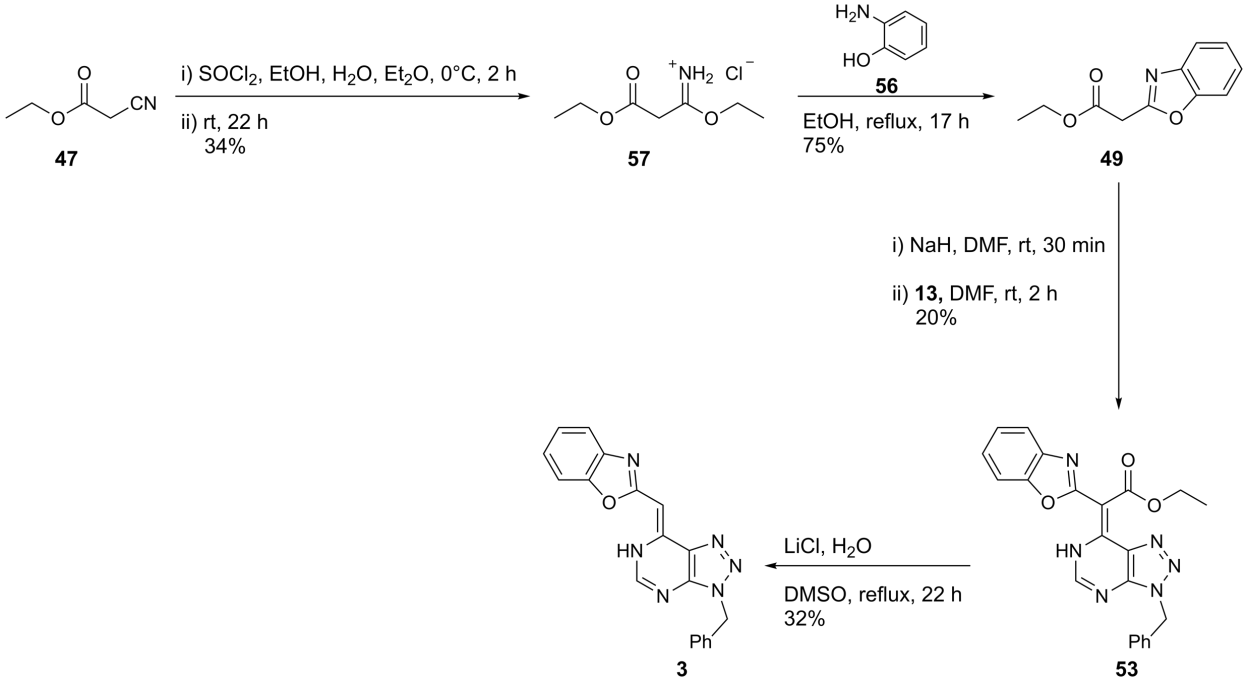

Scheme 2.15 Synthesis of CH derivative **3'** via oxazolylacetate intermediate **53**.[66–68]

A Krapcho decarboxylation was chosen to remove the ester moiety because the mild conditions used should prevent decomposition of the benzoxazole (Scheme 2.16). This was confirmed by analysis of the crude ^{1}H NMR spectrum, which showed only unreacted acetate **53** and desired product **3'**. Although the conditions were mild, I chose to stop the reaction after partial conversion avoid potential thermal decomposition of the benzoxazole moiety.

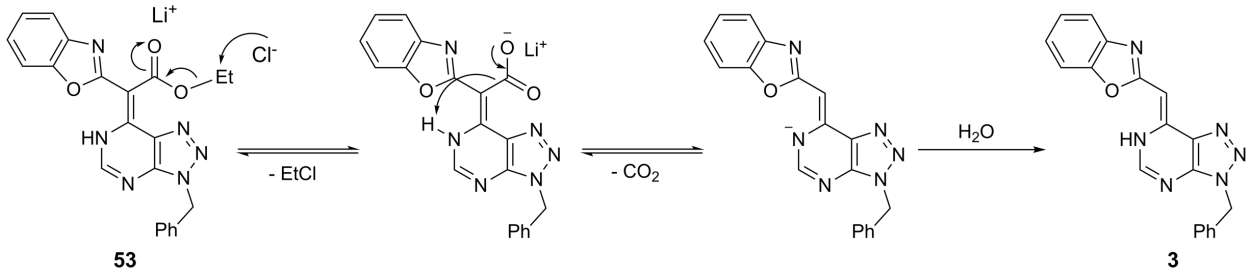

Scheme 2.16 Mechansim of Krapcho decarboxylation to obtain methylene tautomer **3'** from oxazolylacetate **53**.

The exclusive presence of the pyrimidin-7-ylidene tautomer over pyrimid-7-yl tautomer was confirmed by both ^{1}H and ^{13}C NMR spectra (Scheme 2.17). This result was not unexpected, given the naturally observed preference for pyrimidin-7-one over pyrimidin-7-ol.

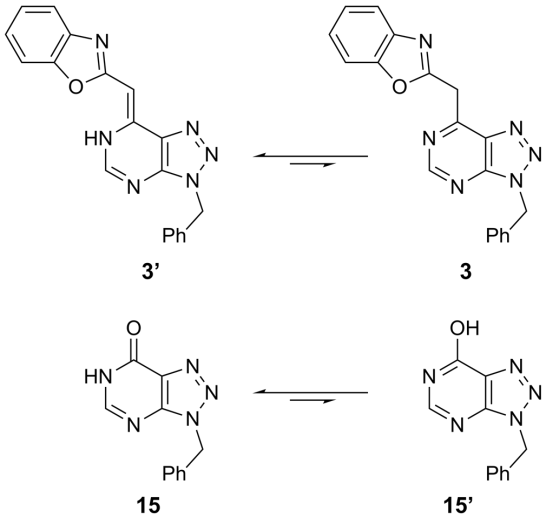

Scheme 2.17 Tautomeric forms of methylene derivative **3** and pyrimidinone **15**.

2.9 ROS INHIBITION: PAST AND PRESENT

With the three triazolopyrimidines (**1**, **2**, and **3'**) in hand, the next step was to determine the best experiment to evaluate their inhibitory effects on ROS production. Several assays have reported using VAS2870 (**1**) as a ROS inhibitor (Table 2.9). These assays found in the literature use several different cell types, each with different ratios of the NOX isozymes. With NOX2 as my main focus, I wanted to find the native cell type with NOX2 as the primary isozyme.[12–14,27,69]

2.9.1 Precedents for ROS Inhibition Using Triazolopyrimidines

There have been a range of concentrations for VAS2870 reported to completely inhibit ROS production in various human cell lines (1-10 μM, Table 2.9). These variations may be a result of the NOX isozymes present, or higher values corresponding to shorter incubation times. The highest concentration, 10 μM, was required for inhibition of vascular smooth muscle cells (VMSCs). These cells contain both NOX1 and NOX4. NOX1 contains the cytosolic component $p47^{phox}$ (like NOX2), which may account some of VAS2870's inhibitory effect. NOX4 is the primary isozyme present, which lacks $p47^{phox}$, but shares the same DH domain as NOX2. When using human leukocyte cells (HL-60, differentiated into neutrophils which contain NOX2), the concentration varied from 2 – 6 μM, and incubation times ranged from 20 – 60 minutes. Human umbilical vein endothelial cells (HUVECs) contain NOX1, 2, 4, and 5, with NOX4 being the primary isozyme present. This may be why a concentration of 5 μM is required for ROS inhibition. Human embryonic kidney (HEK293) cells contain NOX1 and NOX2, and are inhibited by the lowest concentration of VAS2870, 1 μM. The low concentration required may be due to the fact that both isozymes contain the $p47^{phox}$ subunit. For our initial studies, HL-60 cells were chosen because they have been used in previous VAS2870 inhibition experiments and are readily accessible.

Table 2.9 The concentrations of VAS2870 (**1**) required for complete ROS inhibition on various human cell types which express NOX isozymes.

Group	Cell Type	NOX isozyme(s)	Incubation time	Stimulation	[VAS2870] (μM)
Freyhaus et al[27]	VSMC	NOX1 & 4	20 minutes	PDGF	10
Gatto et al[13]	HL-60	NOX1, 2, & 4	20 minutes	PMA	6
Morawietz et al[14]	HUVEC	NOX1, 2, 4, & 5	30 minutes	oxLDL	5
Vasopharm[12]	HL-60	NOX1, 2, & 4	60 minutes	PMA	2
Sandoval et al[69]	HEK293	NOX1 & 2	60 minutes	TNF-α	1
This work	HL-60	NOX2	20 minutes	LPS	10

2.9.2 ROS Inhibition Studies Using N_3-VAS2870 (2) and CH-VAS2870 (3').

With VAS2870 (**1**), N_3-VAS2870 (**2**), and CH-VAS2870 (**3'**) in hand, experiments for ROS inhibition were initiated. First, all three compounds were tested in a respiratory burst assay. A respiratory burst (also known as an oxidative burst) is a process in biological systems involving the rapid release of ROS from cells, often macrophages.[70] This process can be mimicked in assays by incubating cells with compounds that stimulate the release of ROS. Initial studies were performed in the Menard lab by my colleague, Wyatt Slattery.

HL-60 cells were incubated with a control or compounds **1** – **3'** for 20 minutes (Table 2.9, Figure 2.14A). The cells were then stimulated with bacterial lipopolysaccharide (LPS) and the resulting ROS was quantified using chemiluminescence (CHL). Luminol sodium reacted with the ROS byproducts from the respiratory burst, and the emitted light was used to determine the relative ROS production after incubation with compounds **1** – **3'**. Both VAS2870 (**1**) and N_3-VAS2870 (**2**) showed similar degrees of ROS inhibition. CH-VAS2870 (**3'**), however, showed no inhibition compared to the control.

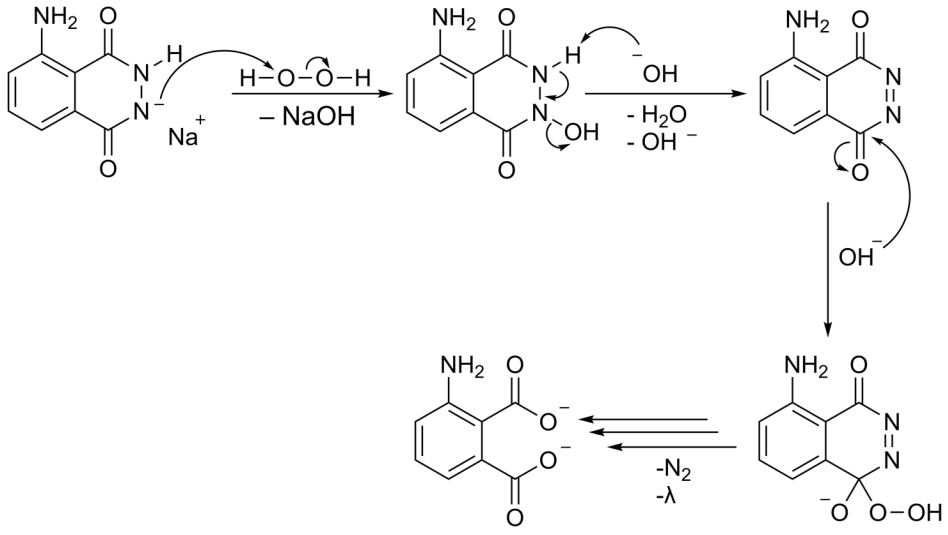

Scheme 2.18 Oxidation of luminol sodium with hydrogen peroxide (a ROS byproduct) results in the release of light (λ).

In a separate experiment, **1** and **3'** were incubated with neurons for 24 h to observe their neuroprotective effects (Figure 2.14B). VAS2870 has been previously shown to inhibit ROS production in neurons, thus preventing neuronal death. Neurons were cultured in nerve growth factor (NGF) for 60 h. They were then kept in NGF or transferred to a culture containing both anti-NGF media and DMSO (control), **1**, or **3'** for 24 h. The neurons incubated with VAS2870 showed more neuronal death than those kept in an NGF media, but less than those in DMSO. Neurons incubated with CH_2-VAS2870 showed no evidence of neuronal protection, with a similar profile as those in DMSO. This experiment was in neurons from dorsal root ganglia (DRG) and conducted by Aaron Johnstone in the Barker lab of UBCO.

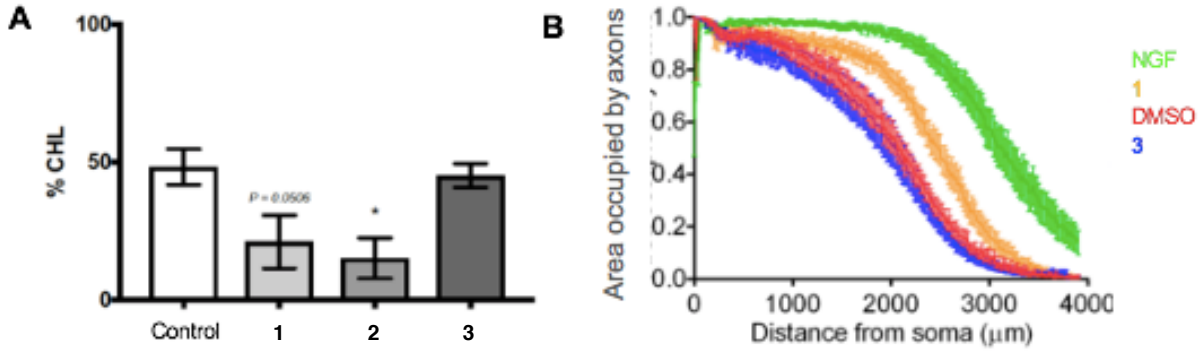

Figure 2.12 The effect of VAS2870 (**1**), N_3-VAS2870 (**2**), and CH-VAS2870 (**3'**) on ROS inhibition in: (A) a respiratory burst assay. Differentiated HL-60 cells were incubated for 20 minutes with a control (DMSO), **1**, **2**, or **3'**. Addition of LPS stimulated ROS production, leading to respiratory bursts. ROS production was measured using chemiluminescence; and (B) neuronal death when exposed to anti-NGF. Neurons were cultured in NGF, then a control (DMSO), **1**, or **3'** was added and incubated for 24 h. Cells were then visualized to determine the neuroprotective effects. Both studies indicate that **1** inhibited ROS production, while **3'** showed no effect (compared to the DMSO). These findings support my hypothesis that **1** inhibits ROS production using thioalkylation.

The results from both independent assays are in agreement. VAS2870 (**1**) inhibited ROS production and CH-VAS2870 (**3'**) did not. This supports my hypothesis that without the ability to undergo thioalkylation by a cysteine residue, methylene tautomer **3'** is unable to prevent ROS production by NOX enzymes. N_3-VAS2870 (**2**) also prevented ROS inhibition, indicating that the *p*-methylazido group does not interfere with binding to its target protein(s). The azide will be used in a future study as an attachment point for a fluorescent dye. This will further test my hypothesis by enabling visualization of the protein-triazolopyrimidine complex.

2.10 SUMMARY AND FUTURE DIRECTIONS

The NOX inhibitor VAS2870 (**1**) along with two derivatives, N_3-VAS2870 (**2**) and CH-VAS2870 (**3'**), have been synthesized. VAS2870 (**1)** was synthesized in 5 steps: addition of benzylamine to chloropyrimidine **20**, followed by formation of the triazole ring to yield chloropyrimidine intermediates **13**, and was completed by the addition of 2-mercaptobenzoxazole (**43**) in an overall yield of 78%. N_3-VAS2870 (**2**) followed the same synthetic route, using benzylamine **22** (2 steps, 77% yield) and chloropyrimidine intermediate **14** with an overall yield of 83%. CH_2-VAS2870 (**3**) used the same synthetic route to chloropyrimidine **13** but required an additional step for the addition of the benzoxazole moiety. Oxazolylacetate **49** (2 steps, 55% yield) was coupled to **13**, and subsequent Krapcho decarboxylation gave methylene tautomer **3'** with an overall yield of 65%.

My hypothesis is that **1** exhibits its inhibitory effects by way of thioalkylating NOX proteins to prevent the active NOX2 complex form forming. To test this hypothesis, I designed two synthetic analogues. **2** has a *p*-methylazido substituent which will be used to click on a fluorescent tag to visualize covalanet binding of **2** to NOX proteins. **3'** was synthesized as an analogue which cannot undergo thioalkylation due replacing the sulphur-carbon bond in **1** and **2** with a carbon-carbon bond. If this compound showed inhibitor effects, it would be through non-covalent ligand-protein interactions. My findings suggest that **1** reacts irreversibly with NOX2 and thus may call several biological assays using it as a reversible inhibitor into question.

VAS2870 (**1**) was used as a standard against **2** and **3'** in reactive oxygen species (ROS) assays. Both **1** and **2** showed inhibitory effects on the production of ROS, while **3'** had no inhibitory effects. This is indicative of a thioalkylation mechanism of inhibition, likely by a cysteine residue of a NOX protein. The *p*-methylazido substituent of **2** will be used in future studies to attach a fluorescent tag for the visualization of the binding site(s) of the triazolopyrimidine backbone to NOX2 to support this hypothesis (Figure 2.15).

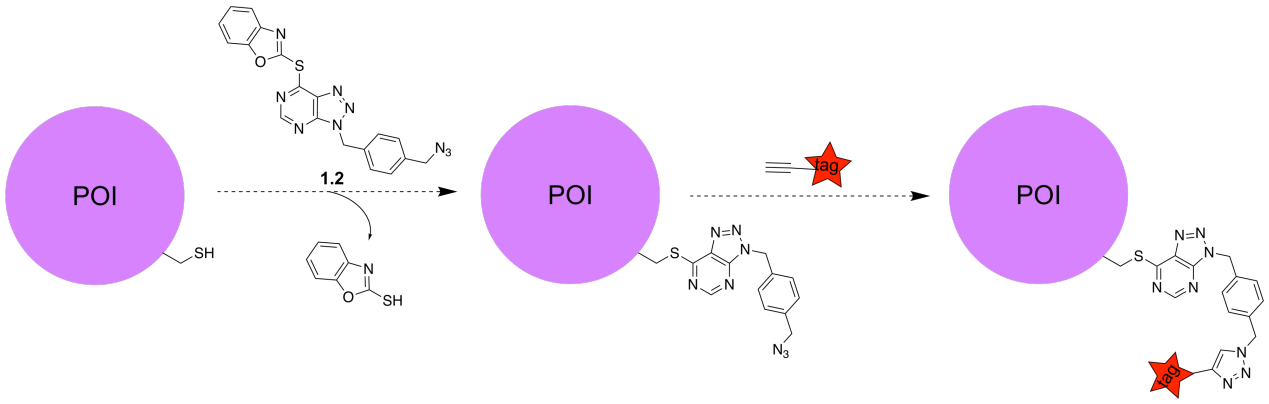

Figure 2.15 Covalent attachment of N_3-VAS2870 (**2**) to a protein of interest (POI) and subsequent cyclization between the *p*-methylazido substituent and alkyne bound to a fluorescent tag.

2.11 Experimental

General Information

Anhydrous EtOH, *n*BuOH, and DMF along with deuterated solvents were purchased from Sigma-Millipore. THF, Et_2O, DMSO, EtOH and DCM were purchased from Fisher and VWR. All other reagents were purchased from one of the three aforementioned companies and were used without further purification.

NMR spectra were obtained on a 400 MHz Varian NMR AS400 unit with an ATB-400 probe at 25 °C. Infrared spectra (IR) were acquired using a PerkinElmer FT-IR Spectrum Two IR Spectrometer with samples prepared as neat film on NaCl plates. High Resolution Mass Spectrometry analyses were obtained with an Agilent G1969A ToF Mass Spectrometer. Column chromatography was performed on silica gel (230-400, Silicycle, Quebec).

Benzyl azide (18)

To a mixture of sodium azide (4.88 g, 76 mmol) in 6 mL H_2O was added a solution of benzyl bromide (4.46 mL, 37.8 mmol) in 75 mL THF. The resulting biphasic mixture was refluxed for 17 hours. The reaction was then cooled to room temperature and diluted with 50 mL of H_2O. The aqueous layer was decanted and extracted with 50 mL Et_2O. The combined organic layers were washed with brine, dried over $MgSO_4$, filtered, and concentrated *in vacuo* to afford benzyl azide (5.0 g, quantitative) as a pale-yellow liquid. The crude was used in the next step without further purification. Characterization data matched reports.[12]

^{1}H NMR (400 MHz, DMSO-d_6) δ = 7.45-7.35 (m, 5H), 4.36 (s, 2H) ppm.

5-Amino-1-benzyl-1*H*-1,2,3-triazole-4-carboxamide (24)

Cyanoacetamide (1.64 g, 19.5 mmol), KOH (1.21 g, 21.7 mmol), and 13 mL EtOH were combined and stirred at rt for 15 minutes. A solution of azide (**18**) (3.24 g, 24.3 mmol) in 8 mL EtOH was added and the resulting mixture was refluxed for 1 hour. The mixture was then cooled to -26 °C and the resulting solid was isolated and dried to afford triazole **24** (3.92g, 92%) as a white solid. The crude was used in the next step without further purification. Characterization data matched reports.[12]

^{1}H NMR (400 MHz, DMSO- d_6) δ = 7.44 (br s, 1H), 7.34-7.30, (m, 2H), 7.28-7.24 (d, 1H), 7.22-7.20 (m, 2H), 7.08 (br s, 1H), 6.24 (s, 2H), 5.44 (s, 2H) ppm.

3-Benzyl-3*H*-[1,2,3]triazolo[4,5-*d*]pyrimidin-7-ol (15)

24 (4.75 g, 21.7 mmol) and ethyl formate (6.98 mL, 86.8 mmol) were added in succession to a 0.045 M solution of NaOEt in 250 mL anhydrous EtOH at rt, under Ar (g). The resulting suspension was brought to reflux for 25 hours. The solvent was removed *in vacuo* and the solids were re-suspended in H_2O. The crude was filtered over a glass frit using vacuum, and the recovered solids were dried over P_2O_5 to yield an off-white powder. The filtrate was evaporated to half volume, resulting in the formation of fluffy (cotton candy- like) off-white crystals. The crystals were isolated using a glass frit and vacuum and were dried over P_2O_5. Both solids were confirmed to be **15** by ^{1}H NMR and were combined to yield 4.5 g (92%). The crude was used in the next step without further purification. Characterization data matched reports.[12]

^{1}H NMR (400 MHz, DMSO- d_6) δ = 7.96 (s, 1H), 7.35-7.25 (m, 5H), 5.58 (s, 2H) ppm.

4,6-Dichloro-5-nitropyrimidine (39)

$POCl_3$ (5.0 mL) was added to **38** (790 mg, 5.0 mmol), followed by *N,N*-dimethylaniline (1 mL, 7.9 mmol). The mixture was heated to reflux for 2 hours. Excess $POCl_3$ was removed by reduced pressure distillation and the resulting liquid was poured into water (100 mL) and extracted with EtOAc (3 x 100 mL). The combined extracts were dried over $MgSO_4$, filtered, and concentrated *in vacuo* to a violet crystalline solid. Purification using a silica plug eluting with DCM gave chloride **39** (0.93 g, 96%) as a yellow crystalline solid. Characterization data matched reports.[58]

^{1}H NMR (400 MHz, $CDCl_3$) δ = 8.92 (s, 1H) ppm.

5-Amino-4,6-dichloropyrimidine (20)

Nitropyrimidine **39** (0.80 g, 3.7 mmol), tin (II) chloride (3.8 g, 18 mmol), and ethanol (8 mL) were combined and brought to reflux for 1 hour. The resulting solution cooled to room temperature and was poured over crushed ice (30 g). $NaHCO_3$ (s) was added until pH = 8, the emulsion was removed by Celite filtration and rinsed with EtOAc (50 mL), then the filtrate was extracted with EtOAc (3 x 150 mL). The combined extracts were dried over $MgSO_4$, filtered, and concentrated *in vacuo* to give amine **20** (0.54 g, 89%) as a pale yellow crystalline solid. Characterization data matched reports.[58]

^{1}H NMR (400 MHz, $CDCl_3$) δ = 8.21 (s, 1H), 4.49 (br s, 2H) ppm.

5-Amino-4-chloro-6-(benzylamino)pyrimidine (40)

Chloride **20** (320 mg, 1.95 mmol), benzylamine (224 μL, 1.63 mmol), TEA (227 μL, 1.63 mmol), and anhydrous *n*BuOH (5 mL) were combined and brought to reflux under Ar (g) for 24 hours. The *n*BuOH was removed by reduced pressure distillation, and the residue was dissolved in DCM (100 mL). The resulting organic solution was washed with water (50 mL), sat. NaCl (aq) (50 mL), dried over $MgSO_4$, filtered, and concentrated *in vacuo* to an orange oily solid (400 mg, 87%) which was used without further purification. Characterization data matched reports.[59]

^{1}H NMR (400 MHz, DMSO-d_6) δ = 7.73 (s, 1H), 7.33 (m, 5H), 5.09 (br s, 2H) 4.63 (d, J= 5.7 Hz, 2H) ppm.

3-Benzyl-7-chloro-3*H*-[1,2,3]triazolo[4,5-*d*]pyrimidine (13)

Diamine **40** (0.40 g, 1.7 mmol), $NaNO_2$ (0.13 g, 1.9 mmol), 50% AcOH (8 mL), and DCM (8 mL) were combined and stirred for 30 minutes. The biphasic mixture was diluted with DCM (50 mL), washed with water (20 mL), sat. $NaHCO_3$ (aq) (3 x 20 mL), water (20 mL), sat. NaCl (aq) (20 mL), dried over $MgSO_4$, and filtered. Removal of solvent *in vacuo* gave chloride **13** (0.36 g, 86%) as a yellow crystalline solid, which was used without further purification. Characterization data matched reports.[60]

^{1}H NMR (400 MHz, $CDCl_3$) δ = 8.96 (s, 1H), 7.49-7.47 (m, 2H), 7.36-7.35 (m, 3H), 5.90 (s, 2H) ppm.

7-(1,3-Benzoxazol-2-ylsulfanyl)-3-benzyl-3H-[1,2,3]triazolo[4,5-d]pyrimidine (1)

Chloride **13** (290 mg, 1.2 mmol), 2-mercaptobenzoxazole (180 mg, 1.2 mmol), TEA (0.16 mL, 1.2 mmol), and anhydrous EtOH (10 mL) were combined and stirred at room temperature for 5 hours. The resulting suspension was diluted with DCM (50 mL), washed with sat. $NaHCO_3$ (10 mL), sat. NaCl (10 mL), dried over $MgSO_4$, filtered, and concentrated *in vacuo* to an orange solid. Purification with flash chromatography using silica gel and eluting with DCM gave **1** as a pale yellow crystalline solid (0.14g, 33%). Characterization data matched reports.[12]

^{1}H NMR (400 MHz, $CDCl_3$) δ = 8.81 (s, 1H), 7.86-7.84 (br d, J = 7.6 Hz, 1H), 7.60-7.58 (br d, J = 7.85 Hz, 1H), 7.48-7.41 (m, 4H), 7.33-7.32 (m, 3H), 5.83 (s, 2H) ppm.

1,4-Bis(azidomethyl)benzene (19)

Dibromide **41** (2.81 g, 10.6 mmol) and NaN_3 (2.07 g, 31.9 mmol) were refluxed in THF/water (36 mL/ 4 mL) for 16 hours. The biphasic mixture was cooled to room temperature and diluted with water (10 mL). The mixture was extracted with Et_2O (2 x 50 mL), dried over $MgSO_4$, filtered, and concentrated *in vacuo* to a pale-yellow oil (2.0 g, 100%). Characterization data matched reports.[61]

^{1}H NMR (400 MHz, $CDCl_3$) δ = 7.31 (s, 4H), 4.32 (s, 4H) ppm.

4-(Azidomethyl)benzylamine (22)

Bisazide **19** (1.67 g, 8.90 mmol), PPh_3 (3.03 g, 11.5 mmol) 1M HCl (32 mL), and Et_2O (42 mL) were combined and vigorously stirred for 22.5 hours. The layers were separated, and the aqueous layer was extracted with Et_2O (3 x 50 mL) to remove starting materials and Ph_3PO. 2.5M KOH was added until pH = 10, then the solution was extracted with DCM (4 x 50 mL). The combined DCM extracts were dried with $MgSO_4$, filtered and concentrated *in vacuo* to give a clear yellow oil (0.79 g, 55%). Characterization data matched reports.[61]

^{1}H NMR (400 MHz, $CDCl_3$) δ = 7.32-7.30 (d, J = 8.21 Hz, 2H), 7.27-7.25 (d, J = 7.63 Hz, 2H), 4.29 (s, 2H), 3.85 (s, 2H), 1.49 (br s, 2H) ppm.

5-Amino-4-chloro-[6-(4-azidomethyl)benzylamino]pyrimidine (42)

Chloride **20** (254 mg, 1.55 mmol), benzylamine **22** (264 mg, 1.63 mmol), TEA (227 μL, 1.63 mmol), and anhydrous *n*BuOH (5 mL) were combined and brought to reflux under Ar (g) for 22.5 hours. The *n*BuOH was removed by reduced pressure distillation, and the residue was dissolved in DCM (100 mL). The resulting organic solution was washed with water (50 mL), sat. NaCl (aq) (50 mL), dried over $MgSO_4$, filtered, and concentrated *in vacuo* to an orange oily solid. Purification by flash chromatography using silica gel eluting with 50% EtOAc/Hexanes gave diamine **42** (330 mg, 67%) as a white crystalline solid. Prepared according to literature procedures for **40**.[59]

FTIR (thin film): 3349, 3245, 2925, 2099, 1576 cm^{-1}.

^{1}H NMR (400 MHz, $CDCl_3$) δ = 8.09 (s, 1H), 7.36-7.28 (dd, J = 7.32 Hz, 4H), 5.21 (bd s, 1H), 4.70-4.69 (d, J = 5.44 Hz, 2H), 4.33 (s, 2H), 3.45 (d, 2H) ppm.

^{13}C NMR (100 MHz, $CDCl_3$) δ = 154.7, 149.5, 143.4, 138.5, 134.8, 128.6, 128.3, 121.9, 54.4, 45.1 ppm.

HRMS (EIS-TOF) m/z: $[M + H]^+$ calcd for $C_{12}H_{12}ClN_7$, 290.0920; found, 290.0915.

7-Chloro-[3-(4-(azidomethyl)benzyl)]-3*H*-[1,2,3]triazolo[4,5-d]pyrimidine (**14**)

Diamine **42** (0.48 g, 1.66 mmol), $NaNO_2$ (126 mg g, 1.82 mmol), 50% AcOH (9 mL), and DCM (9 mL) were combined and stirred for 30 minutes. The biphasic mixture was diluted with DCM (30 mL), washed with water (10 mL), sat. NaCl (aq) (10 mL), dried over $MgSO_4$, and filtered. Removal of solvent *in vacuo* gave chloride **14** (0.34 g, 68%) as a yellow crystalline solid, which was used without further purification. Prepared according to literature procedures for **13**.[60]

FTIR (thin film): 2928, 2101, 1585, 1569 cm^{-1}.

^1H NMR (400 MHz, $CDCl_3$) δ = 8.93 (s, 1H), 7.51-7.48 (d, J = 7.94 Hz, 2H) 7.32-7.30 (d, J = 7.83 Hz, 2H) 5.90 (s, 2H), 4.32 (s, 2H) ppm.

^{13}C NMR (100 MHz, $CDCl_3$) δ = 155.6, 154.3, 149.7, 136.4, 134.2, 133.8, 129.1, 128.8, 54.2, 51.0 ppm.

MS (EIS-TOF) m/z: $[M + H]^+$ calcd for $C_{12}H_{09}ClN_8$, 301; found 283 (indicating the chloropyrimidine had converted to the pyrimidinone).

7-(1,3-Benzoxazol-2-ylsulfanyl)-[3-(4-(azidomethyl)benzyl)]-3H-[1,2,3]triazolo[4,5-d]pyrimidine (**2**)

Chloride **14** (0.27 g, 0.9 mmol), 2-mercptobenzoxazole (133 mg g, 0.9 mmol), TEA (0.13 mL, 0.9 mmol), and anhydrous EtOH (10 mL) were combined and stirred at room temperature for 5 hours under Ar (g). The resulting suspension was concentrated *in vacuo* to a yellow solid, dissolved in chloroform (20 mL), washed with sat. $NaHCO_3$ (10 mL), sat. NaCl (10 mL), dried over $MgSO_4$, filtered, and concentrated *in vacuo* to a brown solid. Purification with flash chromatography using silica gel and eluting with 25% EtOAc/Hexanes gave **2** as a white crystalline solid (0.26 g, 70%). Prepared according to literature procedures for **1**.[12]

FTIR (thin film): 3063, 2926, 2100, 1576, 1563, 1447, 748 cm^{-1}.

^1H NMR (400 MHz, $CDCl_3$) δ = 8.81 (s, 1H), 7.85 (m, 1H), 7.59 (m, 1H), 7.45 (m, 4H), 7.29 (m, 2H), 5.83 (s, 2H), 4.31 (s, 2H) ppm.

^{13}C NMR (100 MHz, $CDCl_3$) δ = 161.4, 155.3, 153.6, 152.9, 148.2, 141.9, 136.2, 134.0, 133.5, 129.0, 128.8, 126.7, 125.2, 124.2, 120.8, 54.2, 50.7 ppm.

HRMS (EIS-TOF) m/z: $[M + H]^+$ calcd for $C_{19}H_{13}N_{09}OS$, 416.1038; found, 416.1037.

Diethyl 2-(3-benzyl-3,6-dihydro-7*H*-[1,2,3]triazolo[4,5-*d*]pyrimidin-7-ylidene)malonate (52)

Diethyl malonate (6.66 mmol) was added dropwise to a suspension of NaH (6.84 mmol) in anhydrous DMF (1 mL) under Ar (g). A solution of chloride **1.4** (3.26 mmol) in DMF (1 ml) was added dropwise and the reaction stirred for 2 h. The mixture was diluted with H_2O (50 mL) and acidified to pH 4 with 12 M HCl. The crude was extracted with DCM (20 mL), dried over $MgSO_4$, filtered, and concentrated *in vacuo* to a yellow oil. Purification with flash chromatography using silica gel and eluting with 50% EtOAc/Hexanes gave **52** (22.9 mg, 19%) as a yellow crystalline solid. Prepared according to literature procedures.[64]

FTIR (thin film): 3158, 3034, 2982, 2904, 2251, 1722, 1633, 1666 cm^{-1}.

^1H NMR (400 MHz, $CDCl_3$) δ = 12.90 (br s, 1H), 7.89 (s, 1H), 7.38-7.27 (m, 5H), 5.63 (s, 2H), 4.46-4.41 (q, 2H), 4.27-4.22 (q, 2H), 1.36-1.26 (m, 6H) ppm.

^{13}C NMR (100 MHz, $CDCl_3$) δ = 168.07, 166.10, 145.87, 144.08, 142.50, 134.57, 134.48, 129.03, 128.73, 128.50, 128,42, 127.54, 91.57, 62.00, 61.00, 50.88, 50.65 ppm.

HRMS (EIS-TOF) m/z: $[M + Na]^+$ calcd for $C_{18}H_{19}N_{05}O_{04}$, 392.1337; found, 392.1329.

Ethyl (*Z*)-2-(3-benzyl-3,6-dihydro-7*H*-[1,2,3]triazolo[4,5-*d*]pyrimidin-7-ylidene)-2-cyanoacetate (51)

Ethyl cyanoacetate (6.66 mmol) was added dropwise to a suspension of NaH (6.84 mmol) in anhydrous DMF (1 mL) under Ar (g). A solution of chloride **1.4** (3.26 mmol) in DMF (1 ml) was added dropwise and the reaction stirred for 2 h. The mixture was diluted with H_2O (50 mL) and acidified to pH 4 with 12 M HCl. The crude was extracted with DCM (20 mL), dried over $MgSO_4$, filtered, and concentrated *in vacuo* to a yellow oil. Purification with flash chromatography using silica gel and eluting with 50% EtOAc/Hexanes gave **51** (32.6 mg, 31%) as a yellow crystalline solid. Prepared according to literature procedures.[65]

FTIR (thin film): 3062, 3027, 2222, 1679, 1558 cm^{-1}.

^1H NMR (400 MHz, DMSO-d_6) δ = 13.25 (br s, 1H), 8.51 (s, 1H), 7.39-7.31 (m, 5H), 5.81 (s, 2H), 4.30-4.25 (q, 2H), 1.31-1.28 (t, 3H) ppm.

^{13}C NMR (100 MHz, DMSO-d_6) δ = 166.96, 148.58,145.61, 135.23, 128.99, 128.44, 128.08, 127.33, 116.76, 66.84, 60.96, 49.96, 14.44 ppm.

HRMS (EIS-TOF) m/z: $[M + Na]^+$ calcd for $C_{16}H_{14}N_{06}O_{02}$, 345.1071; found, 345.1070.

Ethyl 3-ethoxy-3-iminopropanoate hydrochloride (57)

Ethyl cyanoacetate (4.8 mL, 52 mmol), EtOH (5.25 mL, 90 mmol), H_2O (0.75 mL, 42 mmol), and Et_2O (2 mL) were combined and cooled to 0 °C. $SOCl_2$ (3.3 mL, 45 mmol) was added dropwise over several minutes, and the resulting mixture stirred at 0 °C for 2 hours, then 22 hours at room temperature. Et_2O (12 mL) was added and the resulting solids were filtered off, washed with Et_2O (2x 10 mL), and dried to afford 4.0 g of white crystalline solid (4.0 g, 34% yield). Characterization data matched reports.[43]

^{1}H NMR (400 MHz, $CDCl_3$) δ = 12.59 (br s, 1H), 11.88 (br s, 1H), 4.69 (m, 2H), 4.21 (m, 2H), 3.87 (s, 2H), 1.47 (m, 3H), 1.26 (m, 3H) ppm.

Ethyl 2-(benzo[*d*]oxazol-2-yl)acetate (49)

57 (8.0 g, 41 mmol), p-aminophenol (3.44 g, 31.5 mmol), and EtOH (140 mL) were combined and refluxed for 17 hours. The solution was then cooled to room temperature and partitioned between water (140 mL) and EtOAc (140 mL). The organic layer was washed with brine, dried over $MgSO_4$, filtered, and reduced to a pale brown crystalline solid. Purification with flash chromatography using silica gel and eluting with 10% EtOAc/Hexanes gave **2.36** as a light pink crystalline solid (4.83 g, 75%). Characterization data matched reports. [44]

^{1}H NMR (400 MHz, $CDCl_3$) δ = 7.72-7.70 (m, 1H), 7.53-7.51 (m, 1H), 7.36-7.32 (m, 2H), 4.24 (q, 2H), 4.01 (s, 2H), 1.28 (t, 3H) ppm.

Ethyl (*E*)-2-(benzo[*d*]oxazol-2-yl)-2-(3-benzyl-3,6-dihydro-7*H*-[1,2,3]triazolo[4,5-*d*]pyrimidin-7-ylidene)acetate (53)

Acetate **49** (12 mmol) was added, in portions, to a suspension of NaH (13 mmol) in anhydrous DMF (1 mL), under Ar (g). The reaction stirred for 40 min and was quenched by pouring into H_2O (30 mL). The resulting mixture was acidified to pH 4 with 12 M HCl and portioned with chloroform (100 mL). The organic layer was extracted, dried over $MgSO_4$, filtered, and concentrated *in vacuo.* Purification with flash chromatography using silica gel and eluting with 50% EtOAc/hexanes gave **53** (50 mg, 20%) as a yellow-green crystalline solid. Prepared according to literature procedures.[65]

^{1}H NMR (400 MHz, $CDCl_3$) δ = 13.86 (br s, 0.5H), 13,37 (br s, 1H), 8.07 (s, 0.5H), 7.98 (s, 1H), 7.80 (s, 1H), 7.58 (m, 2H), 7.43 (m, 1H), 7.36 (m, 9H), 5.67 (s, 1H), 5.56 (s, 2H), 4.60 (q, 1H), 4.25 (q, 2H) , 1.43 (t, 1.5H), 1.22 (t, 3H) ppm.

^{13}C NMR (100 MHz, $CDCl_3$) δ = 168.99, 165.36, 161.99, 159.22, 151.29, 148.74, 146.18, 144.19, 143.84, 142.05, 140.36, 138.67, 134.45, 134.16, 128.87, 128.62, 128.38, 124.93, 124.58, 124.19, 123.87, 120.36, 117.73, 110.77, 84.09, 62.21, 61.06, 50.52, 14.20, 14.04 ppm.

(*Z*)-2-((3-Benzyl-3,6-dihydro-7*H*-[1,2,3]triazolo[4,5-*d*]pyrimidin-7-ylidene)methyl)benzo[*d*]oxazole (3')

Oxaloacetate **53** (1.2 mmol), LiCl (2.4 mmol), and wet DMSO (.5 ml) were combined and refluxed for 4 h. Contents of the flask were poured into 5 mL of ice water and saturated with NaCl. The resulting suspension was extracted with DCM (3x 5 mL). organic extracts were combined, dried over $MgSO_4$, filtered, and concentrated *in vacuo*. Purification with flash chromatography using silica gel and eluting with 10% EtOAc/Hexanes gave methylene tautomer **3'** as a yellow crystalline solid (12 mg, 29%). Prepared according to literature procedures.[68]

FTIR (thin film): 3060, 1778, 1666 cm^{-1}.

^{1}H NMR (400 MHz, $CDCl_3$) δ = 12.88 (br s, 1H), 7.93 (s, 1H), 7.59-7.57 (d, 1H), 7.49-7.46 (d, 1H), 7.44-7.29 (m, 7H), 6.19 (s, 1H), 5.66 (s, 2H) ppm.

^{13}C NMR (100 MHz, $CDCl_3$) δ = 164.66, 149.04, 146.65, 141.57, 138.54, 134.79, 129.54, 129.08, 128.69, 128.38 124.49, 124.14, 123.87, 122.95, 117.73, 110.32, 51.01 ppm.

HRMS (EIS-TOF) m/z: $[M + H]^+$ calcd for $C_{18}H_{14}N_{05}O_{01}$, 343.1298; found, 343.1302.

Chapter 3: DEVELOPMENT OF A SILICON-BASED TRACELESS-AFFINITY LINKER

The ability to label proteins is a powerful method to help understand their function and localization in living systems.[71,72] Current labels include dyes, affinity tags, and radioactive tracers which can be added to a protein of interest (POI) using a variety of methods.[71,73,74] Three such methods are click chemistry, affinity labelling, and traceless-affinity labelling (Figure 3.1). Click chemistry commonly requires the use of genetic modification to incorperate an azide group to an amino acid in the POI. Affinity labelling uses a probe, composed of a ligand attached to a chemical tag, to selectively label the active site of the POI. Traceless-affinity labelling uses a molecule composed of a ligand, a cleavable linker, and a chemical tag. When the probe binds to the POI the cleavable linker reacts with a surface residue outside of the active site, simultaneously cleaving the ligand from the tag. When the probe dissociates, the active site is freed, and the tag remains bound to the protein. This novel method requires no genetic modification and maintains the POI's native structure and function, making it a very valuable tool for studying proteins in living systems.

3.1 OVERVIEW OF TRACELESS-AFFINITY LABELLING

When studying proteins in living systems, many factors may influence their structure and function, such as expression levels, localization, and interactions with other biomolecules (i.e., ligands and other proteins). Each of these components can be studied by chemically labelling the protein of interest (POI) on an amino acid residue on the surface or in an active site. Many methods exist for selectively labelling proteins, including genetic modification and chemical probes (Chapter 1, Section 1.2).

Click chemistry is a type of genetic modification in which an amino acid containing an azide group is added to an amino acid residue of the POI (Figure 3.1A).[18] While this method is useful for the tagging of a protein *in vitro*, it may become complicated when tagging different proteins simultaneously. Also, the introduction of genetically modified proteins into living organisms is difficult. In contrast, a probe can be delivered to a specific active site (**affinity labeling**) of the POI

(Figure 3.1B). While this method is selective (provided the right ligand-protein pairs are chosen), and enables labelling multiple POIs without genetic modification, it still has limitations. If the ligand readily dissociates, visualizing the protein will be difficult. On the other hand, if the binding interaction is strong, the protein remains labelled but the active site is hindered which may disrupt its native function .[3,73,75]

To overcome the pitfalls of the aforementioned labelling methods, **traceless-affinity labels** were designed (Figure 3.1C).[3] This strategy utilizes a ligand to deliver a chemical label to a protein of interest (POI) via a cleavable linker. Once the ligand is bound to an active site on the POI, the linker is brought in proximity with the protein's surface. The probe is designed to react with nucleophilic residues on the surface, while simultaneously severing its bond to the ligand. The linker remains bound to the chemical tag therefore the tag is now covalently bound to the surface of the POI. The ligand is now free from the tag and when it dissociates the POI's native structure and function should be conserved. Pioneering work by Hayashi and Hamachi in 2012 described a disulfide linker to react with cysteine residues.[3,76] In this work, I propose to develop a cleavable linker that will react with a nucleophilic residue such as lysine. Lysine was chosen because it can act as a nucleophile in physiological conditions, and it is abundant on the surface of proteins.[77]

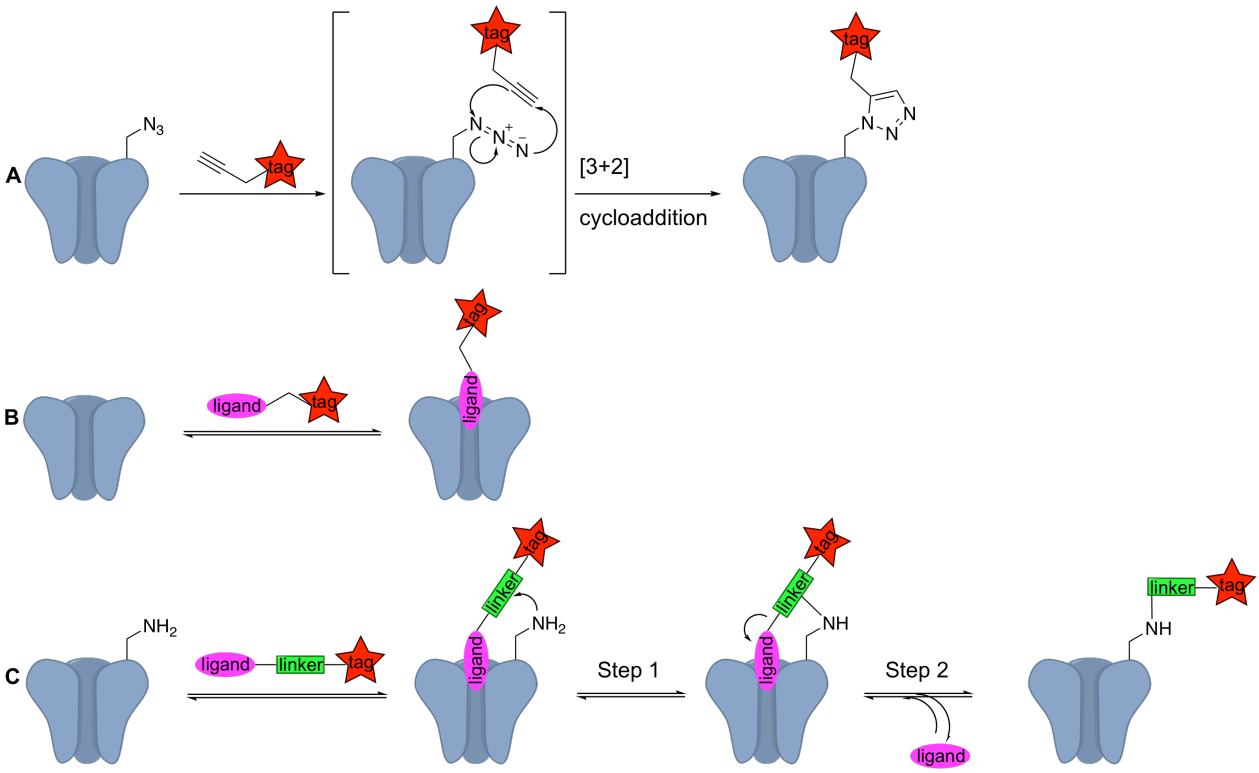

Figure 3.1 General examples of click chemistry (A), affinity labelling (B), and traceless-affinity labeling (C) of a protein.[3]

There are two important factors to consider when designing the cleavable linker required for the above strategy: compatibility and reactivity. The linker must be compatible with a wide variety of ligands and chemical tags. Once coupled to a ligand and tag, the linker must remain bioorthogonal towards chemical processes within the cell until it is brought into proximity of the POI's active site.

3.1.1 Existing Methods for Covalent Tagging of Surface Lysine Residues

Lysine is a common target for covalently tagging proteins because of the nucleophilic nature of the amine residue.[78] Although lysine is mostly protonated at physiological pH (Scheme 3.1), it is able to chemoselectively react with electrophiles in the presence of other nucleophilic residues (such as cysteine and serine).[79]

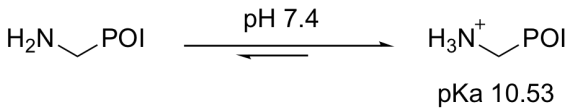

Scheme 3.1 Protonation of lysine residue at physiological pH (7.4).

Examples of current tagging methods for the surface residues in cellular conditions are summarized in Table 3.1. In 1986, Bernad *et al.* first showed that maleic anhydride (**58**) could acylate lysines under basic conditions (pH 8.2) producing amide **59**.[80] Side reactions with the α-NH_2 of amino acids, serine, and threonine were also observed, prompting investigations into more selective methods. Now, more than thirty years of research efforts have led to the discovery of a range of electrophiles which selectively label lysines *in vitro* under physiological conditions with short reaction times.[81–83]

Table 3.1 Examples of current tagging methods for the surface lysine residues.

Reaction Type	Electrophile	Conditions	Product	Side Reactions
Trans-acylation	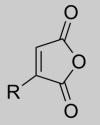 **58** Bernad, *et al.*, 1986[80]	HEPES buffer, pH 8.2, overnight	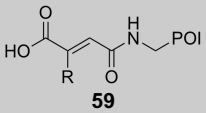 **59**	Alpha-NH_2, serine, threonine
Electroacylation	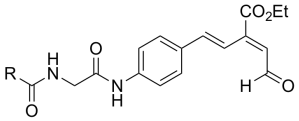 **60** Tanaka *et al.*, 2008[81]	PBS, pH 7.0, 30 min.	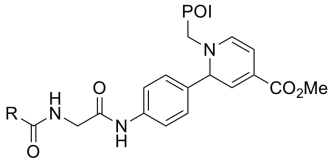 **61**	None reported
Azidation/ Trans-acylation	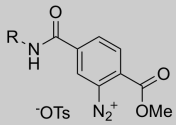 **62** Dietheim *et al.*, 2014[82]	PBS, pH 7.0, 2h	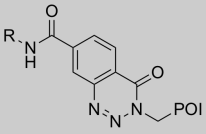 **63**	None reported
Phthalimidine formation	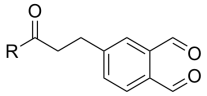 **64** Tung *et al.*, 2016[83]	PBS, pH 7.4, 30 min.	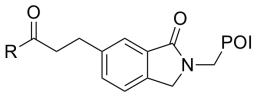 **65**	None reported

A proposed linker that may meet the above criteria is an α-silyl-β-lactone (**4**, Figure 3.2). Based on reactions of existing β-lactones with serine proteases, **4** may undergo transacylation reactions with nucleophilic residues to covalently attach to the POI. The intermediate can then, via an intramolecular rearrangement, cleave to form a tag-POI complex and silanol-ligand by-product. When the ligand dissociates from the POI, the protein can then be studied in its native state.

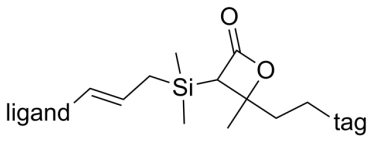

4

Figure 3.2 Proposed cleavable linker containing an α-silyl-β-lactone (**4**).

3.1.2 Reactions of β-Lactones with Primary and Secondary Amines

β-Lactones (**66**) are known to react with primary and secondary amines to give amides **67** and/or amino acids **68** (Scheme 3.2).[84] The ratio of the two ring-opened products depends on the conditions used and can be modified to favor a particular product. The three main factors contributing to the ratio of products are: the amine used, solvent, and the order of reagent addition.

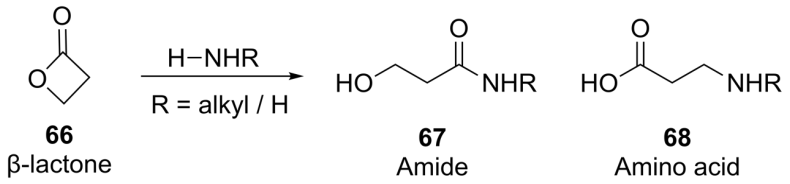

66 β-lactone **67** Amide **68** Amino acid

Scheme 3.2 Reactions of β-lactone **66** with amines yields a mixture of amide **67** (via trans-acylation) and amino acid **68** (via S_N2).

In water, reactions of β-lactones with primary amines (e.g., lysine) favor the formation of amides, regardless of the order of reagent addition. This suggests that when the proposed α-silyl- β-lactone reacts with lysine, it should form an amide intermediate, prior to cleavage.

3.1.3 β-Lactones React with Nucleophilic Residues of Enzymatic Active Sites

A variety of electrophiles have been shown to chemoselectively react with lysines under physiological conditions (i.e., dienal **60**, diazonium **62**, phthaldehyde **64**, Table 3.1). Although synthetic methods exist for reactions between amines and lactones, reactions of **66** and lysine in physiological conditions have never been reported. Yet, there are examples of natural and synthetic β-lactones reacting selectively with serine and cysteine residues of enzymes.[85–87]

By coupling a ligand with **66**, the lactone can be brought into proximity with a surface lysine residue of the POI. I hypothesize that the proximity to the lysine's amine will facilitate acylation by **66**, thereby completing the first step in traceless-affinity labelling.

3.1.4 β-Lactones in Natural Products Acylate Nucleophilic Residues

The β-lactone moiety was chosen as a component of proposed cleavable linker **4** because it is present in natural products which acylate nucleophilic residues (i.e., serine and cysteine) (Figure 3.3).

The serine and cysteine residues that get acylated are found in the active sites of enzymes, with no side reactions with other residues observed. This reactivity likely arises from the selectivity of the compounds for the active site of the enzymes, bringing the β-lactone into proximity of the nucleophilic residue.

Table 3.2 Examples of natural products containing β-lactones.

Natural Product containing β-lactone	Source	Inhibits
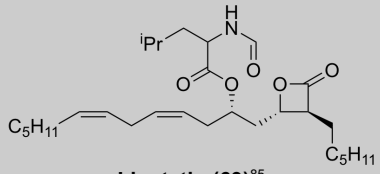 **Lipstatin (69)**[85]	*Streptomyces toxytricini*	Pancreatic Lipase
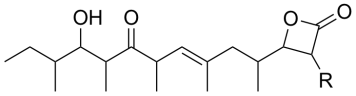 **Ebelactone A (70, R = Me)** **Ebelactone B (71, R = Et)**[86]	*Streptomyces aburaviensis*	Homoserine transacetylase (HTA)
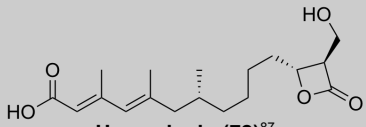 **Hymeglusin (72)**[87]	*Enterococcus faecalis*	Hydroxymethylglutaryl (HMG)-CoA Synthase

The four β-lactones in Table 3.2 (**69** – **72**) undergo nucleophilic attack by a Ser or a Cys, followed by ring opening and protonation. Lipstatin (**69**) and Ebelactone A (**70**) and B (**71**) acylate serine residues within the active sites of their respective serine protease targets. It should be noted that these serine residues are more nucleophilic than normal because they are part of a catalytic triad. The triad is composed of serine, histidine, and aspartate residues which are responsible for the activity of the enzymes.[88] The carboxylate group of Asp polarizes the His, which then deprotonates the Ser, and the oxyanion then attacks the lactone's carbonyl carbon (Scheme 3.3).[89]

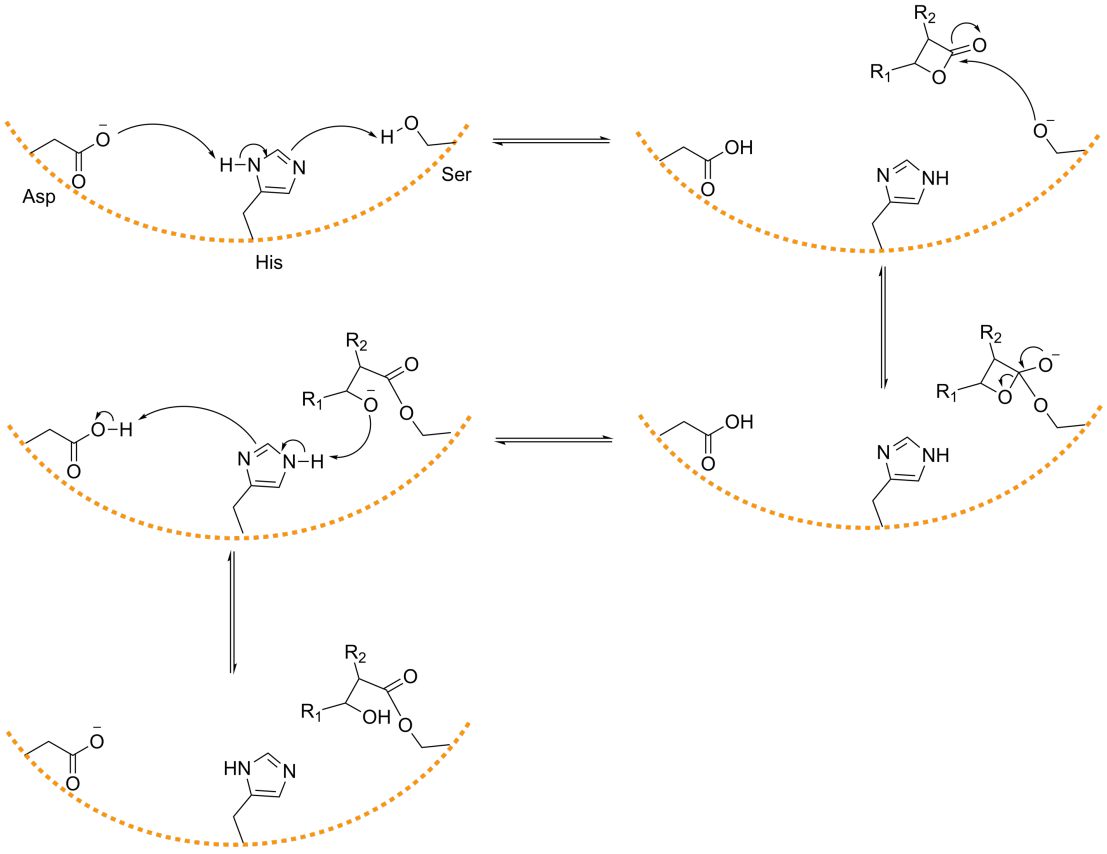

Scheme 3.3 Simplified mechanism for the acylation of a serine by a β-lactone. The serine in the catalytic site is activated by assistance from neighbouring His/Asp pair.

Hymeglusin (**72**) acylates the cysteine residue in the catalytic site of HMG-CoA synthase.[87] Aside from the cysteine, the other residues involved in the catalytic process are not identified. It has been postulated Glu is the catalytic base, and His may act as a proton donor (Scheme 3.4).[90]

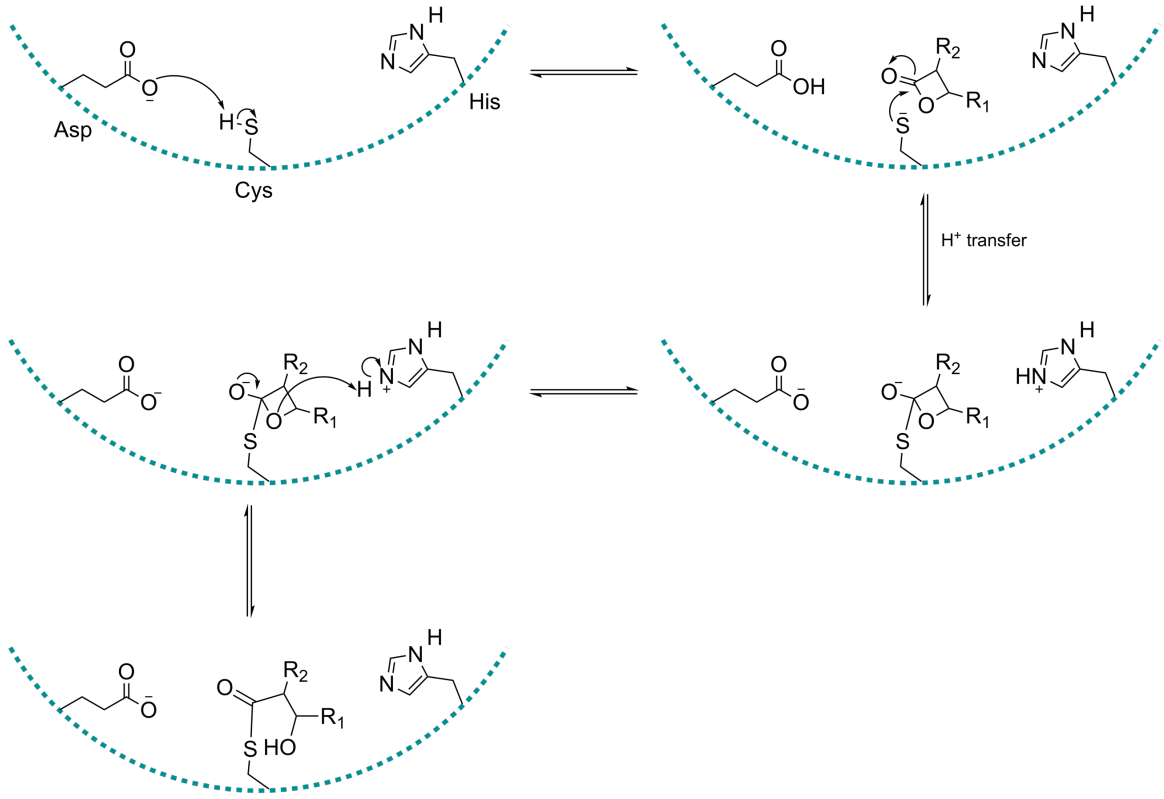

Scheme 3.4 Putative mechanism for the acylation of a cysteine residue by a β-lactone in the active site of an HMG-CoA synthase.

3.1.5 Synthetic β-Lactones that Acylate Nucleophilic Residues

Based on the natural β-lactones in the previous section, in 2008 Böttcher and Sieber developed a series of β-lactones to covalently tag the active sites of enzymes.[79] Each lactone bore a substituent on the α-carbon to increase selectivity towards a specific enzyme class, and an alkyne group on the β-carbon. Once the lactone has reacted with its enzyme target, click chemistry is used to attach a fluorescent tag to visualize the protein.

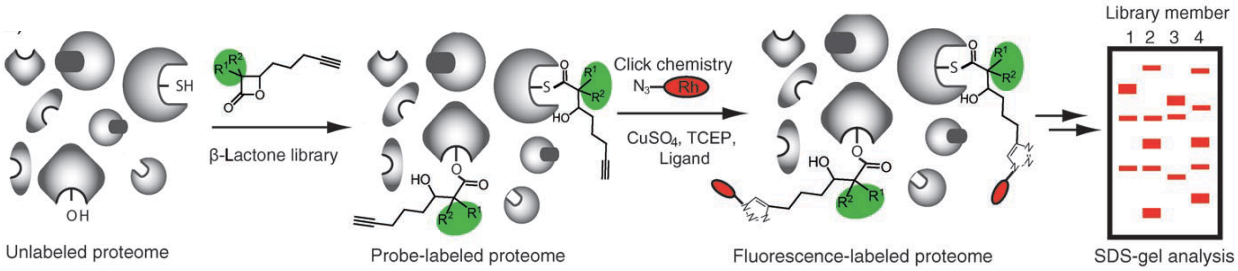

Figure 3.3 A two-step method for tagging enzymes. First, a β-lactone (with an alkyne on C-4) acylates a cysteine or serine residue. Next, the alkyne is reacted with an azide on a Rhodamine (Rh)-fluorescent tag, in the presence of copper (II) sulfate, tris(2-carboxyethyl)phosphine (TCEP), and a ligand resulting in covalent tagging of the enzymes.[79]

While this affinity labelling provides a selective method for visualization of enzymes, the active site ends up inhibited by design. I propose utilizing a related method for traceless-affinity labelling, in which the β-lactone is brought into proximity of a lysine on the surface of the POI through a ligand-protein interaction. This will enable the acylation of the lysine's amine in the absence of a catalytic base (such as glutamate or histidine in the active sites of enzymes). This would complete the first step in traceless-affinity labelling (Scheme 3.5).

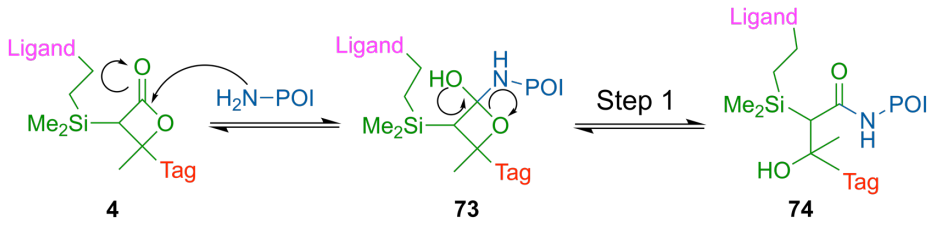

Scheme 3.5 Proposed nucleophilic attack of a lysine residue on the β-lactone of traceless-affinity molecule **4**.

3.2 RESEARCH PROPOSAL: CLEAVAGE OF A α-SILYL-β-LACTONE LINKER VIA A PETERSON OLEFINATION

Upon association of the ligand and protein of interest (POI), the proposed acylation of a lysine residue will covalently tag the protein (**74**, Scheme 3.5). The resulting amide intermediate contains a silicon and oxygen in a 1,2-relationship. A subsequent Peterson olefination would cleave the ligand from the linker and tag, completing the second step of traceless-affinity labelling (Figure 3.5). After cleavage and dissociation of the ligand, the native function of the protein is expected to be restored. Having the tag remaining bound to the protein would allow us to monitor its activity in real-time.

3.2.1 Mechanism of the Peterson Olefination

The Peterson olefination traditionally involves reacting an α-silyl organometallic reagent (**75**) with an aldehyde or ketone (**76**) to produce an alkene and a silanol.[91] This reaction proceeds in a two-step process (Scheme 3.6). First, the α-silyl organometallic reagent reacts with the carbonyl compound to form β-hydroxysilane intermediate **77** or **80**. These intermediates may be isolated if desired or taken directly to the next step. Elimination of the silanol yields alkene **78** or **79** and can occur under acidic or basic conditions.

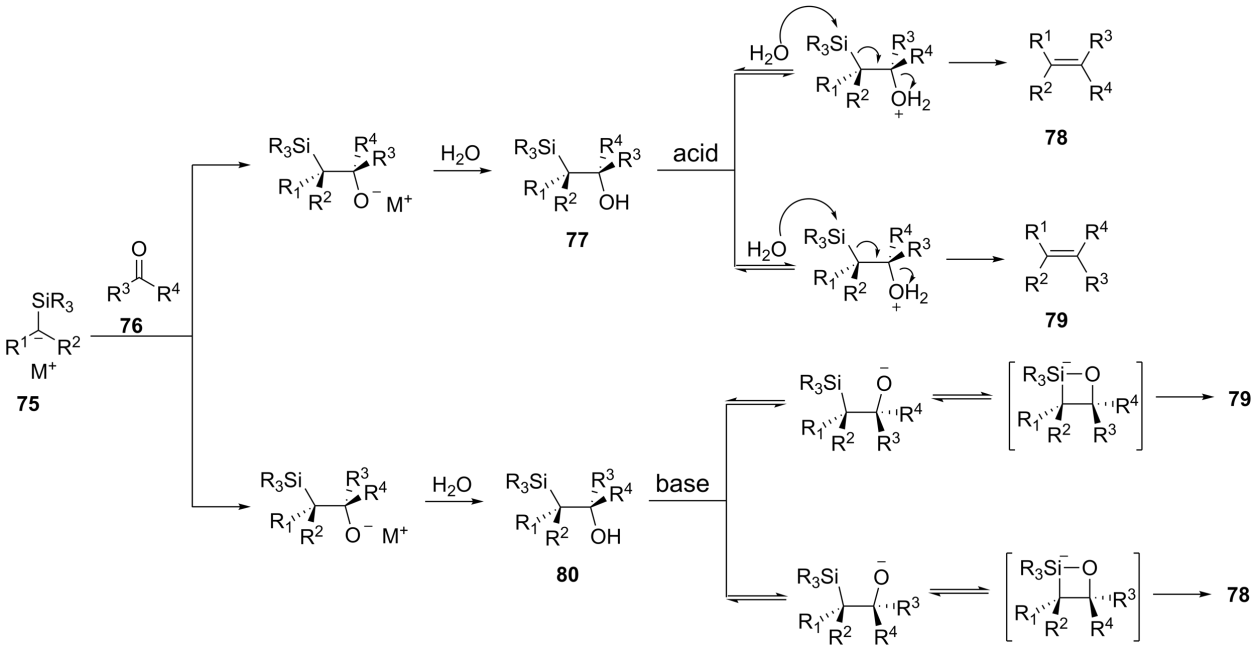

Scheme 3.6 The classic Peterson olefination of the hydroxysilane intermediates **77** and **80** can both proceed in acidic or basic conditions. Molecules **77** and **80** are each only shown in one condition for simplicity.[92]

The mechanism of elimination depends on the conditions used.[92] Under acidic conditions the hydroxyl group is protonated. A molecule of water then attacks the silicon, facilitating *anti*-periplanar elimination of water to produce the alkene and silanol. Under basic conditions the hydroxyl group is deprotonated and attacks the silicon, forming a pentacoordinate silicon intermediate. This is followed by *syn*-periplanar elimination to yield the alkene and silanol.

3.2.2 A Peterson Olefination Under Physiological Conditions?

The proposed traceless-affinity molecule **4** has silicon and oxygen atoms in a 1,2-relationship, which may facilitate cleavage via a Peterson olefination. Traditionally, the Peterson olefination requires strongly acidic or basic conditions, each proceeding through different mechanisms (Scheme 3.6). I propose that the steric strain of a β-lactone will favor ring-opening after nucleophilic attack by lysine, and the resulting β-hydroxysilane intermediate **74** will undergo Peterson olefination. If successful, this will liberate a silanol bound to the ligand, and an alkene bound to the tag and POI (Scheme 3.7). For protein labelling, the stereochemistry of the alkene is inconsequential, so either of the aforementioned mechanisms will yield a functional product.

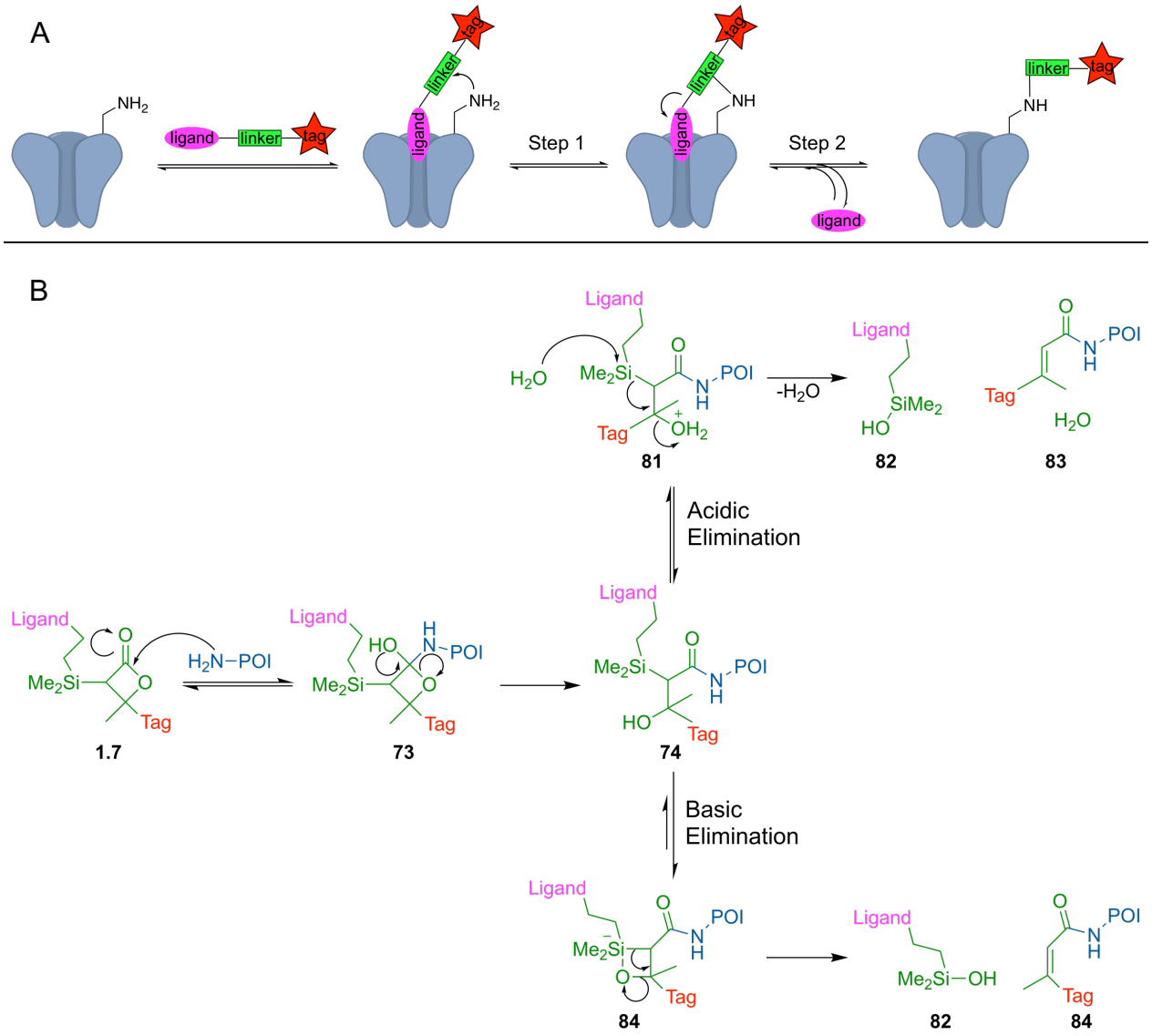

Scheme 3.7 (A) General concept of traceless affinity labelling. (B) the nucleophilic attack of traceless-affinity molecule **4** and a lysine residue, followed by Peterson olefination.

3.3 STRATEGY: SYNTHESIS OF AN α-SILYL-β-LACTONE LINKER

When designing a synthesis for the linker **4**, an α-silyl ester was chosen because the preparation of similar esters has been described in a one-step reaction. The starting material, dichlorodimethylsilane (**85**), may be functionalized with an allyl group and an ester.[93,94] The allyl group of **88** would be used to attach a ligand via cross-metathesis. The ester **90** can cyclize to the α-silyl-β-lactone **92** with an aldehyde or ketone **91** (which contains the chemical tag). If successful, this

will produce a traceless-affinity compound in four steps (Scheme 3.8). It is expected that the lengths of the carbon chains will need to be optimized for the best reactivity profile.

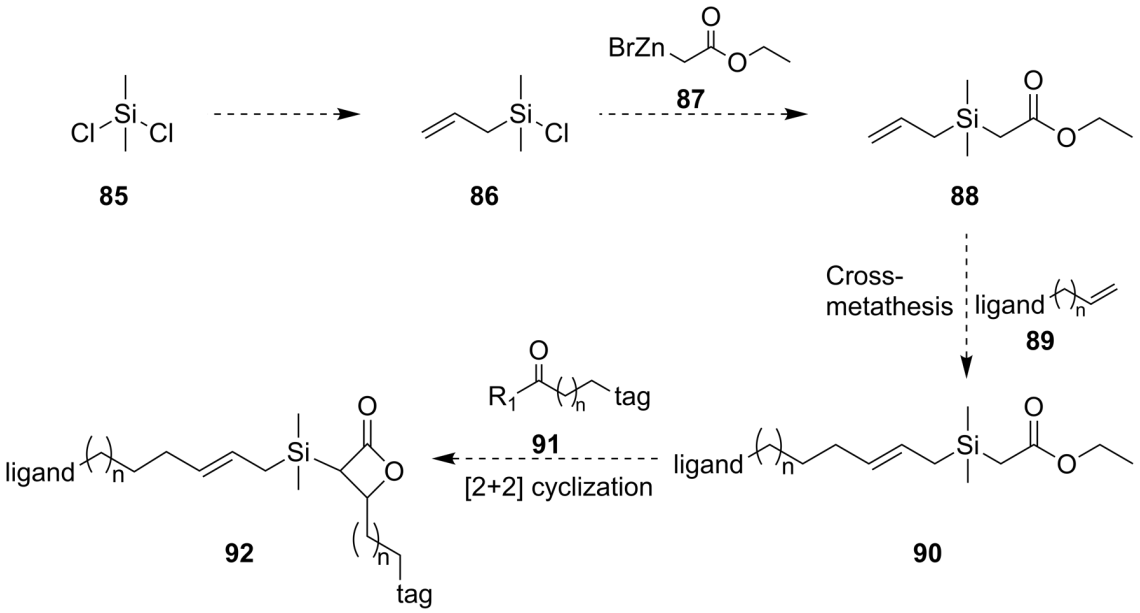

Scheme 3.8 The proposed synthetic route for traceless-affinity molecule **92**.

3.3.1 Early Attempts to Prepare an α-Silyl-β-lactone

Initial efforts toward the development of the proposed α-silyl lactone began with the synthesis of allyl(diemethyl)chlorosilane (**86**) from dichlorodimethylsilane (**85**). Several attempts to mono-alkylate **85** were unsuccessful, with diallyldimethylsilane (**93**) as the only identified product (Table 3.3). The crude ^{1}H NMR spectra were examined, and the mono- and di-allyl products identified by their sp^3 CH_2 doublets at approximately 1.75 and 1.5 ppm, respectively.

Table 3.3 Attempted coupling of dichlorodimethylsilane (**85**) and alkylating agent.

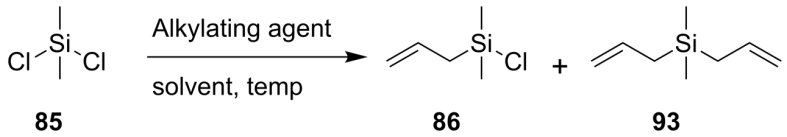

85 **86** **93**

Entry	Alkylating agent (eq)	3.41 eq	Solvent	Temp (°C)	3.42 yield (%)	Comments
1	AllylMgBr (1.0)	1.0	Et_2O	30	0	**93** obtained
2	AllylMgBr (1.2-1.5)	1.0	Et_2O	0-rt	0	**93** obtained
3	AllylZnBr	1.0	THF	0	0	**93** obtained
4	AllylInBr (1.0)	1.0	Et_2O	rt	<10	**93** major product

Each reaction was performed under anhydrous, inert conditions and monitored by thin layer chromatography (TLC). The Grignard and allyl zinc attempts (entries 1-3) resulted in the exclusive formation of diallylsilane **93**, despite the equivalents, temperatures, and addition times of the organometallic reagent used. I then explored the use of an allyl indium species, which has been reported to yield the mono allylsilane **86** in a 92% isolated yield.[93] I was unable to replicate these yields, with yields below 10%. The unreacted dichlorosilane in each reaction was visualized by TLC throughout the reaction but was hydrolyzed upon workup. Since the desired allyl(chloro)silane **86** is commercially available, it was purchased to continue on with this route.

3.4 DEVELOPMENT OF A MODEL CLEAVABLE LINKER

Before continuing on with the synthesis of traceless-affinity molecule **92**, I wanted to confirm whether the α-silyl-β-lactone moiety could undergo a Peterson olefination with an amine under physiological conditions. This led me to postpone the synthesis of the full traceless-affinity molecule **92** and first produce a model linker from trimethylsilylchloride (TMSCl). The model linker may be synthesized in two steps: by generating the TMS ester **95** followed by a [2+2] cycloaddition to a carbonyl (**96**, **98**, or **100**) to yield an α-silyl-β-lactone (**97**, **99**, or **101**; Table 3.4).

Table 3.4 General synthesis of model α-silyl-β-lactones.

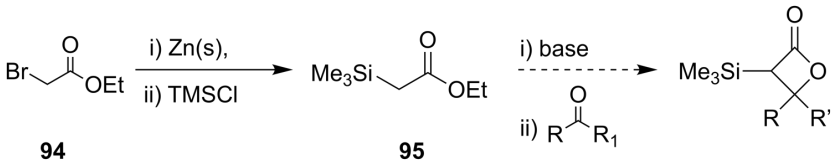

94 95

Entry	Aldehyde/Ketone	R	R'	Lactone
1	**96**	H	*i*-Pr	**97**
2	**98**	Me	*i*-Pr	**99**
3	**100**	Me	Me	**101**

3.4.1 Synthesis of a Model β-Lactone Via Enolate Chemistry

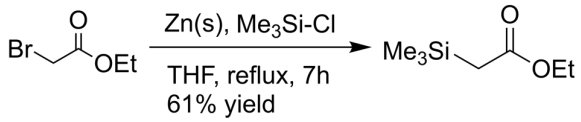

94 95

Scheme 3.9 Synthesis of α-silyl ester **95** using the Reformatsky reagent.

The TMS ester was synthesized using the Reformatsky reagent. In a one pot reaction, the Reformatsky reagent was generated *in situ* by adding bromoacetate **94** to a refluxing mixture of zinc powder and TMSCl in anhydrous THF (Scheme 3.9). It was then reacted with TMSCl to yield α-silyl ester **95** in a 61% yield. This yield was slightly below that of Fessenden and Fessenden in 1967 (72%), but provided enough material to move on to the next step.[94] This reaction was not optimized further.

Scheme 3.10 Attempted cyclization of α-silyl ester **95** and carbonyls **96**, **98**, and **100**.

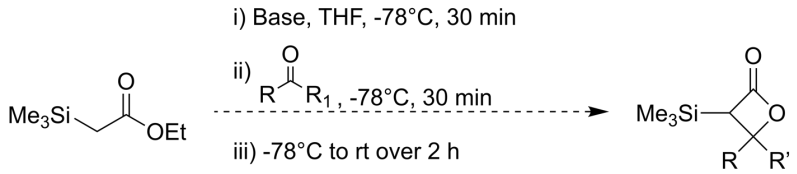

95

The first base used to attempt cyclization between α-silyl ester **95** and a carbonyl was MeLi (Scheme 3.10). The crude ^{1}H NMR spectrum when using aldehyde **96** showed neither starting material nor lactone **97** and was primarily Et_2O (from workup). In the crude ^{1}H NMR spectrum with ketone **98**, TMS ester **95** was present, but not the ketone or desired product, **99**. There were new peaks in the aliphatic region, which may have been a result of an undesired reaction between the methyl anion and the TMS ester **95** (suggesting the MeLi acted through a different mechanism than that in scheme 3.11) but could not be identified.

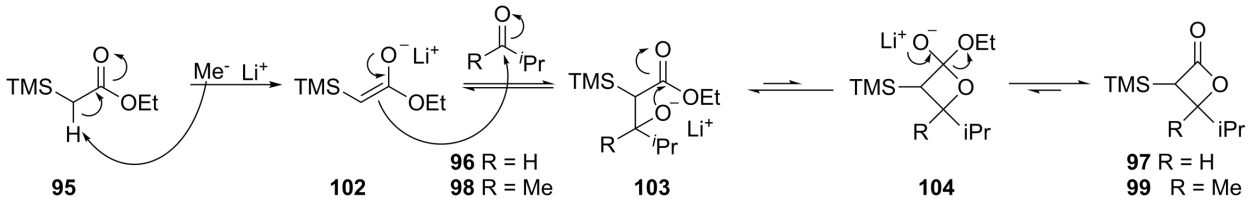

Scheme 3.11 Mechanism for the cyclization of TMS ester enolate **102** with aldehyde **96** or ketone **98** to form α-silyl lactone **97** or **99**, respectively.

The cyclization was then attempted with LDA as the base, as it is bulkier it should not be nucleophilic. Again, the crude ^{1}H NMR spectrum showed no evidence of a lactone. It is possible that the lactone cyclization was unsuccessful because the ethoxy substituent was a poor leaving group, so a different ester was explored next.

Next, I attempted to synthesize the α-silyl lactone **99** from phenyl bromoacetate (**107**) and ketone **98** (Scheme 3.12). The phenoxide moiety is known to be a better leaving group, and phenyl esters have been used to synthesize β-lactones by Schick et al. in 1995.[95] I also chose to use the more substituted carbonyl, ketone **98**, because cyclization should be more successful due to the *gem*-dialkyl effect. The rationale behind this effect is that replacing the aldehyde's hydrogens with alkyl groups increases the rate of cyclization due to repulsion between the groups.[96] The repulsion results in a smaller angle between the oxyanion and ester in the intermediate **103** (Scheme 3.11), favoring intramolecular ring formation.

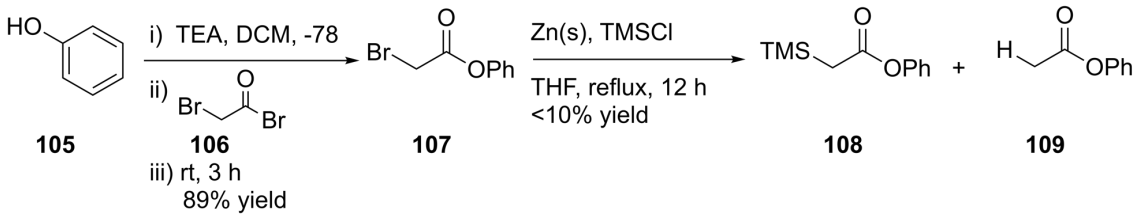

Scheme 3.12 Attempted synthesis of phenyl TMS acetate (**108**) from bromoacetate **107**.

The first approach to phenyl ester **108** utilized conditions of the Reformatsky reagent in Scheme 3.9. Bromo ester **107** was prepared by deprotonation of phenol (**105**) by TEA (triethylamine), followed by addition to bromo acetylbromide (**106**) in DCM, in a good yield (89%). It was then subjected to the conditions in the Reformatsky reagent (Scheme 3.4) to yield a 1:12 mixture of the TMS ester **108** and phenyl acetate (**109**). Due to the high boiling points of both **108** and **109**, and the instability of the TMS ester **108** on silica columns, I was unable to isolate the desired ester for subsequent lactonization.

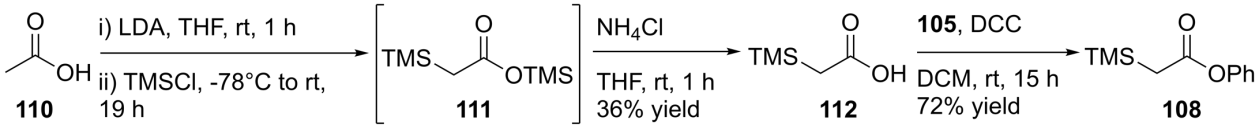

Scheme 3.13 Synthesis of phenyl TMS acetate **108** from acetic acid (**110**).

The second approach began with acetic acid (**110**) undergoing double deprotonation by LDA (Scheme 3.13). The subsequent addition of TMSCl gave the bis-silylnated intermediate **111**, which was hydrolyzed to TMS acid **112** in a modest yield (36%).[97] The acid was coupled with phenol in the presence of DCC to yield the desired phenyl TMS ester **108** in a good yield (72%).

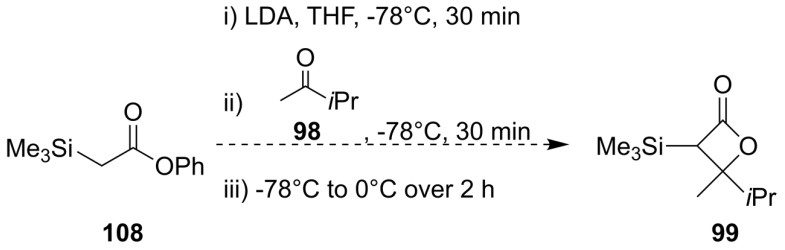

Scheme 3.14 Attempted lactonization of phenyl ester **108** and ketone **98** using LDA.

Using the procedure from Schick *et al.*, lactonization was still unsuccessful (Scheme 3.14). The crude ^{1}H NMR was similar to that of the reaction using the ethyl ester (Scheme 3.11). This may indicate that the TMS enolate undergoes decomposition, therefore TMS esters are not suitable intermediates for the synthesis of TMS lactones.

With these results in hand, and no literature directly supporting the cyclization between a TMS ester and aldehyde/ketone, an alternate synthesis was explored. An ideal synthesis would avoid generating an anion in the lactonization, thus avoiding potential side reactions with the TMS group.

3.4.2 Synthesis of a Model β-Lactone via [2+2] Cycloaddition

An alternative using a [2+2] cyclization between TMS ketene **113** and ketone **98** was explored to produce the desired lactone **99** (Scheme 3.15). This synthesis has been previously reported and may provide an alternate, modular synthesis that could be used for a cleavable linker.[95,98] Two routes were explored for generation of the ketene: thermal rearrangement of TMS acetylene **115** and intramolecular dehydration of TMS acid (**112**).

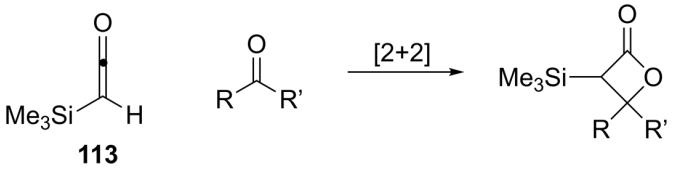

Scheme 3.15 General strategy for a [2 + 2] cycloaddition.

The thermal rearrangement was first introduced by Shchukovskaya *et al* in 1965 via pyrolyisis of TMS acetylene **115**.[98] Later procedures were successfully achieved the thermal rearrangement at 120°C. Once generated, the TMS ketene is very stable. It is isolated via distillation at 82°C, does not dimerize when heated, and can be stored for long periods of time.

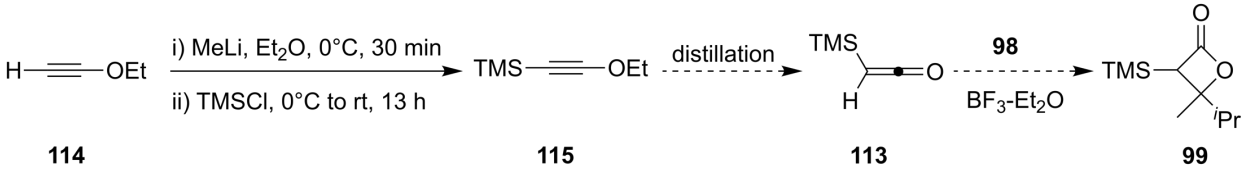

Scheme 3.16 Attempted synthesis of the proposed model α-silyl lactone from TMS ketene **113**.[99]

The thermal rearrangement was attempted in a one pot reaction (Scheme 3.16). Ethoxyacetylene (**114**) was deprotonated with MeLi at 0 °C and coupled with TMSCl to generate TMS acetylene intermediate **115**. The acetylene was removed by distillation under nitrogen and a second distillation in a 120 °C oil bath was used to achieve rearrangement to ketene **113**. Analysis of the ^{1}H NMR spectrum of the second distillate showed acetylene **115** and Et_2O. This may have been due to the small scale used here (1 g) compared to that in literature (20 g).[98,100]

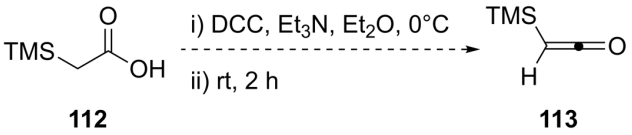

112 **113**

Scheme 3.17 Synthesis of TMS ketene **113** via intramolecular dehydration of TMS acid **112**.[100]

When the thermal rearrangement was unsuccessful, a new route was explored. This involved the intramolecular dehydration of TMS acid **112** in the presence of DCC and trace TEA (Scheme 3.17).[100] Olah *et al*. used this method to successfully generate several stable dialkyl ketenes on a 20 g scale. This route was appealing because it avoided the high temperatures of the thermal rearrangement. Unfortunately, this route was also fruitless on a 1 g scale.

Since all pre-existing methods of generating silyl ketenes rely on large scale syntheses, this was not considered a feasible route to the desired silyl lactone **99**. Due to time constraints, I was unable to continue on with this synthesis and explore further alternative syntheses.

3.5 SUMMARY & FUTURE DIRECTIONS: A γ-SILYL-β-LACTONE

A cleavable linker for traceless affinity labelling via a transacylation cascade has been proposed. The development of a synthetic route to key α-silyl-β-lactone **98** proved more challenging than anticipated. The initial route attempted to cyclize enolate **102** with carbonyls **96** and **98** gave no evidence of lactone formation, possibly due to rearrangement of the enolate. The second route, a [2+2] cyclization between TMS ketene **113** and ketone **98** was also unsuccessful because of difficulties generating the desired ketene, possibly due to the small scale of the reaction.

Due to these results, an alternative route to explore revisits enolate chemistry to generate a γ-silyl-β-lactone. Here, the enolate generated does not contain the TMS group, which may prevent

undesired rearrangements between the oxyanion and TMS group. For this route, I would begin with the TMS group on the ketone rather than on the ester **109** (Scheme 3.18). I believe this may circumvent the problems faced when generating the TMS enolate. TMS acetone **116** and phenyl acetate (**109**) would be good starting points, as they are both readily available.

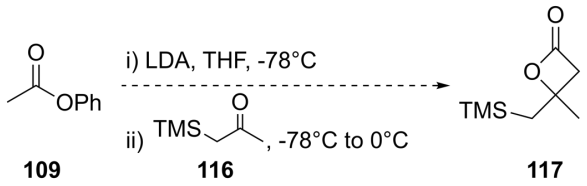

Scheme 3.18 Proposed synthesis of γ-silyl-β-lactone **116**.

While β-lactone **117** bears the silyl group on the γ-carbon, it still maintains the 1,2-relationship between the silicon and heterocyclic oxygen. This may also facilitate the Peterson olefination required for traceless-affinity labelling of a protein of interest (POI, Scheme 3.19). Here once transacylation has occurred, intermediate **120** can undergo an intermolecular rearrangement to yield alkene **122**. Lack of time prevented me from fully exploring this route, but it is a good starting point for the next researcher on this project.

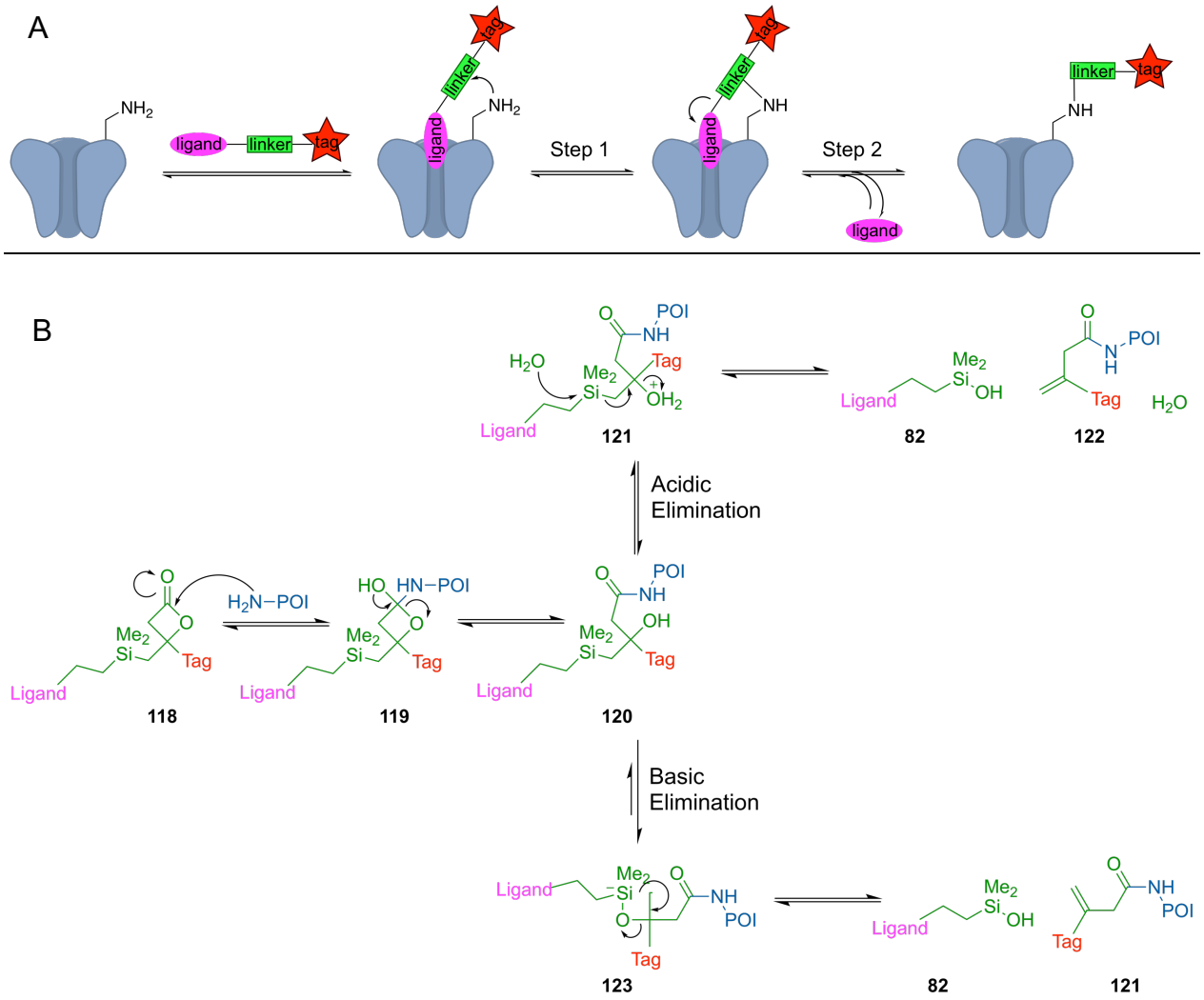

Scheme 3.19 **(**A) General concept of traceless affinity labelling. (B) Next-generation: γ-silyl-β-lactone strategy. The nucleophilic attack of traceless-affinity molecule **118** by a lysine residue, followed by Peterson olefination.

3.6 EXPERIMENTAL

General Information

THF, Et_2O, EtOH and DCM were purchased from Fisher and VWR. Deuterated solvents were purchased from Sigma-Millipore. All other reagents were purchased from one of the three aforementioned companies and were used without further purification.

NMR spectra were obtained on a 400 MHz Varian NMR AS400 unit with an ATB-400 probe at 25 °C. Infrared spectra (IR) were acquired using a PerkinElmer FT-IR Spectrum Two IR Spectrometer with samples prepared as neat film on NaCl plates. Column chromatography was performed on silica gel (230-400, Silicycle, Quebec).

Ethyl trimethylsilylacetate (95)

Zinc powder (27.6 mmol) and anhydrous THF (15 mL) were combined under Ar (g) and brought to reflux. A solution of TMSCl (18.4 mmol), ethyl bromoacetate (27.6 mmol), and THF (5 mL) was added dropwise. The mixture refluxed for 7 h, until nearly all zinc was consumed. The reaction was cooled on an ice bath, quenched with 1 M HCl (10 mL), and stirred for 5 min. The remaining zinc was filtered off using glass wool and extracted with Et_2O (3x 20 mL). The organic layers were combined, neutralized with saturated $NaHCO_3$, washed with brine, dried over $MgSO_4$, filtered and concentrated *in vacuo* to yield **95** (1.79 g, 61%) as a fragrant, clear colourless liquid. Characterization data matched reports.[94]

^{1}H NMR (400 MHz, $CDCl_3$) δ = 4.06 (q, 2H), 1.83 (s, 2H), 1.20 (t, 3H), 0.06 (s, 9H) ppm.

Phenyl Bromoacetate (107)

Triethylamine (25 mmol) was added dropwise to a solution of phenol (25 mmol) in DCM (50 mL) at -78 °C, under Ar (g), and stirred for 10 min. Bromoacetyl bromide (25 mmol) was added slowly and the solution stirred at -78 °C for 1 h, then at rt for 2 h. The reaction was quenched with 1 M HCl (30 mL) and diluted with DCM (40 mL). The organic layer was separated, washed with brine, dried over $MgSO_4$, filtered, and concentrated *in vacuo* to a yield **107** (4.85g, 90%) as a yellow-brown liquid. Characterization data matched reports.[101]

^{1}H NMR (400 MHz, $CDCl_3$) δ = 7.41-7.35 (m, 2H), 7.27-7.23 (m, 1H), 7.13-7.11 (m, 2H), 4.04 (s, 2H) ppm.

2-(Trimethylsilyl) acetic acid (112)

A solution of LDA was prepared by adding nBuLi (2.3 M in hexanes, 45 mmol) dropwise to a solution of DIPA (47.3 mmol) in anhydrous THF (20 mL) at -78 °C under Ar (g). After 15 min., a solution of glacial acetic acid (22.5 mmol) in THF (4 mL) was added dropwise and stirred for 1 h at rt. The solution was cooled again to -78 °C and TMSCl (63 mmol) was added dropwise and the solution was gradually warmed to rt and stirred for 19 h. The resulting precipitate was removed using a glass frit and vacuum and the filtrate was reduced to yield trimethylsilyl 2-(trimethylsilyl)acetate (3.63) as a white solid. 3.63 was dissolved in THF (25 mL) and saturated NH_4Cl (5 mL) and stirred at rt for 1 h. The organic layer was separated, dried over $MgSO_4$, filtered, and concentrated in vacuo to yield 3.64 (1.07 g, 36%) as a pale yellow crystalline solid. Characterization data matched reports.[100]

^{1}H NMR (400 MHz, CDCl3) δ = 1.92 (s, 2H), 0.15 (s, 9H) ppm.

Phenyl trimethylsilylacetate (108)

Phenol (4.16 mmol) was added to a mixture of **112** (3.78 mmol), DCC (4.16 mmol), and anhydrous DCM (10 mL) under Ar (g) and stirred for 15 h. The mixture was filtered using a glass frit and vacuum, and the precipitate was washed twice with DCM. The filtrate was reduced and triturated in pentane. The resulting precipitate was filtered through a glass frit and the filtrate was reduced to a yellow solid. Purification with flash chromatography using silica gel and eluting with 30% EtOAc/Hexanes gave **108** as a clear colourless oil (0.57 g, 72%).

^{1}H NMR (400 MHz, $CDCl_3$) δ = 7.35-7.33 (m, 2H), 7.19-7.18 (m, 1H), 7.06-7.04 (m, 2H), 2.12 (s, 2H), 0.23 (s, 9H) ppm.

^{13}C NMR (100 MHz, $CDCl_3$) δ = 172.62, 152.22, 130.59, 126.77, 123.00, 28.25, 0.01 ppm.

Chapter 4: GENERAL CONCLUSIONS

Chemical probes – small molecules that modulate a protein's activity – have enabled us to study proteins in their native environments.[2,102] Knowledge of their interactions with other biological molecules (other proteins, hormones, neurotransmitters, etc.) can allow us to design drugs to target these specific interactions, potentially reducing the side effects. This thesis presented the design and synthesis of two types of chemical probes. The first described the development of two novel NADPH oxidase 2 (NOX2) inhibitors to probe the activity of a known inhibitor, VAS2870. The second focused on the development of a novel traceless-affinity compound for universal protein tagging.

Chapter two described the synthesis of a known NOX2 inhibitor, VAS2870, and two derivatives (Figure 4.1). NOX enzymes are composed of several proteins that come together to produce reactive oxygen species (ROS).[10,41,103] These ROS have been implicated in the onset and progression of neurodegenerative diseases.[10,25,104] VAS2870 (**1**) has been used in several neurobiological studies to inhibit ROS production, but its mechanism of action is not yet understood. Recent studies have shown it thioalkylates ryanodine receptors and glutathione.[28] It was my hypothesis that the triazolopyrimidine moiety of VAS2870 thioalkylates one or more cysteine residues of NOX2 proteins, prior to assembly, inhibiting ROS production.

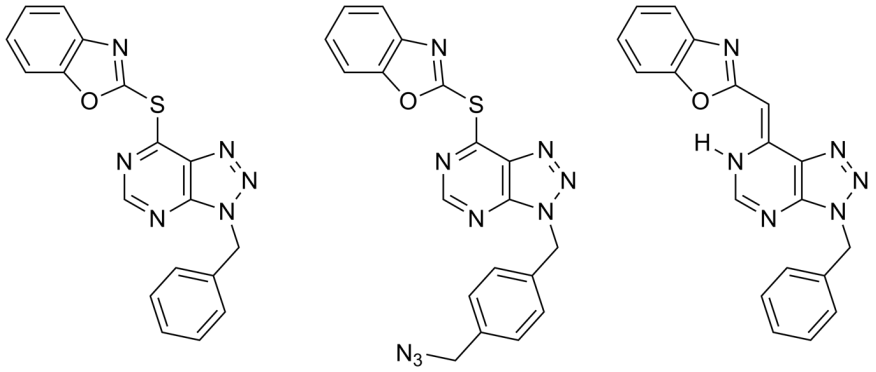

Figure 4.1: VAS2870 (**1**), azidomethyl derivative **2**, and methylene tautomer **3'**.

To test this hypothesis, I developed a derivative of VAS, the methylene tautomer **3'**, which replaces the sulfur atom of VAS2870 with a methylene group. This compound is unable to thioalkylate cysteines, thus was not expected to inhibit ROS production. Initial studies showed no inhibitory effect

of the methylene derivative, providing strong evidence that VAS2807 does indeed thioalkylate NOX2 proteins. Next, I wanted to visualize which proteins were affected by VAS2870. This required the design of a second analogue (**2**) with a methylazido substituent on the para position of VAS's benzyl group. If thioalkylation does occur, the azide would be covalently bound to the proteins and click chemistry could be used to attach a fluorescent tag for visualization. Initial studies showed a similar inhibitory effect to VAS2870, but time constraints prevented me from developing a protocol for tagging and visualization of the affected proteins. If visualization is achieved in future studies, it may call into question the use of VAS2870 in both past and future neurobiological studies.

Chapter three described efforts towards the development of a novel traceless affinity compound.[3,83] This compound has three components: a ligand, a cleavable linker, and a chemical tag. The ligand delivers the tag to the protein of interest (POI) when it binds to the POI. Upon binding, the linker reacts with an amino acid residue on the surface of the POI, which results in cleavage of the ligand and tag. When the ligand dissociates, the tag remains bound to the POI's surface. This leaves the active site free and unobstructed. For this to be successful, the cleavable linker must be unreactive in biological conditions until it is brought into proximity of the desired residue by the linker. Also, the linker must react with said residue before the ligand dissociates from the POI.

My work focused on the design of a cleavable linker containing an ∝-silyl-β-lactone moiety (**4**, Figure 4.2). Previous work uses β-lactones to selectively inhibit serine proteases, in which they remained stable in biological conditions until brought into proximity of the catalytic triad.[86,105] With the addition of the ∝-silyl group, I propose the following reaction cascade: when brought into proximity of a nucleophilic lysine residue (by a ligand), the β-lactone will acylate the lysine's amine, resulting in ring opening due to steric strain. Next, a Peterson olefination will liberate a ligand-silanol compound, and an alkene that is bound to both the tag and the POI.

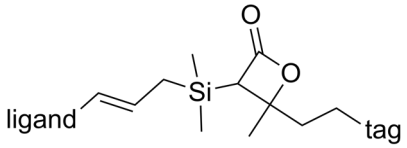

4

Figure 4.2: General structure of the traceless-affinity compound **4**.

Once synthesized in future work, **4** will be subjected to reactions to determine if it is able to undergo a Peterson olefination (or another kind of cleavage). From here, several ligand/tag

combinations can be added to test the linker's stability in the presence of various functional groups. If successful, it will be a valuable tool in the visualization of several proteins in their native systems.

References

(1) Ali Tavassoli, Andrew D. Hamilton, D. R. S. Small Molecules in Biology Themed Issue. *Chem. Soc. Rev.* **2011**, *40* (8), 4332–4345.

(2) Arrowsmith, C. H.; Audia, J. E.; Austin, C.; Baell, J.; Bennett, J.; Blagg, J.; Bountra, C.; Brennan, P. E.; Brown, P. J.; Bunnage, M. E.; et al. The Promise and Peril of Chemical Probes. **2015**, *11* (August).

(3) Hayashi, T.; Hamachi, I. Traceless Affinity Labeling of Endogenous Proteins for Functional Analysis in Living Cells. *Acc. Chem. Res.* **2012**, *45* (9), 1460–1469.

(4) Deluca, D. C.; York, J. L. Enzymes. 625–626.

(5) Patrick, G. L. *An Introduction to Medicinal Chemistry*, Fifth.; Oxford University Press: Oxford, 2013.

(6) Saboury, A. A. Enzyme Inhibition and Activation : A General Theory. **2009**, *6* (2), 219–229.

(7) Xu, L.; He, D.; Bai, Y. Microglia-Mediated Inflammation and Neurodegenerative Disease. *Mol. Neurobiol.* **2016**, *53* (10), 6709–6715.

(8) Dickinson, B. C.; Peltier, J.; Stone, D.; Schaffer, D. V.; Chang, C. J. Nox2 Redox Signaling Maintains Essential Cell Populations in the Brain. *Nat. Chem. Biol.* **2011**, *7* (2), 106–112.

(9) Diebold, B. A.; Smith, S. M. E.; Li, Y.; Lambeth, J. D. NOX2 As a Target for Drug Development: Indications, Possible Complications, and Progress. *Antioxid. Redox Signal.* **2015**, *23* (5), 375–405.

(10) Park, L.; Anrather, J.; Girouard, H.; Zhou, P.; Iadecola, C. Nox2-Derived Reactive Oxygen Species Mediate Neurovascular Dysregulation in the Aging Mouse Brain. *J. Cereb. Blood Flow Metab.* **2007**, *27* (12), 1908–1918.

(11) Block, M. L. NADPH Oxidase as a Therapeutic Target in Alzheimer's Disease. *BMC Neurosci.* **2008**, *9* (SUPPL. 2), 1–8.

(12) Tegtmedt, Frank; Ulrich, Walter; Schinzel, Reinhard; Wingler, Kirstin; Scheurer, Peter; Schmidt, H. Compounds Containing a N-Heteroaryl Moiety Linked to Fused Ring Moieties for the Inhibition of NAD(P)H Oxidases and Platlet Activation. WO 2005/111041 A1, 2005.

(13) Gatto, G. J.; Ao, Z.; Kearse, M. G.; Zhou, M.; Morales, C. R.; Daniels, E.; Bradley, B. T.; Goserud, M. T.; Goodman, K. B.; Douglas, S. A.; et al. NADPH Oxidase-Dependent and -Independent Mechanisms of Reported Inhibitors of Reactive Oxygen Generation. *J. Enzyme Inhib. Med. Chem.* **2013**, *28* (1), 95–104.

(14) Stielow, C.; Catar, R. A.; Muller, G.; Wingler, K.; Scheurer, P.; Schmidt, H. H. H. W.; Morawietz, H. Novel Nox Inhibitor of OxLDL-Induced Reactive Oxygen Species Formation in Human Endothelial Cells. *Biochem. Biophys. Res. Commun.* **2006**, *344* (1), 200–205.

(15) Kleinschnitz, C.; Grund, H.; Wingler, K.; Armitage, M. E.; Jones, E.; Mittal, M.; Barit, D.; Schwarz, T.; Geis, C.; Kraft, P.; et al. Post-Stroke Inhibition of Induced NADPH Oxidase Type 4 Prevents Oxidative Stress and Neurodegeneration. *PLoS Biol.* **2010**, *8* (9).

(16) Altenhöfer, S.; Radermacher, K. A.; Kleikers, P. W. M.; Wingler, K.; Schmidt, H. H. H. W. Evolution of NADPH Oxidase Inhibitors: Selectivity and Mechanisms for Target Engagement. *Antioxid. Redox Signal.* **2015**, *23* (5), 406–427.

(17) Altenhöfer, S.; Kleikers, P. W. M.; Radermacher, K. A.; Scheurer, P.; Hermans, J. J. R.; Schiffers, P.; Ho, H.; Wingler, K.; Schmidt, H. H. H. W. The NOX Toolbox: Validating the Role of NADPH Oxidases in Physiology and Disease. *Cell. Mol. Life Sci.* **2012**, *69* (14), 2327–2343.

(18) Baskin, J. M.; Bertozzi, C. R. Bioorthogonal Click Chemistry: Covalent Labeling in Living Systems. *QSAR Comb. Sci.* **2007**, *26* (11–12), 1211–1219.

(19) Thirumurugan, P.; Matosiuk, D.; Jozwiak, K. Click Chemistry for Drug Development and Diverse Chemical Biology Applications. **2013**.

(20) Pickens, C. J.; Johnson, S. N.; Pressnall, M. M.; Leon, M. A.; Berkland, C. J. Practical Considerations, Challenges, and Limitations of Bioconjugation via Azide-Alkyne Cycloaddition. *Bioconjug. Chem.* **2018**, *29* (3), 686–701.

(21) Gao, H. M.; Hong, J. S. Why Neurodegenerative Diseases Are Progressive: Uncontrolled Inflammation Drives Disease Progression. *Trends Immunol.* **2008**, *29* (8), 357–365.

(22) Ma, M. W.; Wang, J.; Zhang, Q.; Wang, R.; Dhandapani, K. M.; Vadlamudi, R. K.; Brann, D. W. NADPH Oxidase in Brain Injury and Neurodegenerative Disorders. *Mol. Neurodegener.* **2017**, *12* (1), 1–28.

(23) Gao, H.-M.; Zhou, H.; Hong, J.-S. NADPH Oxidases: Novel Therapeutic Targets for Neurodegenerative Diseases. *Trends Pharmaxology Sci.* **2013**, *33* (6), 295–303.

(24) Barrett, J. P.; Henry, R. J.; Villapol, S.; Stoica, B. A.; Kumar, A.; Burns, M. P.; Faden, A. I.; Loane, D. J. NOX2 Deficiency Alters Macrophage Phenotype through an IL-10/STAT3 Dependent Mechanism: Implications for Traumatic Brain Injury. *J. Neuroinflammation* **2017**, *14* (1), 1–17.

(25) Bedard, K.; Krause, K.-H. The NOX Family of ROS-Generating NADPH Oxidases:

Physiology and Pathophysiology. *Physiol. Rev.* **2007**, *87* (1), 245–313.

(26) Cifuentes-Pagano, E.; Meijles, D. N.; Pagano, P. J. The Quest for Selective Nox Inhibitors and Therapeutics: Challenges, Triumphs and Pitfalls. *Antioxid. Redox Signal.* **2014**, *20* (17), 2741–2754.

(27) ten Freyhaus, H.; Huntgeburth, M.; Wingler, K.; Schnitker, J.; Bäumer, A. T.; Vantler, M.; Bekhite, M. M.; Wartenberg, M.; Sauer, H.; Rosenkranz, S. Novel Nox Inhibitor VAS2870 Attenuates PDGF-Dependent Smooth Muscle Cell Chemotaxis, but Not Proliferation. *Cardiovasc. Res.* **2006**, *71* (2), 331–341.

(28) Sun, Q. A.; Hess, D. T.; Wang, B.; Miyagi, M.; Stamler, J. S. Off-Target Thiol Alkylation by the NADPH Oxidase Inhibitor 3-Benzyl-7-(2-Benzoxazolyl)Thio-1,2,3-Triazolo[4,5-d]Pyrimidine (VAS2870). *Free Radic. Biol. Med.* **2012**, *52* (9), 1897–1902.

(29) Lull, M. E.; Block, M. L. Microglial Activation and Chronic Neurodegeneration. *Neurotherapeutics* **2010**, *7* (4), 354–365.

(30) Fu, R.; Shen, Q.; Xu, P.; Luo, J. J.; Tang, Y. Phagocytosis of Microglia in the Central Nervous System Diseases. *Mol. Neurobiol.* **2014**, *49* (3), 1422–1434.

(31) Neumann, H.; Kotter, M. R.; Franklin, R. J. M. Debris Clearance by Microglia: An Essential Link between Degeneration and Regeneration. *Brain* **2009**, *132* (2), 288–295.

(32) Leumann, P. A. K. C. J. Oxidative Damage on RNA Nucleobases. *Chem. Biol. Nucleic Acids* **2014**, 76–89.

(33) Auten, R. L.; Davis, J. M. The Role of Oxygen in Health and Disease - A Series of Reviews Oxygen Toxicity and Reactive Oxygen Species : The Devil Is in the Details. *Pediatr. Res.* **2009**, *66* (2), 121–127.

(34) Beckerman, M. *Biological and Medical Physics, Biomedical Engineering: Cellular Signalling in Health and Disease*; Springer: New York, 2009.

(35) Winterbourn, C. C. Toxicity of Iron and Hydrogen Peroxide: The Fenton Reaction. *Toxicol. Lett.* **1995**, *82–83* (C), 969–974.

(36) Lapouge, K.; Smith, S. J. M.; Groemping, Y.; Rittinger, K. Architecture of the P40-P47-P67phox Complex in the Resting State of the NADPH Oxidase. A Central Role for P67phox. *J. Biol. Chem.* **2002**, *277* (12), 10121–10128.

(37) Diebold, B. A.; Bokoch, G. M. Molecular Basis for Rac2 Regulation of Phagocyte NADPH Oxidase. *Nat. Immunol.* **2001**, *2* (3), 211–215.

(38) Lapouge, K.; Smith, S. J. M.; Walker, P. A.; Gamblin, S. J.; Smerdon, S. J.; Rittinger, K.

Structure of the TPR Domain of P67 Phox in Complex with Rac{□ } GTP. *Mol. Cell* **2000**, *6* (4), 899–907.

(39) Docking of Apocynin , Diapocynin and 5-Nitroapocynin with 1K4U Sub-Section of Human Neutrophil NADPH Oxidase System and MD Simulation A Thesis Presented to The Faculty of the Graduate School Southern University and A & M College In Partial Fulfillment Of . **2011**.

(40) Groemping, Y.; Lapouge, K.; Smerdon, S. J.; Rittinger, K. Molecular Basis of Phosphorylation-Induced Activation of the NADPH Oxidase. *Cell* **2003**, *113* (3), 343–355.

(41) Sumimoto, H. Structure, Regulation and Evolution of Nox-Family NADPH Oxidases That Produce Reactive Oxygen Species. *FEBS J.* **2008**, *275* (13), 3249–3277.

(42) Vignais, P. V. The Superoxide-Generating NADPH Oxidase : Structural Aspects and Activation Mechanism. *Cell. Mol. Life Sci.* **2002**, *59*, 1428–1459.

(43) Assari, T. Chronic Granulomatous Disease; Fundamental Stages in Our Understanding of CGD. *Med. Immunol.* **2006**, *5*, 1–8.

(44) McBean, G. J.; López, M. G.; Wallner, F. K. Redox-Based Therapeutics in Neurodegenerative Disease. *Br. J. Pharmacol.* **2017**, *174* (12), 1750–1770.

(45) Hobbs, G. A.; Mitchell, L. E.; Arrington, M. E.; Gunawardena, H. P.; Decristo, M. J.; Loeser, R. F.; Chen, X.; Cox, A. D.; Campbell, S. L. Redox Regulation of Rac1 by Thiol Oxidation. *Free Radic. Biol. Med.* **2015**, *79*, 237–250.

(46) Debeurme, F.; Picciocchi, A.; Dagher, M. C.; Grunwald, D.; Beaumel, S.; Fieschi, F.; Stasia, M. J. Regulation of NADPH Oxidase Activity in Phagocytes: Relationship between FAD/NADPH Binding and Oxidase Complex Assembly. *J. Biol. Chem.* **2010**, *285* (43), 33197–33208.

(47) Ren, Z.; Mao, X.; Mertens, C.; Krishnaraj, R.; Qin, J.; Mandal, P. K.; Romanowski, M. J.; McMurray, J. S.; Chen, X. Crystal Structure of Unphosphorylated STAT3 Core Fragment. *Biochem. Biophys. Res. Commun.* **2008**, *374* (1), 1–5.

(48) Nagarkoti, S.; Dubey, M.; Awasthi, D.; Kumar, V.; Chandra, T.; Kumar, S.; Dikshit, M. S-Glutathionylation of P47phox Sustains Superoxide Generation in Activated Neutrophils. *Biochim. Biophys. Acta - Mol. Cell Res.* **2018**, *1865* (2), 444–454.

(49) Butturini, E.; Darra, E.; Chiavegato, G.; Cellini, B.; Cozzolino, F.; Monti, M.; Pucci, P.; Dell'Orco, D.; Mariotto, S. S-Glutathionylation at Cys328 and Cys542 Impairs STAT3 Phosphorylation. *ACS Chem. Biol.* **2014**, *9* (8), 1885–1893.

(50) Change in the Conformation of P47phox by Sodium Dodecyl Sulfate, an Activator of the Leukocyte NADPH Oxidase. *Journam Biochem. Moecular Biol.* **1993**, *31* (3), 227–232.

(51) Meijles, D. N.; Fan, L. M.; Howlin, B. J.; Li, J. M. Molecular Insights of P47phox Phosphorylation Dynamics in the Regulation of NADPH Oxidase Activation and Superoxide Production. *J. Biol. Chem.* **2014**, *289* (33), 22759–22770.

(52) Arnott, E. A.; Chan, L. C.; Cox, B. G.; Meyrick, B.; Phillips, A. POCl3 Chlorination of 4-Quinazolones. *J. Org. Chem.* **2011**, *76* (6), 1653–1661.

(53) Snyder, D. C. Conversion of Alcohols to Chlorides by TMSCl and DMSO. *J. Org. Chem.* **1995**, *60*, 2638–2639.

(54) Belaj, F.; Dojer, B. Chlorination of Aromatic Rings by PCL5. *Phosphorus. Sulfur. Silicon Relat. Elem.* **2013**, *188* (1–3), 132–136.

(55) Herman Gershon, A. T. G. Pyrimidines. 7. A Study of Chorination of Pyrimidines with POCl3 in the Presence of N,N-Dimethylaniline. *J. Heterocycl. Chem.* **1984**, *21*, 1161–1167.

(56) Jessie Sandosham, K. U. SYNTHESIS OF PYRIMIDINYL TRIFLATES AND PALLADIUMCATALYZED COUPLING WITH ORGANOTIN AND ORGANOZINC REAGENTS. *Heterocycles* **1994**, *37* (1), 501–514.

(57) Acid, R.; Mylari, B. L.; Oates, P. J.; Beebe, D. A.; Brackett, N. S.; Coutcher, J. B.; Dina, M. S.; Zembrowski, W. J. Sorbitol Dehydrogenase Inhibitors (SDIs): A New Potent, Enantiomeric SDI, 4-[2-1R-Hydroxy-Ethyl)-Pyrimidin-4-Yl]-Piperazine-1-Sulfonic Acid Dimethylamide. *J. Med. Chem.* **2001**, *40* (17), 2695–2700.

(58) Latli, B.; Jones, P. J.; Krishnamurthy, D.; Senanayake, C. H. Synthesis of [14C]-, [13C4]-, and [13C4, 15N2]-5-Amino-4-Iodopyrimidine. *J. Label. Compd. Radiopharm.* **2008**, *51* (1), 54–58.

(59) Read, M. L.; Brændvang, M.; Miranda, P. O.; Gundersen, L. L. Synthesis and Biological Evaluation of Pyrimidine Analogs of Antimycobacterial Purines. *Bioorganic Med. Chem.* **2010**, *18* (11), 3885–3897.

(60) Khoje, A. D.; Kulendrn, A.; Charnock, C.; Wan, B.; Franzblau, S.; Gundersen, L. L. Synthesis of Non-Purine Analogs of 6-Aryl-9-Benzylpurines, and Their Antimycobacterial Activities. Compounds Modified in the Imidazole Ring. *Bioorganic Med. Chem.* **2010**, *18* (20), 7274–7282.

(61) Peptide, A. P.; Using, N. Dendronized Polymer Organogels from Click Chemistry – Remarkable Gelation Property Due to Synergistic Functional Group Binding and Dendritic

Size Effect. *Angew. Chemie* **2008**, *36*, 98–103.

(62) Houpis, I. N.; Molina, A.; Lynch, J.; Reamer, R. A.; Volante, R. P.; Reider, P. J. Condensation of 2-Methylbenzoxazole with Aromatic Aldehydes Bearing Acidic Protons. A Convenient Coupling in the Synthesis of the HIV-Reverse Transcriptase Inhibitor L-696,229. *J. Org. Chem.* **1993**, *58* (11), 3176–3178.

(63) Ralph P. Volante, Cranbury; Joseph E. Lynch, Plainfield; Ioannis Houpis, Edison; Audrey Molina, Elizabeth, all of N. J. Facile Condensation of Methylbenzoxazoles with Aromatic Aldehydes. 5,290,941, 1994.

(64) Freeman, F. *Ethyl Cyanoacetate*; John Wiley & Sons. Ltd., 2001.

(65) Zakhs, E. R.; Ponyaev, A. I.; Subbotina, M. A. Synthesis and Photochromic Properties of 2-(3-Nitro-2-Pyridylmethyl)Benzazoles. *Russ. J. Gen. Chem.* **2001**, *71* (7), 1076–1087.

(66) Philippa B. Cranwell*, Andrew T. Russell*, C. D. S. A New Synthesis of 2-Aminoindoles and 6-Aminopyrrolo[3,2-d]Pyrimidines from π-Deficient 1,2-Dihaloarenes and Geminal Enediamines. *Synlett* **2016**, No. 27, 131–135.

(67) Woll, M. G.; Qi, H.; Turpoff, A.; Zhang, N.; Zhang, X.; Chen, G.; Li, C.; Huang, S.; Yang, T.; Moon, Y. C.; et al. Discovery and Optimization of Small Molecule Splicing Modifiers of Survival Motor Neuron 2 as a Treatment for Spinal Muscular Atrophy. *J. Med. Chem.* **2016**, *59* (13), 6070–6085.

(68) Krapcho, A. P.; Weimaster, J. F.; Eldridge, J. M.; Jahngen, E. G. E.; Lovey, A. J.; Stephens, W. P. Synthetic Applications and Mechanism Studies of the Decarbalkoxylations of Geminal Diesters and Related Systems Effected in MeaSO by Water and/or by Water with Added Salts. *J. Org. Chem.* **1978**, *43* (1), 138–147.

(69) Sandoval, R.; Lazcano, P.; Ferrari, F.; Pinto-Pardo, N.; González-Billault, C.; Utreras, E. TNF-α Increases Production of Reactive Oxygen Species through Cdk5 Activation in Nociceptive Neurons. *Front. Physiol.* **2018**, *9* (FEB).

(70) Yang, P.; Huang, S.; Xu, A. *The Oxidative Burst System in Amphioxus*; China Science Publishing & Media Ltd., 2016.

(71) Yan, Q.; Bruchez, M. P.; Laboratories, E.; Biosensor, M. HHS Public Access. **2016**, *360* (1), 179–194.

(72) Giepmans, B. N. G.; Adams, S. R.; Ellisman, M. H.; Tsien, R. Y. The Fluorescent Toolbox for Assessing Protein Location and Function. *Science (80-.).* **2006**, *312* (5771), 217–224.

(73) Lichty, J. J.; Malecki, J. L.; Agnew, H. D.; Michelson-Horowitz, D. J.; Tan, S. Comparison

of Affinity Tags for Protein Purification. *Protein Expr. Purif.* **2005**, *41* (1), 98–105.

(74) Mchowat, J.; Mchowat, J.; Jones, J. H.; Jones, J. H.; Creer, M. H.; Creer, M. H. On Methodology. *J. Lipid Res.* **1996**, *37*, 2450–2460.

(75) Boersema, P. J.; Raijmakers, R.; Lemeer, S.; Mohammed, S.; Heck, A. J. R. Multiplex Peptide Stable Isotope Dimethyl Labeling for Quantitative Proteomics. *Nat. Protoc.* **2009**, *4* (4), 484–494.

(76) Tamura, T.; Hamachi, I. Chemistry for Covalent Modification of Endogenous/Native Proteins: From Test Tubes to Complex Biological Systems. *J. Am. Chem. Soc.* **2018**, *141*, 2782–2799.

(77) Lodish H, Berk A, Zipursky SL, et al. *Molecular Cell Biology*, Fourth.; Freeman, W. H., Ed.; New York, 2000.

(78) DeGruyter, J. N.; Malins, L. R.; Baran, P. S. Residue-Specific Peptide Modification: A Chemist's Guide. *Biochemistry* **2017**, *56* (30), 3863–3873.

(79) Bottcher, T.; Sieber, S. A. Beta-Lactones As Privileged Structures for the Active-Site Labeling of Versatile Bacterial Enzyme Classes. *Angew. Chemie - Int. Ed.* **2008**, *47* (24), 4600–4603.

(80) Bernad, A.; Nieto, M. A.; Vioque, A.; Palacihn, E. Biochimica et Biophysica Acta 873 (1986) 350-355. **1986**, *873*, 350–355.

(81) Tanaka, K.; Fujii, Y.; Fukase, K. Site-Selective and Nondestructive Protein Labeling through Azaelectrocyclization-Induced Cascade Reactions. *ChemBioChem* **2008**, *9* (15), 2392–2397.

(82) Diethelm, S.; Schafroth, M. A.; Carreira, E. M. Amine-Selective Bioconjugation Using Arene Diazonium Salts. *Org. Lett.* **2014**, *16* (15), 3908–3911.

(83) Tung, C. L.; Wong, C. T. T.; Fung, E. Y. M.; Li, X. Traceless and Chemoselective Amine Bioconjugation via Phthalimidine Formation in Native Protein Modification. *Org. Lett.* **2016**, *18* (11), 2600–2603.

(84) Jansen, J. E.; Shaver, F. W.; Bankert, R. A.; Vol, F. T. F.; Fiedorek, F. T. Reactions with Ammonia. *J. Am. Chem. Soc.* **1951**, *73*, 3168–3171.

(85) Weibel, E. K.; Hadvary, P.; Hochuli, E.; Kupfer, E.; Lengsfeld, H. Lipstatin, an Inhibitor of Pancreatic Lipase, Produced by Streptomyces Toxytricini. I. Producing Organism, Fermentation, Isolation and Biological Activity. *J. Antibiot. (Tokyo).* **1987**, *40* (8), 1081–1085.

(86) De Pascale, G.; Nazi, I.; Harrison, P. H. M.; Wright, G. D. β-Lactone Natural Products and Derivatives Inactivate Homoserine Transacetylase, a Target for Antimicrobial Agents. *J. Antibiot. (Tokyo).* **2011**, *64* (7), 483–487.

(87) Skaff, D. A.; Ramyar, K. X.; McWhorter, W. J.; Barta, M. L.; Geisbrecht, B. V.; Miziorko, H. M. Biochemical and Structural Basis for Inhibition of *Enterococcus Faecalis* Hydroxymethylglutaryl-CoA Synthase, MvaS, by Hymeglusin. *Biochemistry* **2012**, *51* (23), 4713–4722.

(88) Colin, D. Y.; Deprez-Beauclair, P.; Allouche, M.; Brasseur, R.; Kerfelec, B. Exploring the Active Site Cavity of Human Pancreatic Lipase. *Biochem. Biophys. Res. Commun.* **2008**, *370* (3), 394–398.

(89) Mirza, I. A.; Nazi, I.; Korczynska, M.; Wright, G. D.; Berghuis, A. M. Crystal Structure of Homoserine Transacetylase from Haemophilus Influenzae Reveals a New Family of Alpha/Beta-Hydrolases. *Biochemistry* **2005**, *44* (48), 15768–15773.

(90) Theisen, M. J.; Misra, I.; Saadat, D.; Campobasso, N.; Miziorko, H. M.; Harrison, D. H. T. 3-Hydroxy-3-Methylglutaryl-CoA Synthase Intermediate Complex Observed in "Real-Time". *Proc. Natl. Acad. Sci. U. S. A.* **2004**, *101* (47), 16442–16447.

(91) Edwin, L.; Hudrlik, A. M. 1 4 6 5. **1989**, *68* (23), 5613–5618.

(92) 1 - The Peterson Olefination Reaction.Pdf.

(93) Li, Z.; Yang, C.; Zheng, H.; Qiu, H.; Lai, G. Selective Mono- and Di-Allylation and Allenylation of Chlorosilanes Using Indium. *J. Organomet. Chem.* **2008**, *693* (25), 3771–3779.

(94) Fessenden, R. J.; Fessenden, J. S. Convenient Synthesis of .Alpha.-Silyl Esters. *J. Org. Chem.* **1967**, *32* (11), 3535–3537.

(95) Wedler, C.; Kunath, A.; Schick, H. Synthesis of β-Lactones via a Spontaneous Intramolecular Cyclization of O-Lithiated Phenyl Β′-Hydroxyalkanoates Obtained by Aldolization of Ketones or Aldehydes with Lithium Enolates of Phenyl Esters. *J. Org. Chem.* **1995**, *60* (3), 758–760.

(96) Jung, M. E.; Piizzi, G. Gem-Disubstituent Effect : Theoretical Basis and Synthetic Applications Gem-Disubstituent Effect : Theoretical Basis and Synthetic Applications. *Chem. Rev.* **2005**, *105* (5), 1735–1766.

(97) Bellassoued, M.; Dubois, J. E.; Bertounesque, E. A Simple Preparation of Trimethylsilyl Acetic Acid. *Synth. Commun.* **2006**, No. December 2014, 37–41.

(98) Brady, W. T.; Saidi, K. Trimethylsilylketene. Cycloadditions of Ketenes and Aldehydes. *J. Org. Chem.* **1979**, *44* (5), 733–737.

(99) Ramachandran, V. A Bird' s Eye View. *Sanctuary Asia* **2009**, *5*, 60–65.

(100) George A. Olah, An-hsiang Wu, O. F. Intramolecular Dehydration of Dialkylacetic Acids

and Trimethylsilylacetic Acid with DCC to the Corresponding Ketenes.Pdf. *Synthesis (Stuttg).* **1989**, *7*, 568.

(101) Ma, M.; Hao, W.; Ma, L.; Zheng, Y.; Lian, P.; Wan, X. Interception of Radicals by Molecular Oxygen and Diazo Compounds: Direct Synthesis of Oxalate Esters Using Visible-Light Catalysis. *Org. Lett.* **2018**, *20* (18), 5799–5802.

(102) Schwarz, D. M. C.; Gestwicki, J. E. Revisiting the "Art of the Chemical Probe." *ACS Chem. Biol.* **2018**, *13* (5), 1109–1110.

(103) Babior, B. M. NADPH Oxidase: An Update. **2018**, *93* (5), 1464–1476.

(104) Rosales-Corral, S.; Reiter, R. J.; Tan, D.-X.; Ortiz, G. G.; Lopez-Armas, G. Functional Aspects of Redox Control during Neuroinflammation. *Antioxid. Redox Signal.* **2010**, *13* (2), 193–247.

(105) Böttcher, T.; Sieber, S. A. β-Lactams and β-Lactones as Activity-Based Probes in Chemical Biology. *Medchemcomm* **2012**, *3* (4), 408–417.

(106) Unsain, N.; Heard, K. N.; Higgins, J. M.; Barker, P. A. Production and Isolation of Axons from Sensory Neurons for Biochemical Analysis Using Porous Filters. *J. Vis. Exp.* **2014**, *89* (July), 1–8.

Appendices

Appendix A NMR DATA

Figure AA-1. ^{1}H NMR spectrum for benzyl azide (18)

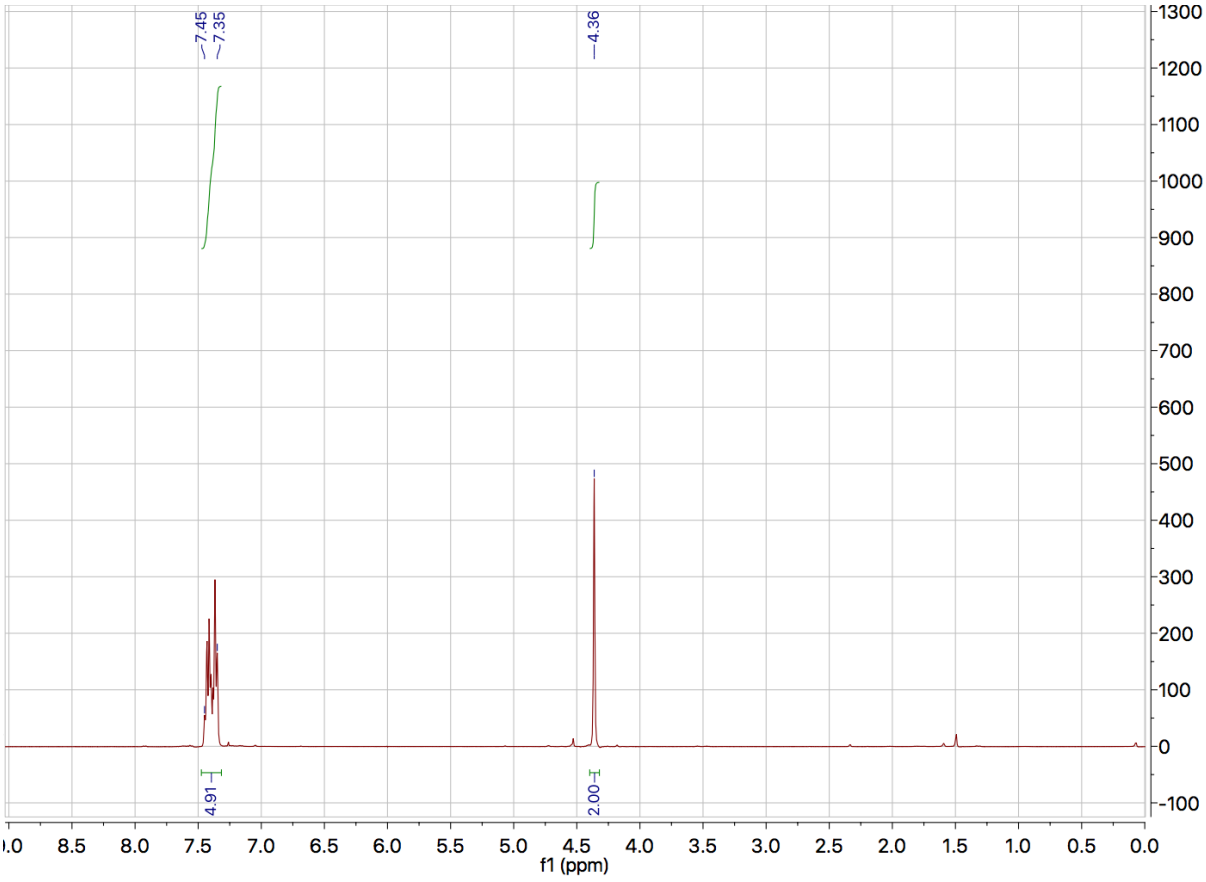

Figure AA-2. ^{1}H NMR spectrum for 5-Amino-1-benzyl-1*H*-1,2,3-triazole-4-carboxamide (24)

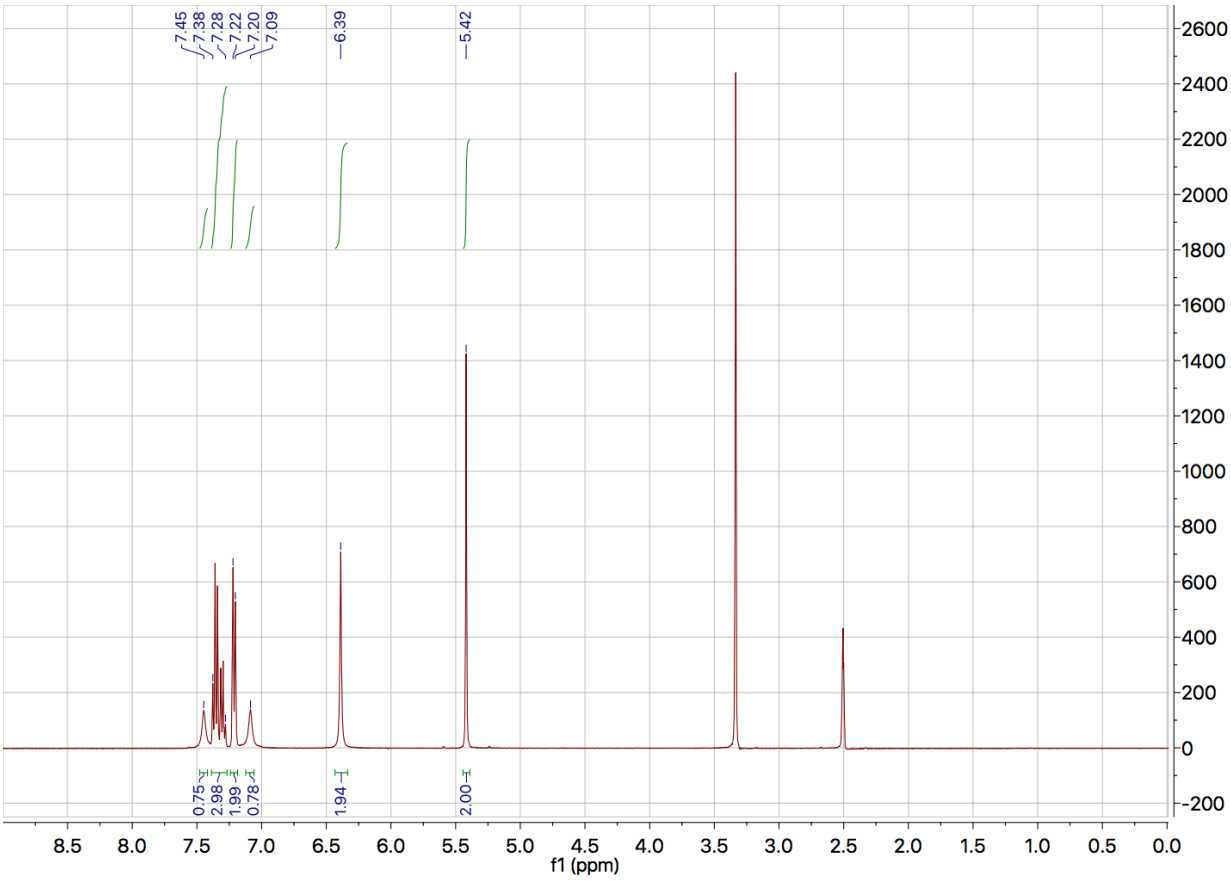

Figure AA-3. ^{1}H NMR spectrum for 3-Benzyl-3*H*-[1,2,3]triazolo[4,5-*d*]pyrimidin-7-ol (15)

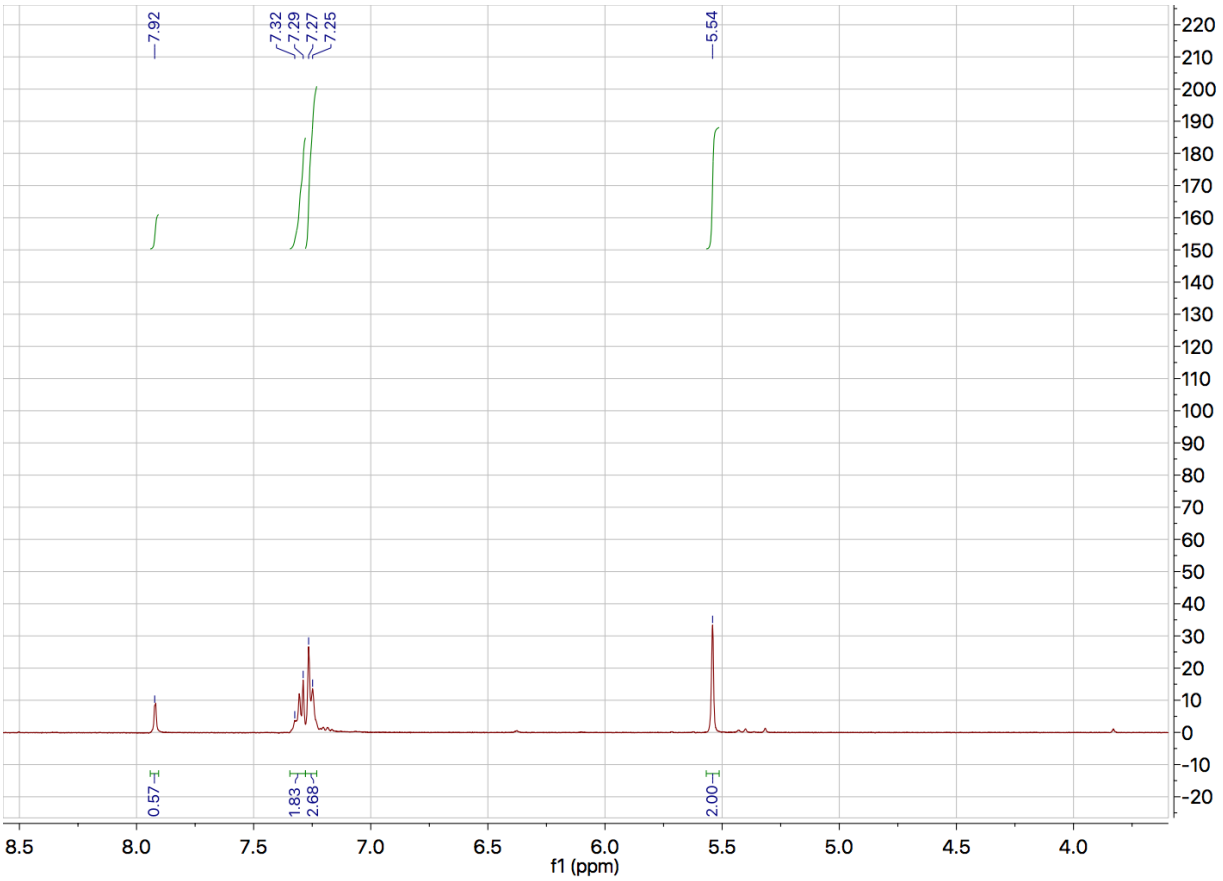

Figure AA-4. ^{1}H NMR spectrum for 4,6-Dichloro-5-nitropyrimidine (39)

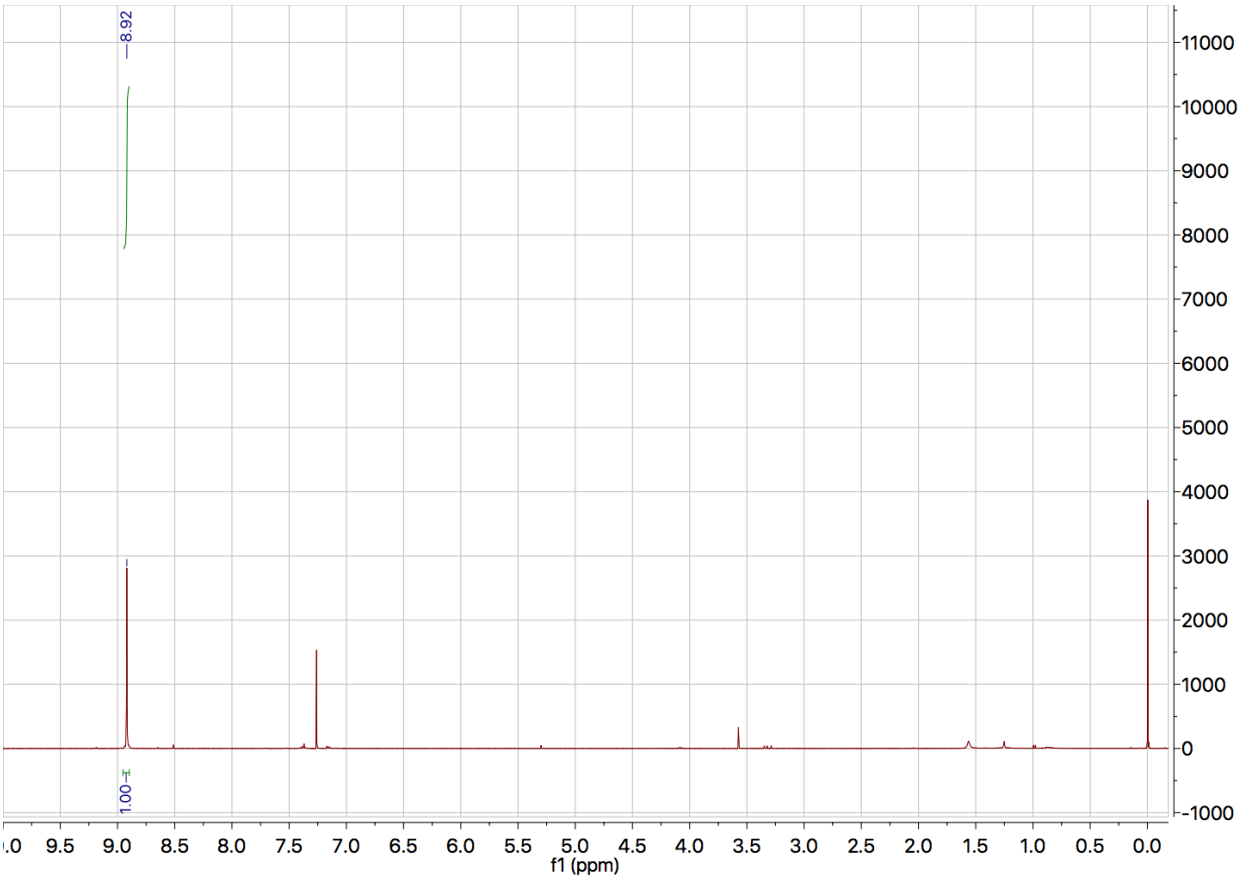

Figure AA-5. ^{1}H NMR spectrum for 5-Amino-4,6-dichloropyrimidine (20)

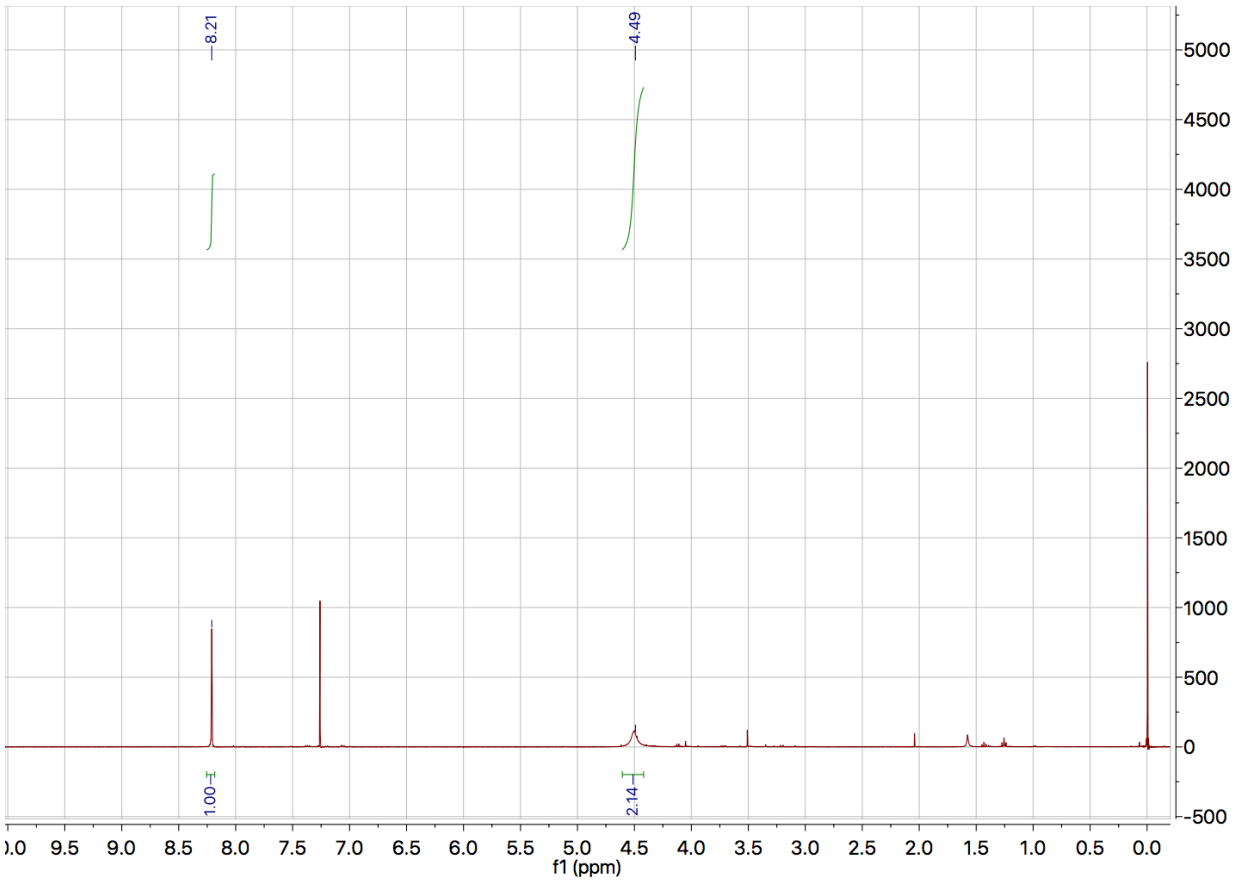

Figure AA-6. ^{1}H NMR spectrum for 5-Amino-4-chloro-6-(benzylamino)pyrimidine (40)

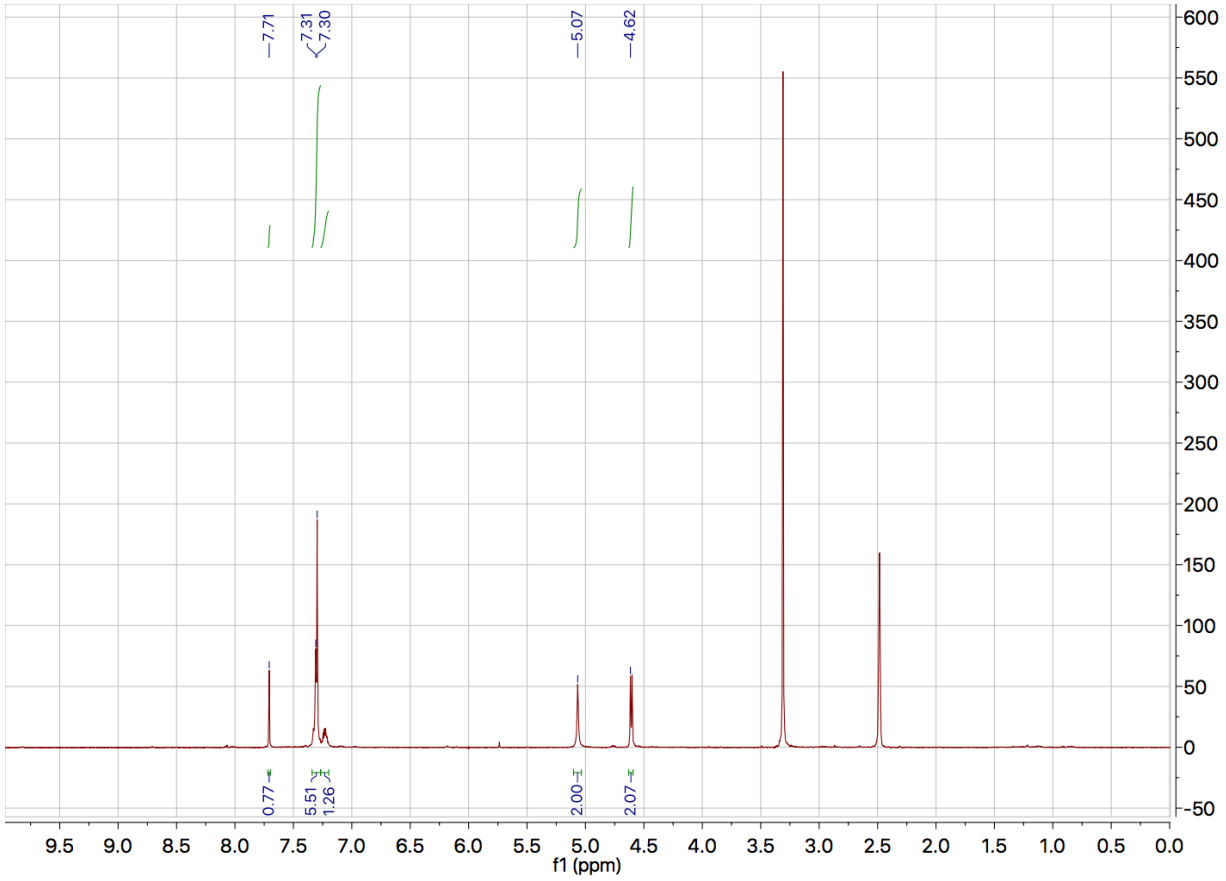

Figure AA-7. ^{1}H NMR spectrum for 3-Benzyl-7-chloro-3*H*-[1,2,3]triazolo[4,5-*d*]pyrimidine (13)

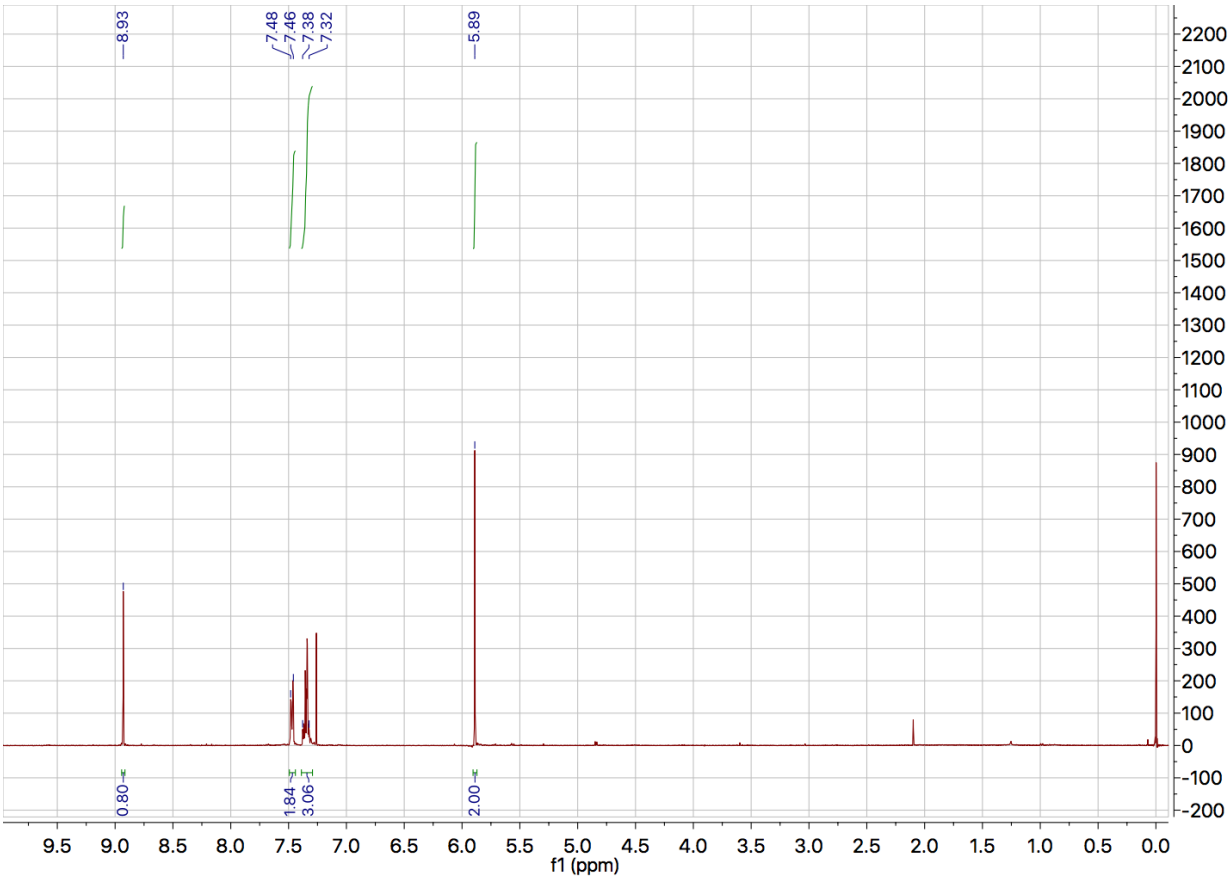

Figure AA-8. ^{1}H NMR spectrum for 7-(1,3-Benzoxazol-2-ylsulfanyl)-3-benzyl-3H-[1,2,3]triazolo[4,5-d]pyrimidine (1)

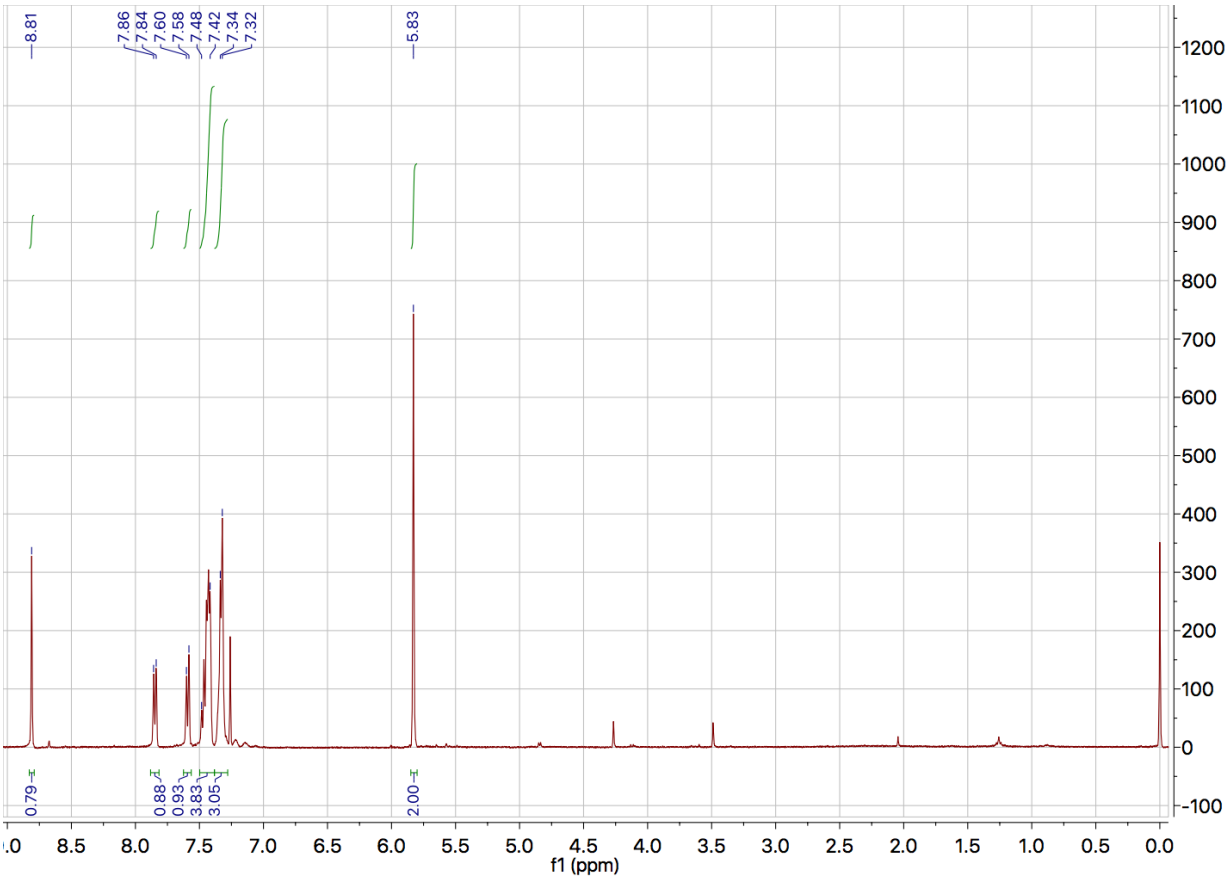

Figure AA-9. ^{1}H NMR spectrum for 1,4-Bis(azidomethyl)benzene (19)

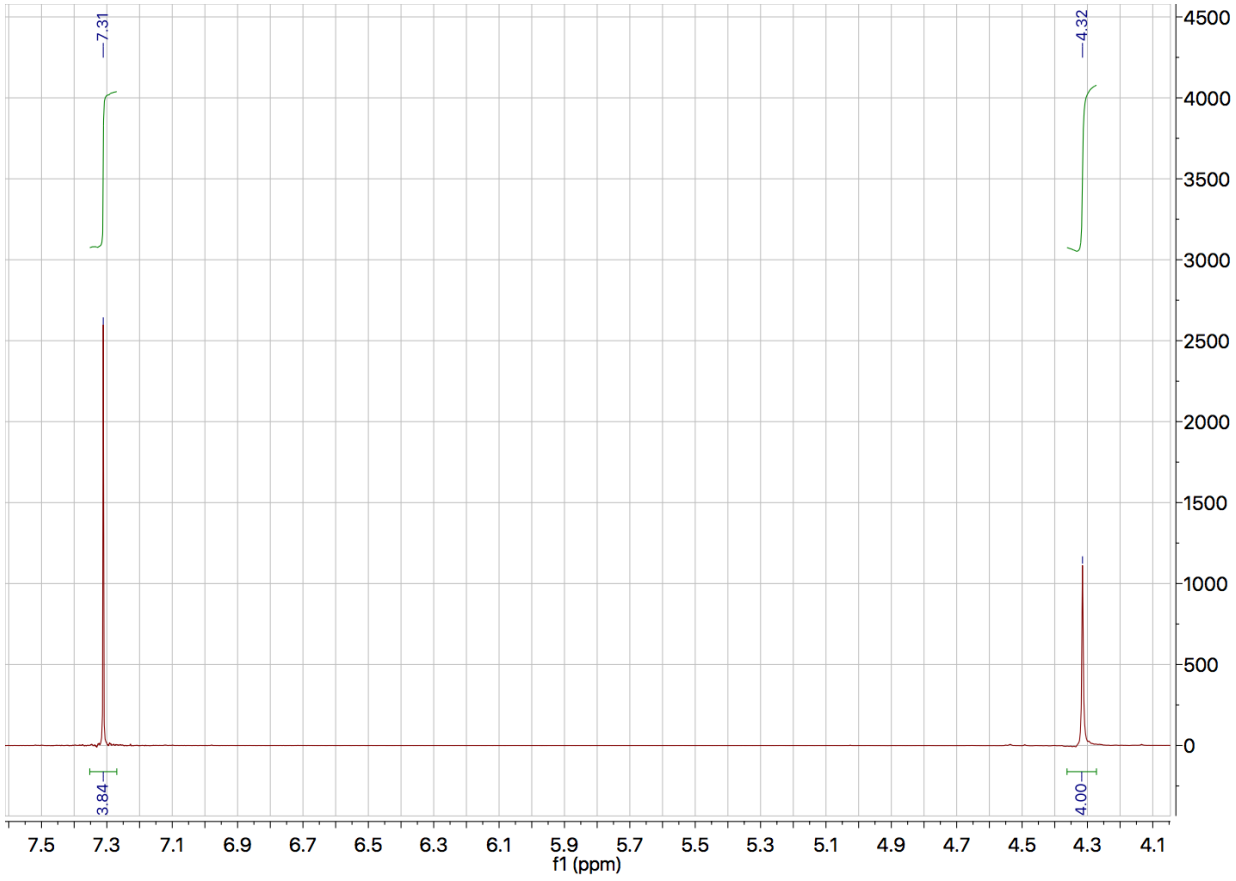

Figure AA-10. ^{1}H NMR spectrum for 4-(Azidomethyl)benzylamine (22)

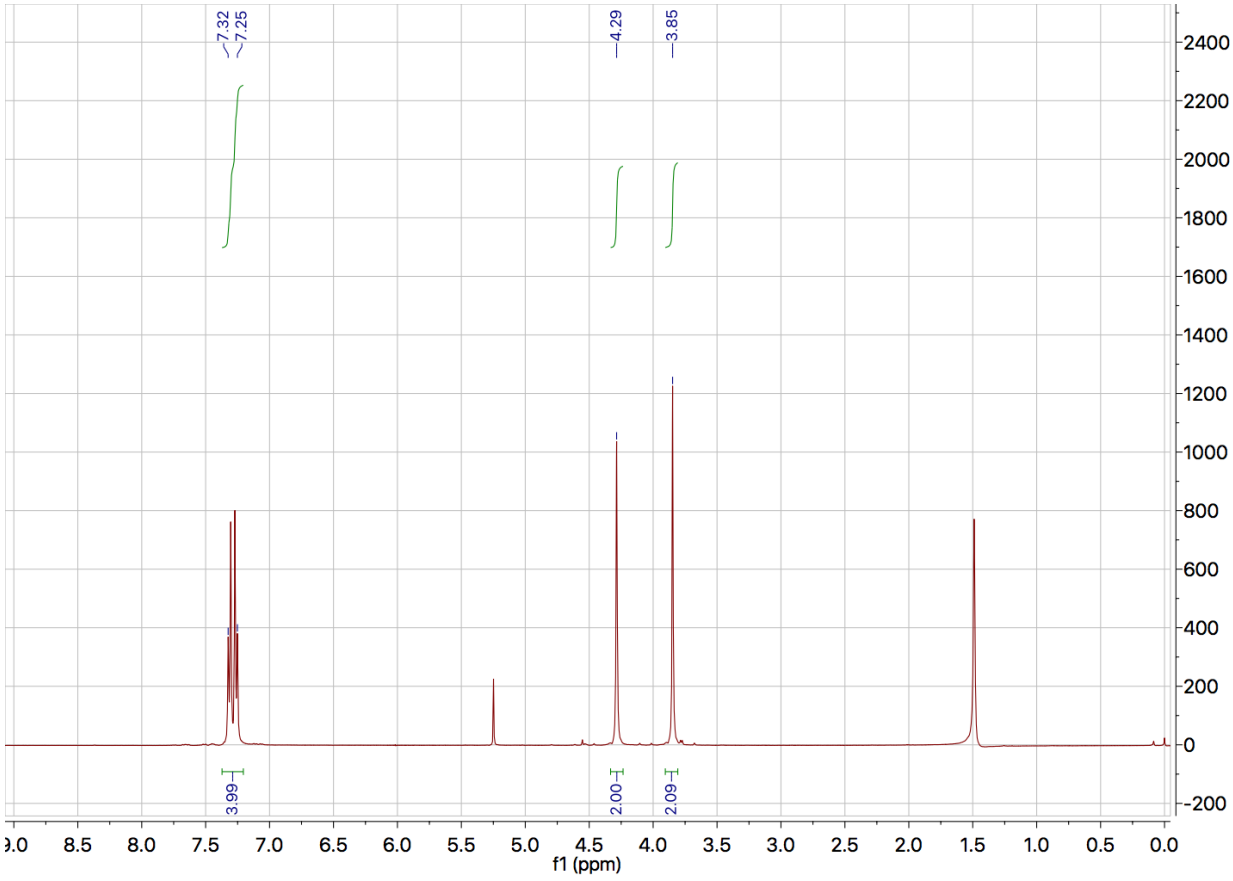

Figure AA-11. ^{1}H NMR spectrum for 5-Amino-4-chloro-[6-(4-azidomethyl)benzylamino]pyrimidine (42)

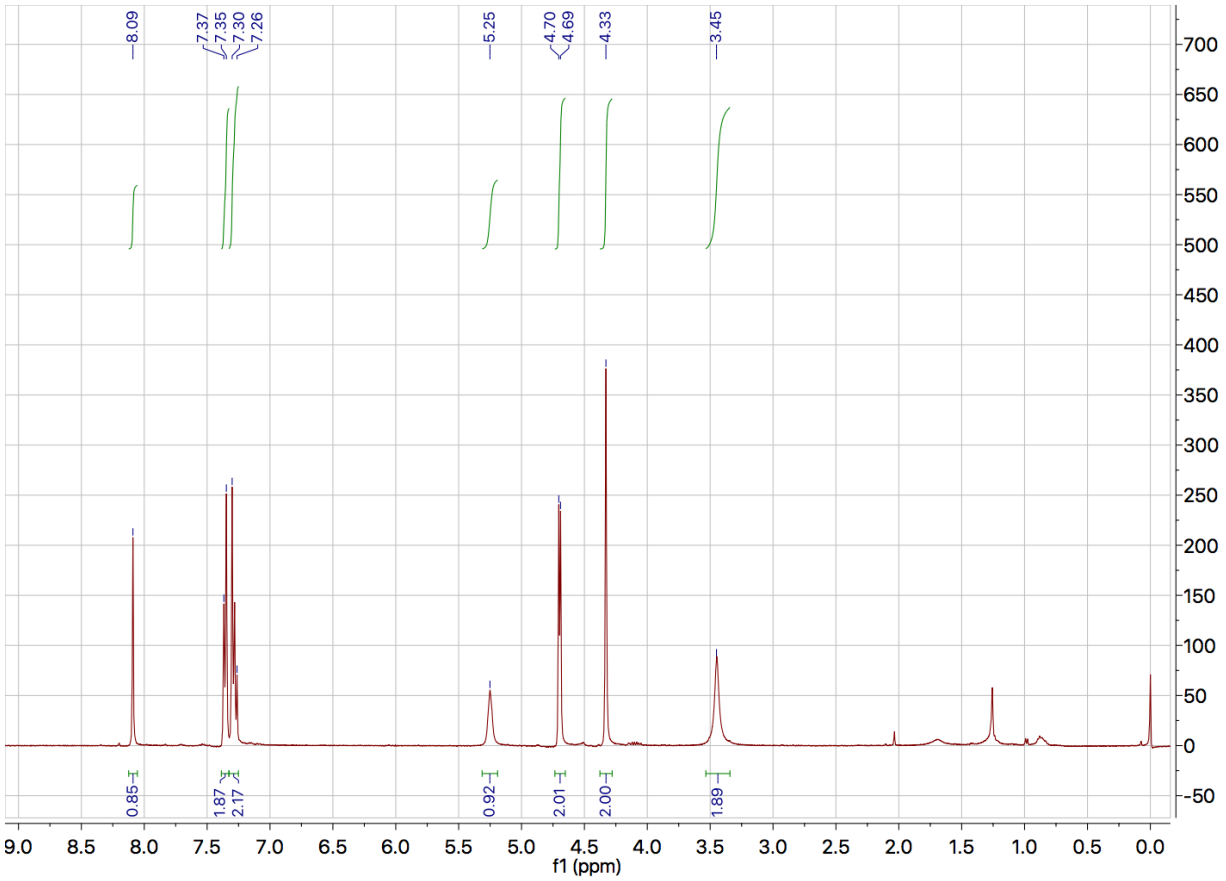

Figure AA-12. ^{13}C NMR spectrum for 5-Amino-4-chloro-[6-(4-azidomethyl)benzylamino]pyrimidine (42)

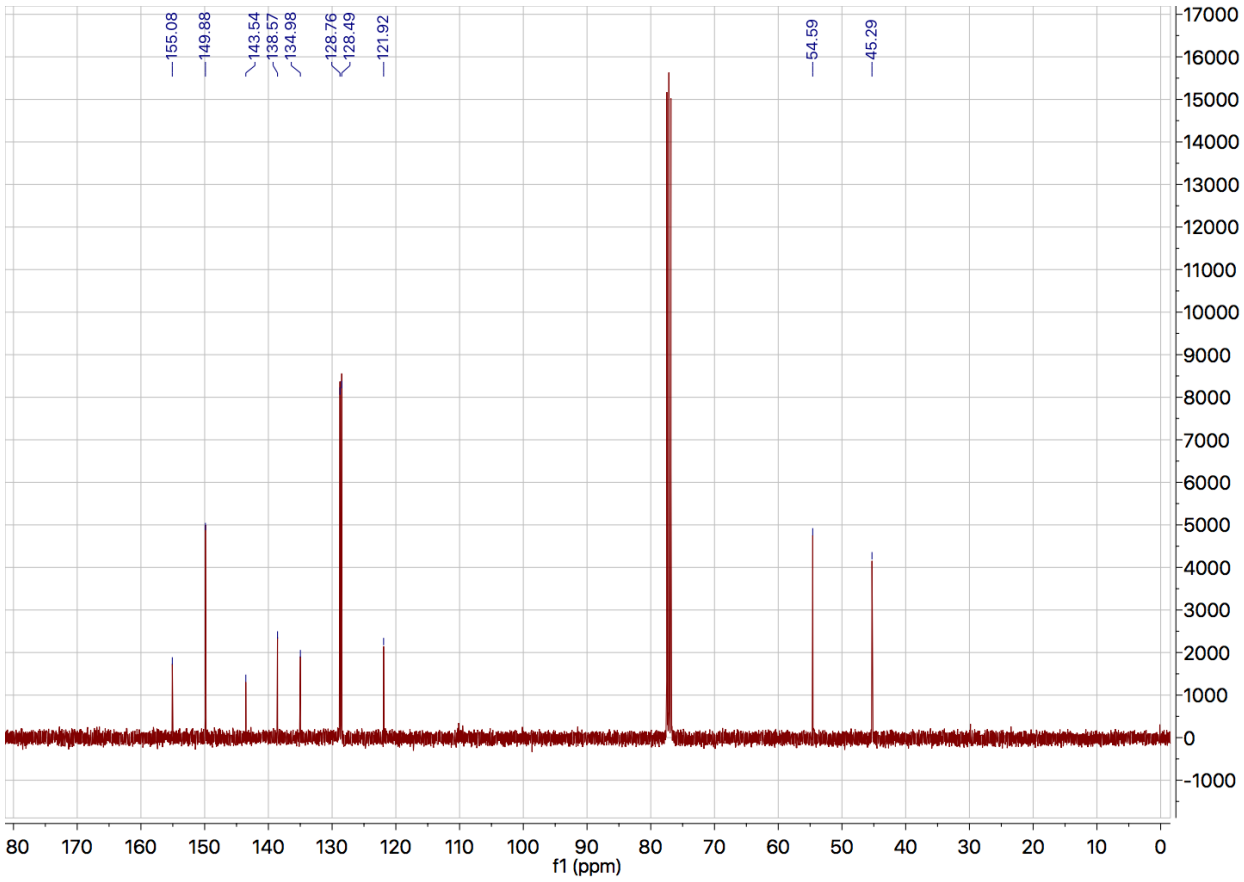

Figure AA-13. ^{1}H NMR spectrum for 7-Chloro-[3-(4-(azidomethyl)benzyl)]-3*H*-[1,2,3]triazolo[4,5-d]pyrimidine (14)

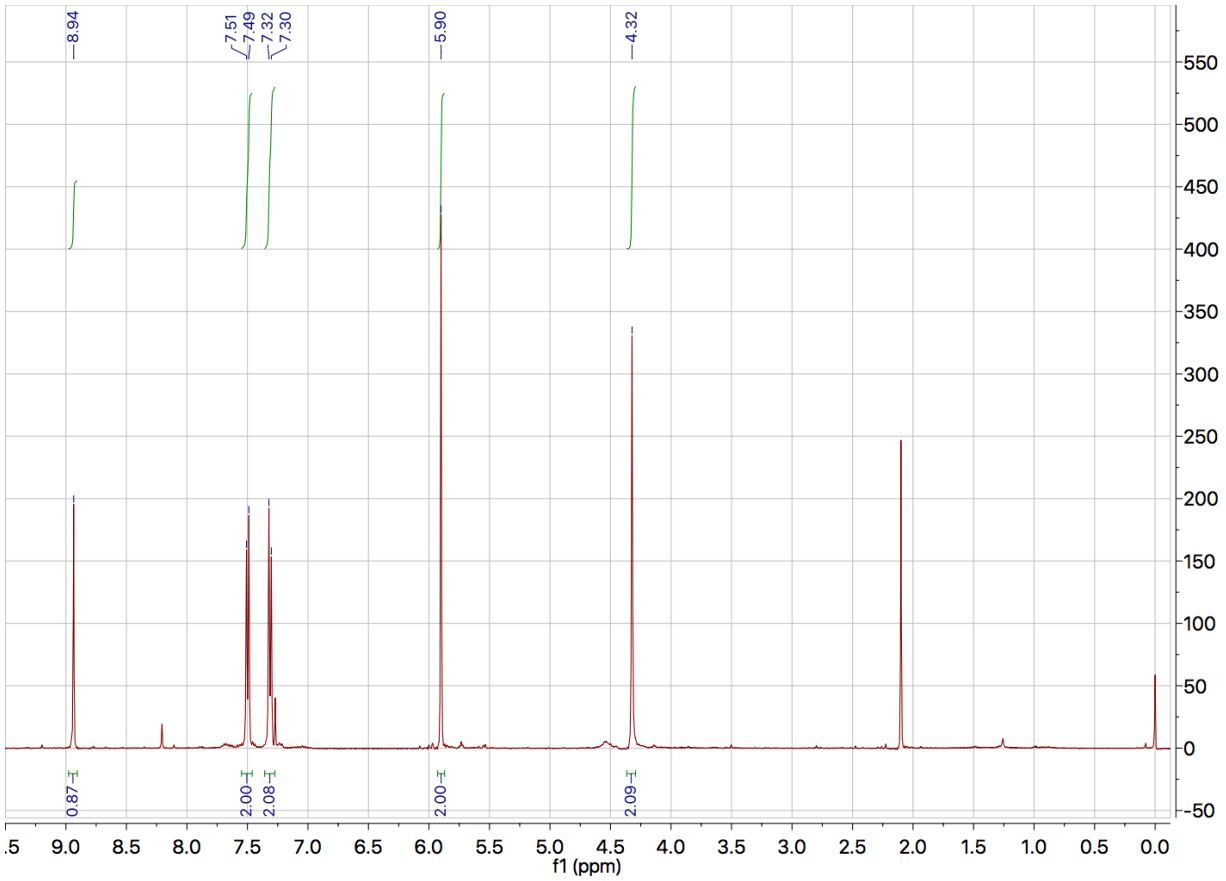

Figure AA-14. ^{13}C NMR spectrum for 7-Chloro-[3-(4-(azidomethyl)benzyl)]-3*H*-[1,2,3]triazolo[4,5-d]pyrimidine (14)

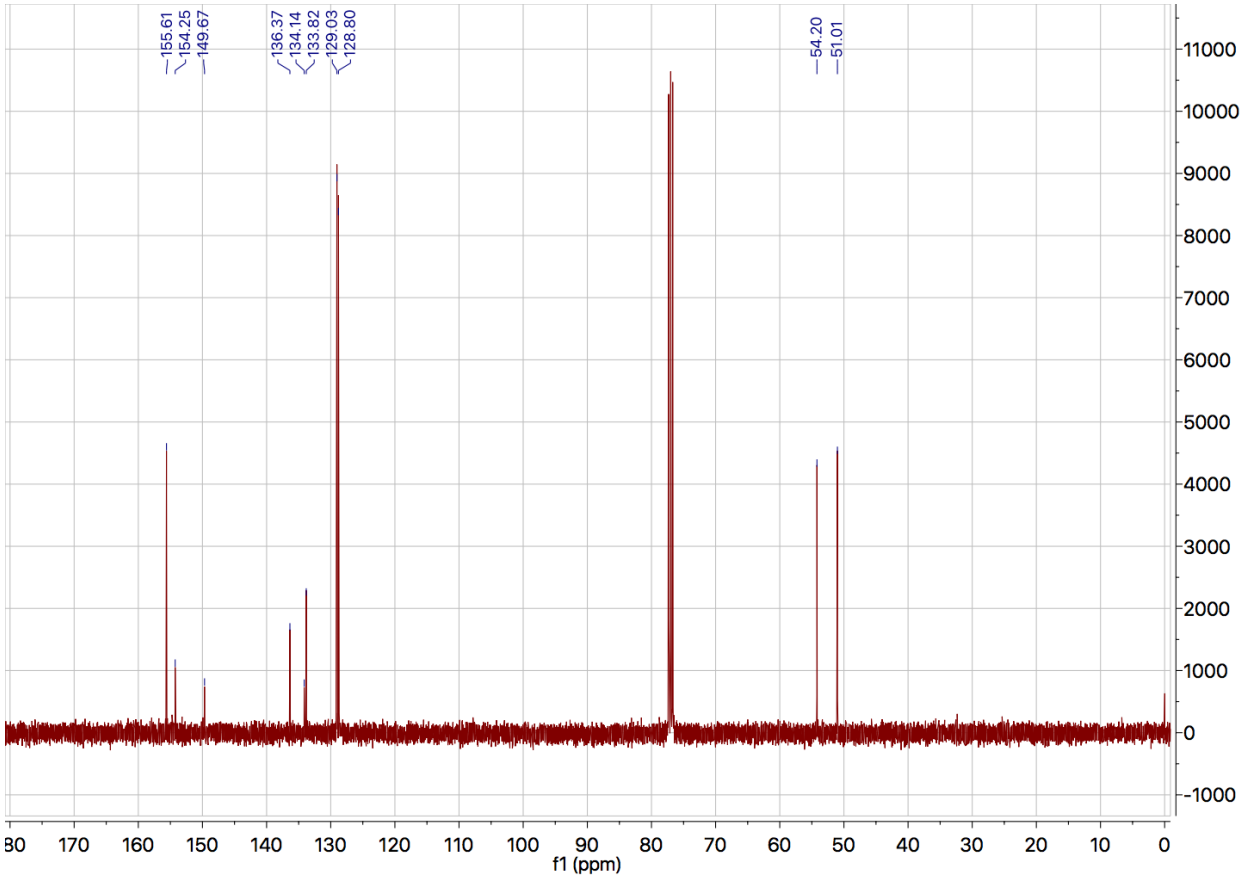

Figure AA-15. ^{1}H NMR spectrum for 7-(1,3-Benzoxazol-2-ylsulfanyl)-[3-(4-(azidomethyl)benzyl)]-3H-[1,2,3]triazolo[4,5-d]pyrimidine (2)

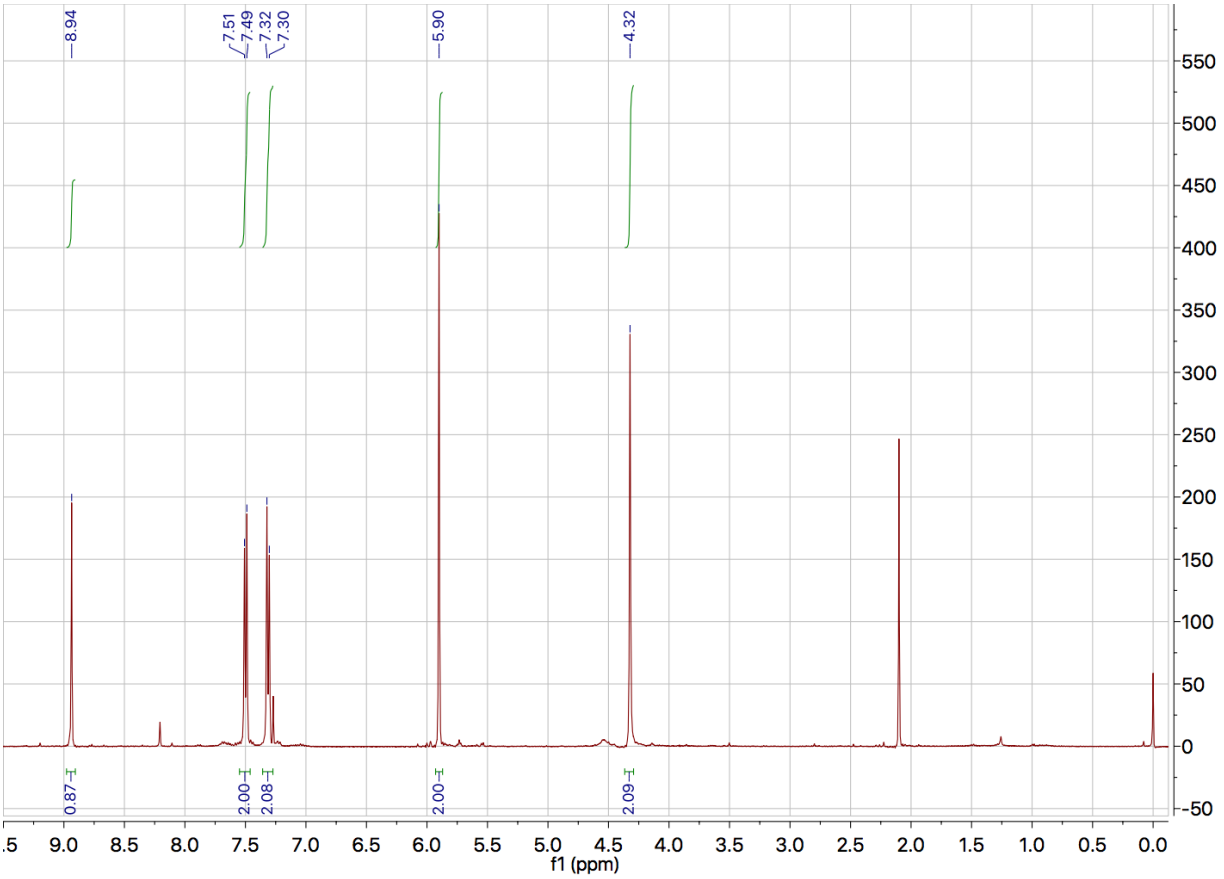

Figure AA-16. ^{13}C NMR spectrum for 7-(1,3-Benzoxazol-2-ylsulfanyl)-[3-(4-(azidomethyl)benzyl)]-3H-[1,2,3]triazolo[4,5-d]pyrimidine (2)

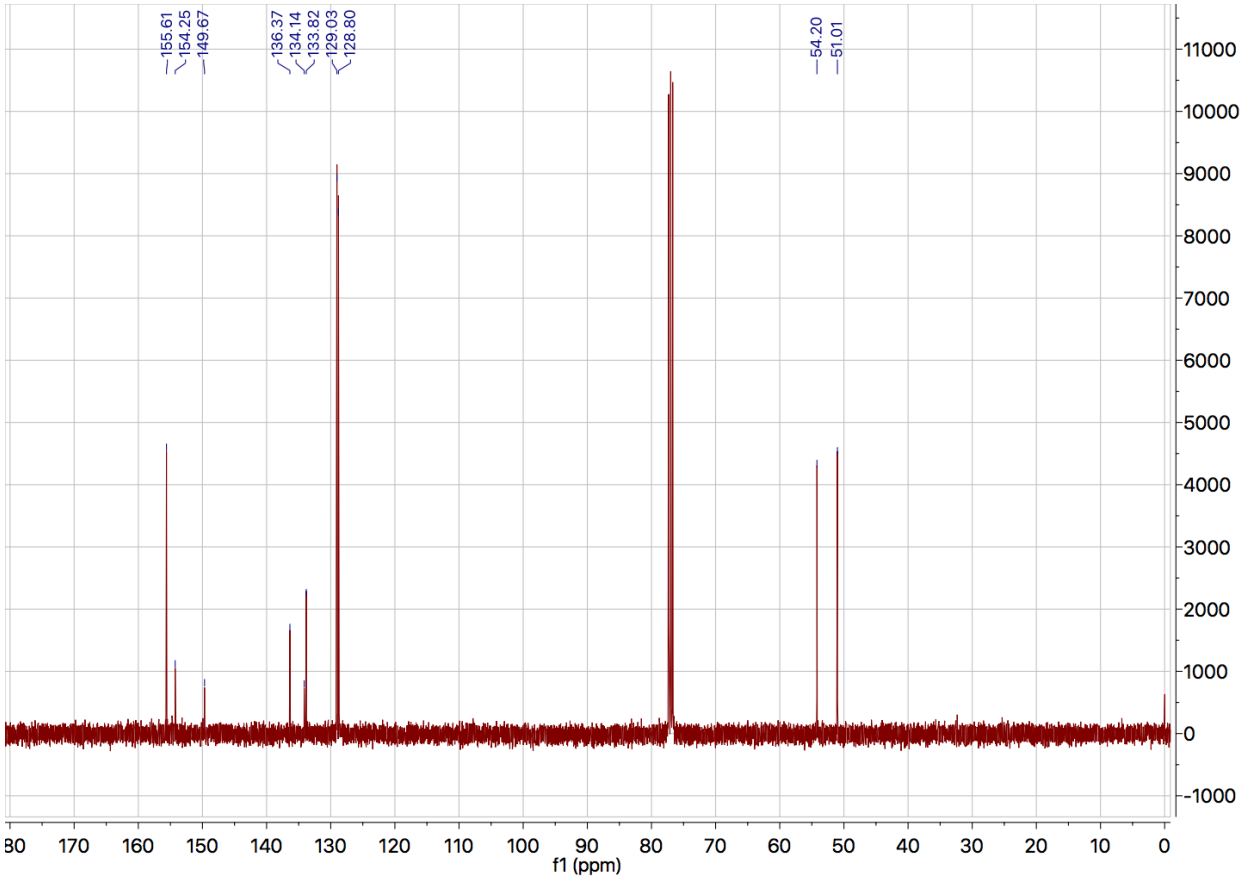

Figure AA-17. ^{1}H NMR spectrum for diethyl 2-(3-benzyl-3,6-dihydro-7*H*-[1,2,3]triazolo[4,5-*d*]pyrimidin-7-ylidene)malonate (52)

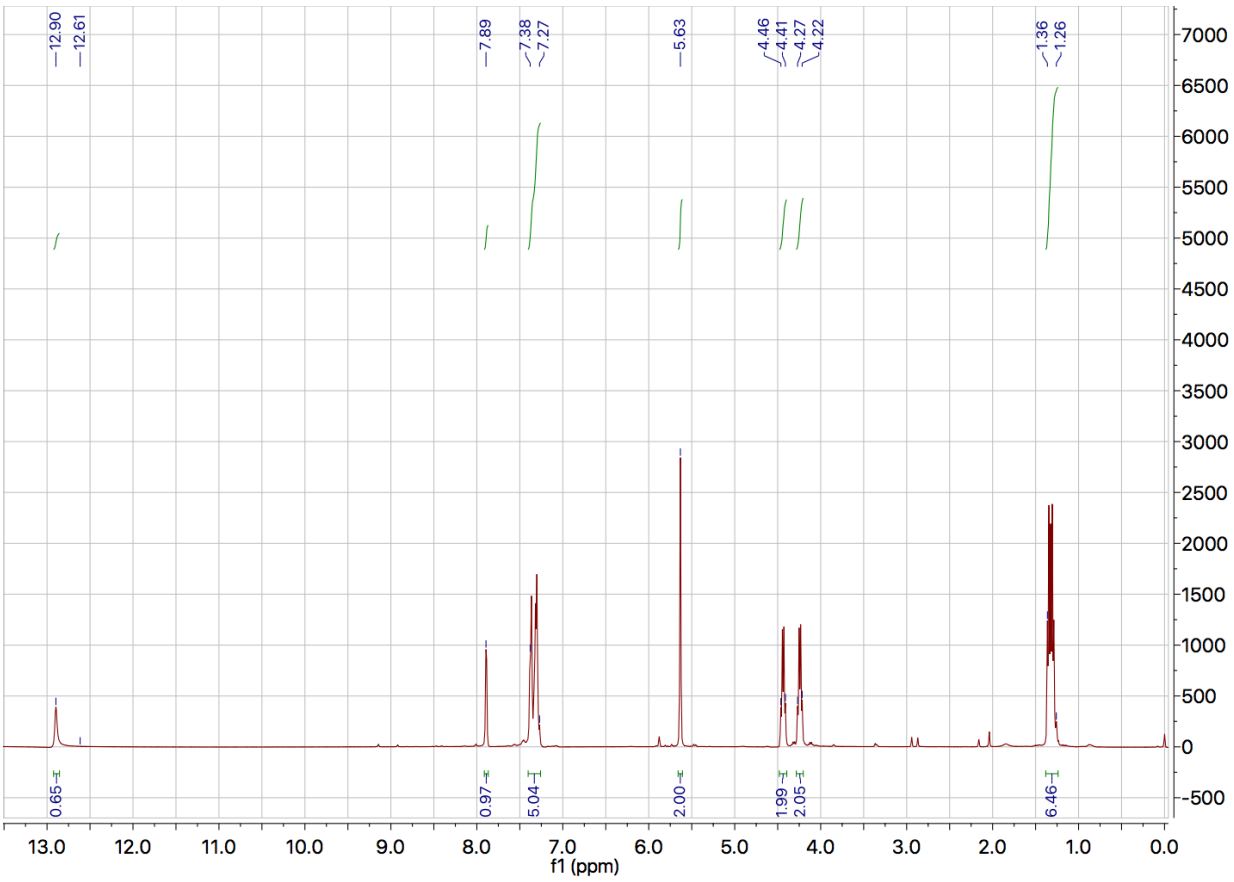

Figure AA-18. ^{13}C NMR spectrum for diethyl 2-(3-benzyl-3,6-dihydro-7*H*-[1,2,3]triazolo[4,5-*d*]pyrimidin-7-ylidene)malonate (52)

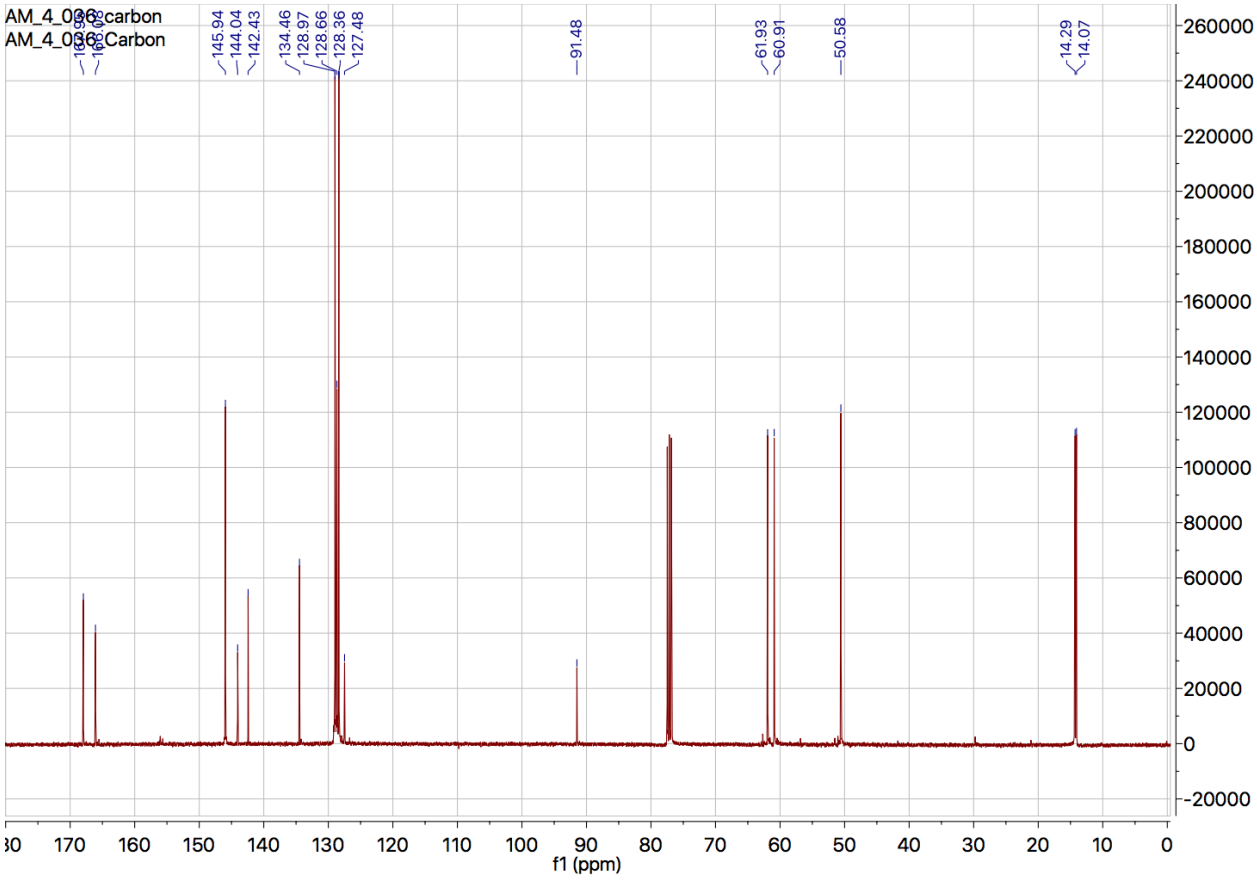

Figure AA-19. ^{1}H NMR spectrum for ethyl (*Z*)-2-(3-benzyl-3,6-dihydro-7*H*-[1,2,3]triazolo[4,5-*d*]pyrimidin-7-ylidene)-2-cyanoacetate (51)

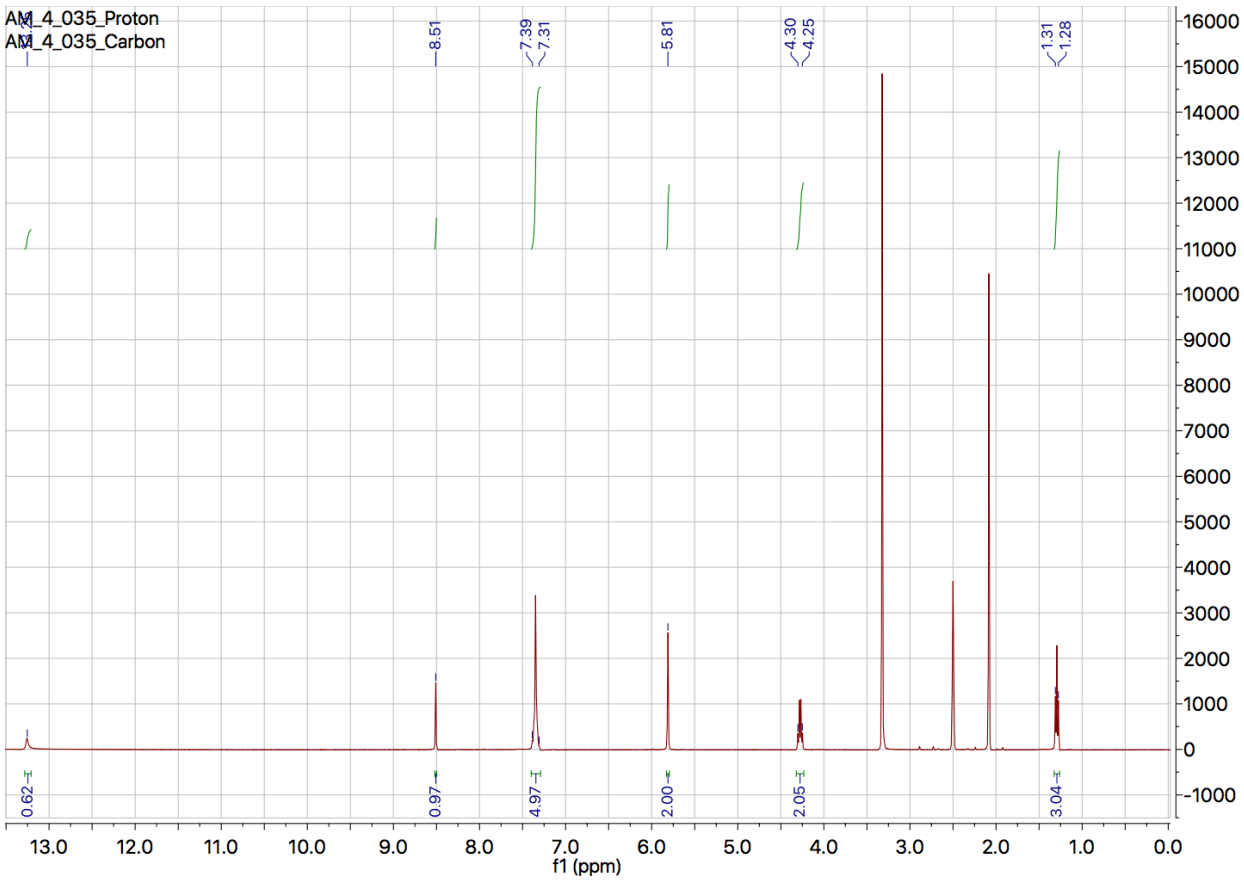

Figure AA-20. ^{13}C NMR spectrum for ethyl (*Z*)-2-(3-benzyl-3,6-dihydro-7*H*-[1,2,3]triazolo[4,5-*d*]pyrimidin-7-ylidene)-2-cyanoacetate (51)

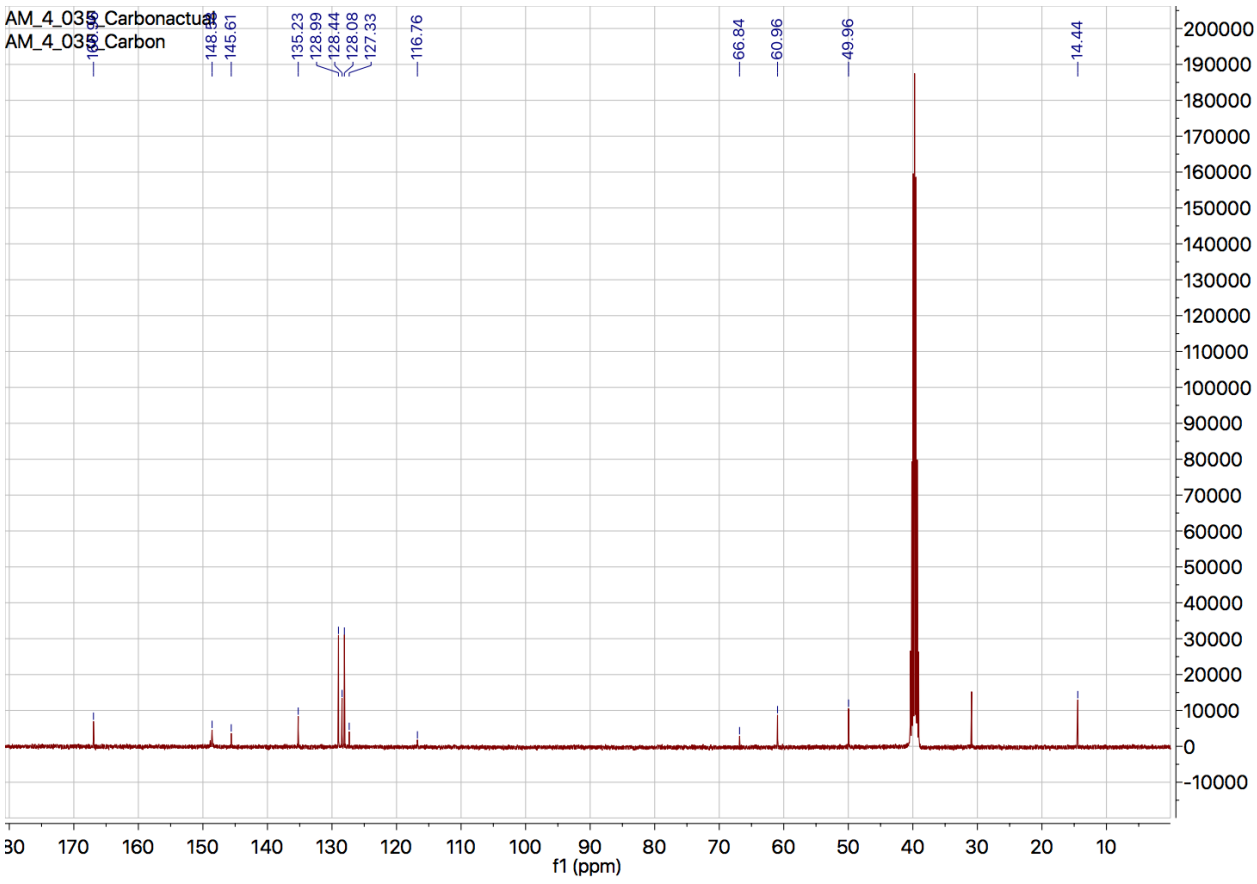

Figure AA-21. ^{1}H NMR spectrum for ethyl 3-ethoxy-3-iminopropanoate hydrochloride (57)

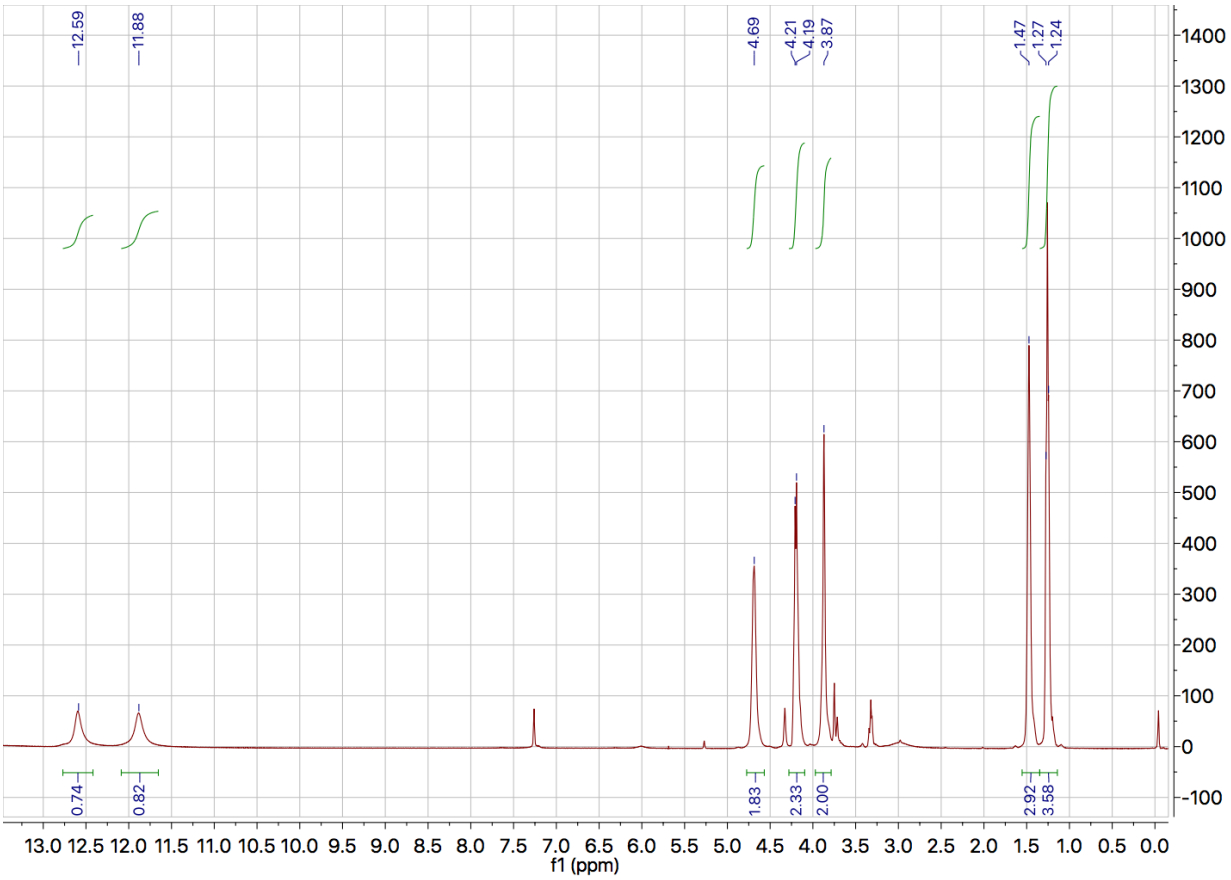

Figure AA-22. ^{1}H NMR spectrum for ethyl 2-(benzo[*d*]oxazol-2-yl)acetate (49)

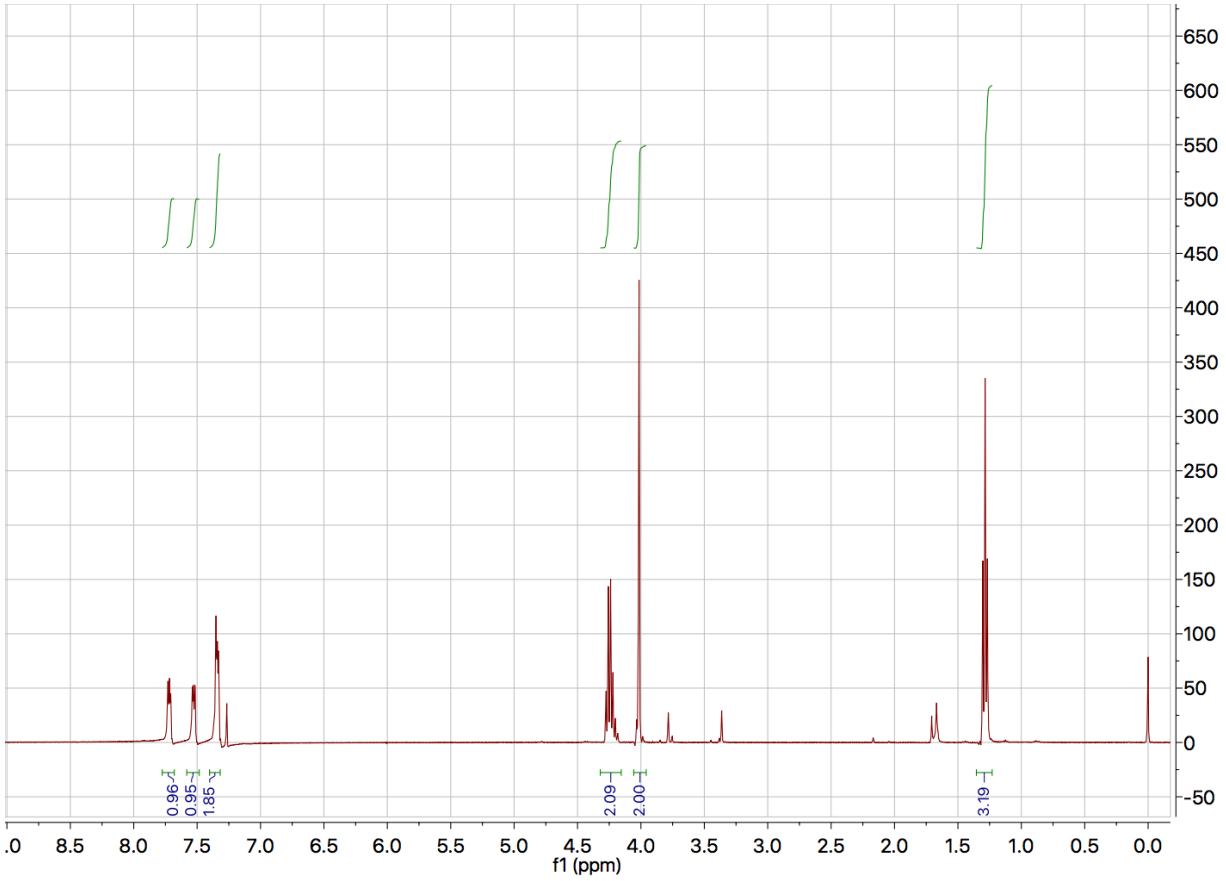

Figure AA-23. ^{1}H NMR spectrum for ethyl (*E*)-2-(benzo[*d*]oxazol-2-yl)-2-(3-benzyl-3,6-dihydro-7*H*-[1,2,3]triazolo[4,5-*d*]pyrimidin-7-ylidene)acetate (53)

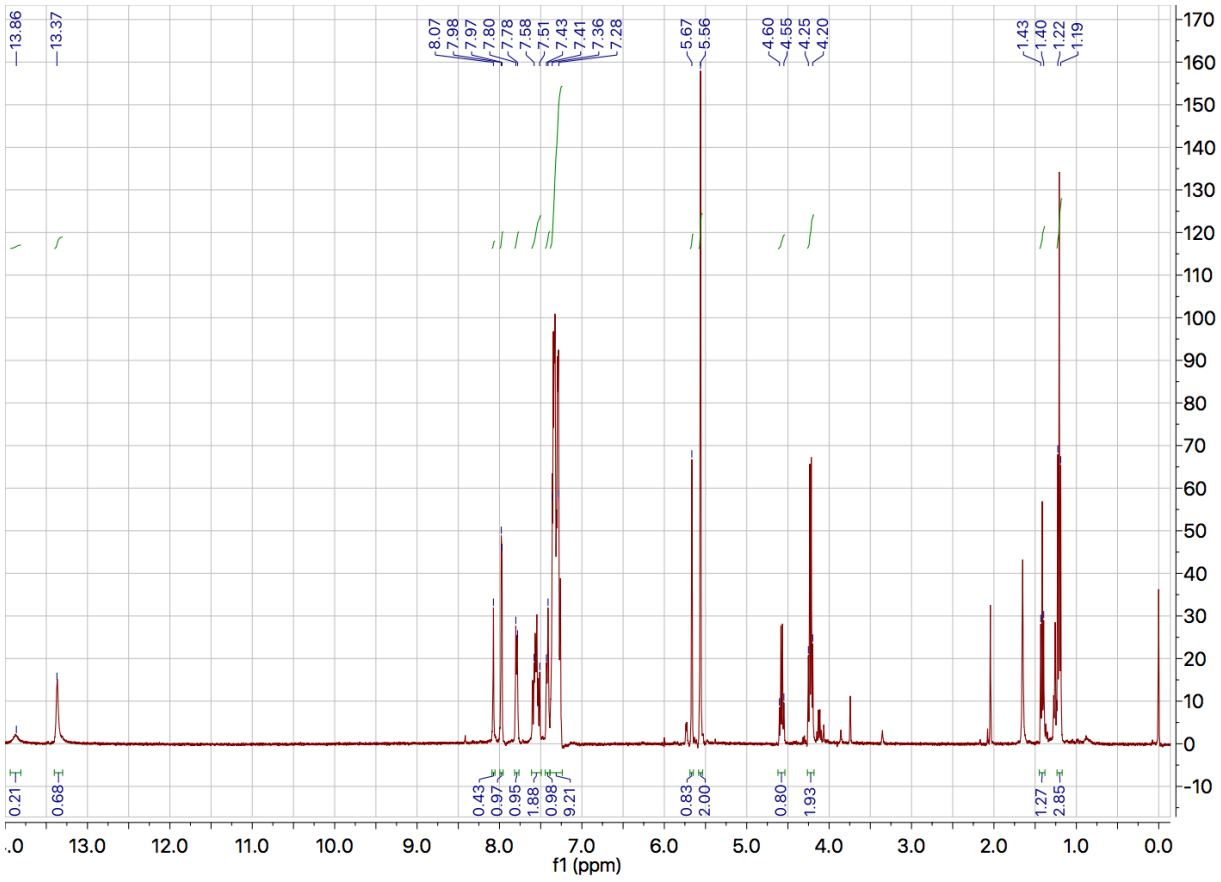

Figure AA-24. ^{13}C NMR spectrum for ethyl (*E*)-2-(benzo[*d*]oxazol-2-yl)-2-(3-benzyl-3,6-dihydro-7*H*-[1,2,3]triazolo[4,5-*d*]pyrimidin-7-ylidene)acetate (53)

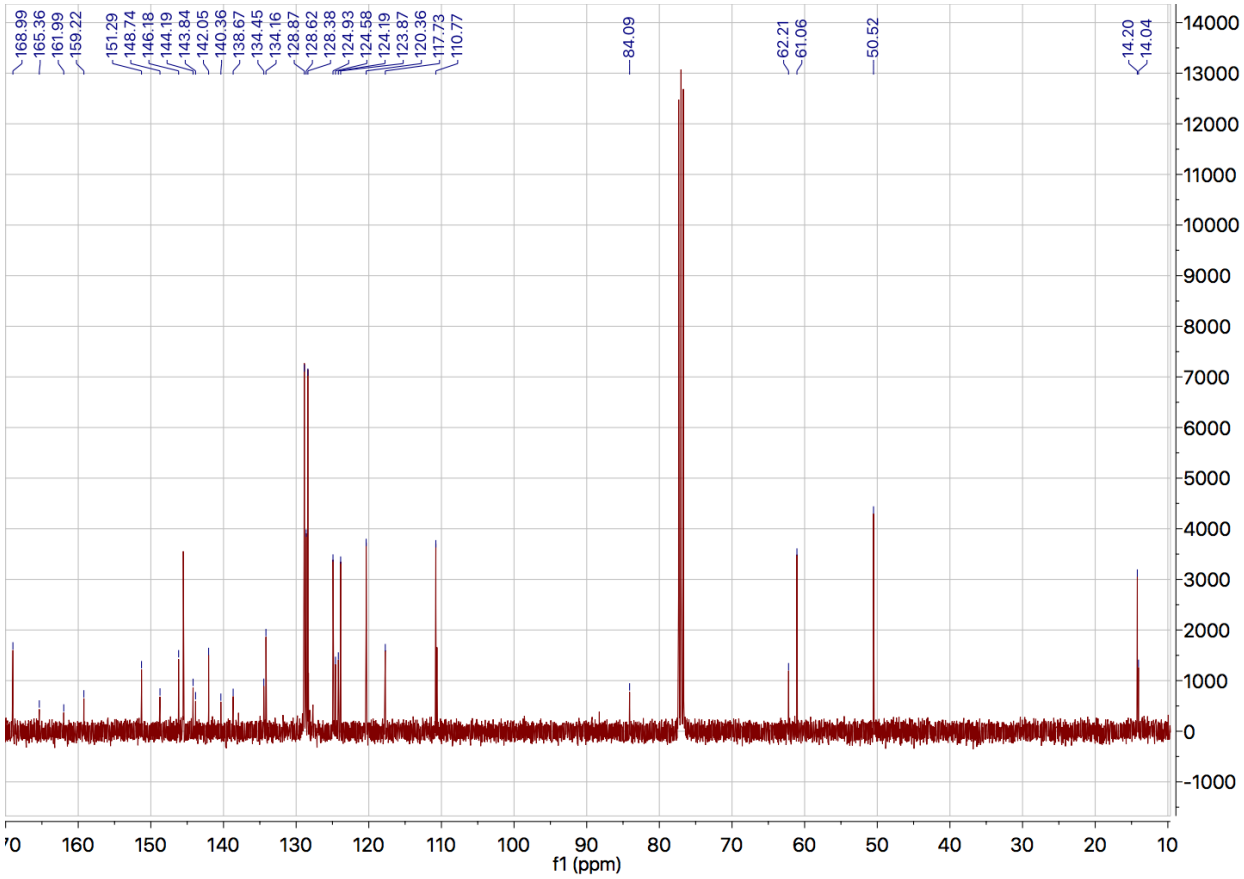

Figure AA-25. ^{1}H NMR spectrum for (*Z*)-2-((3-benzyl-3,6-dihydro-7*H*-[1,2,3]triazolo[4,5-*d*]pyrimidin-7-ylidene)methyl)benzo[*d*]oxazole (3')

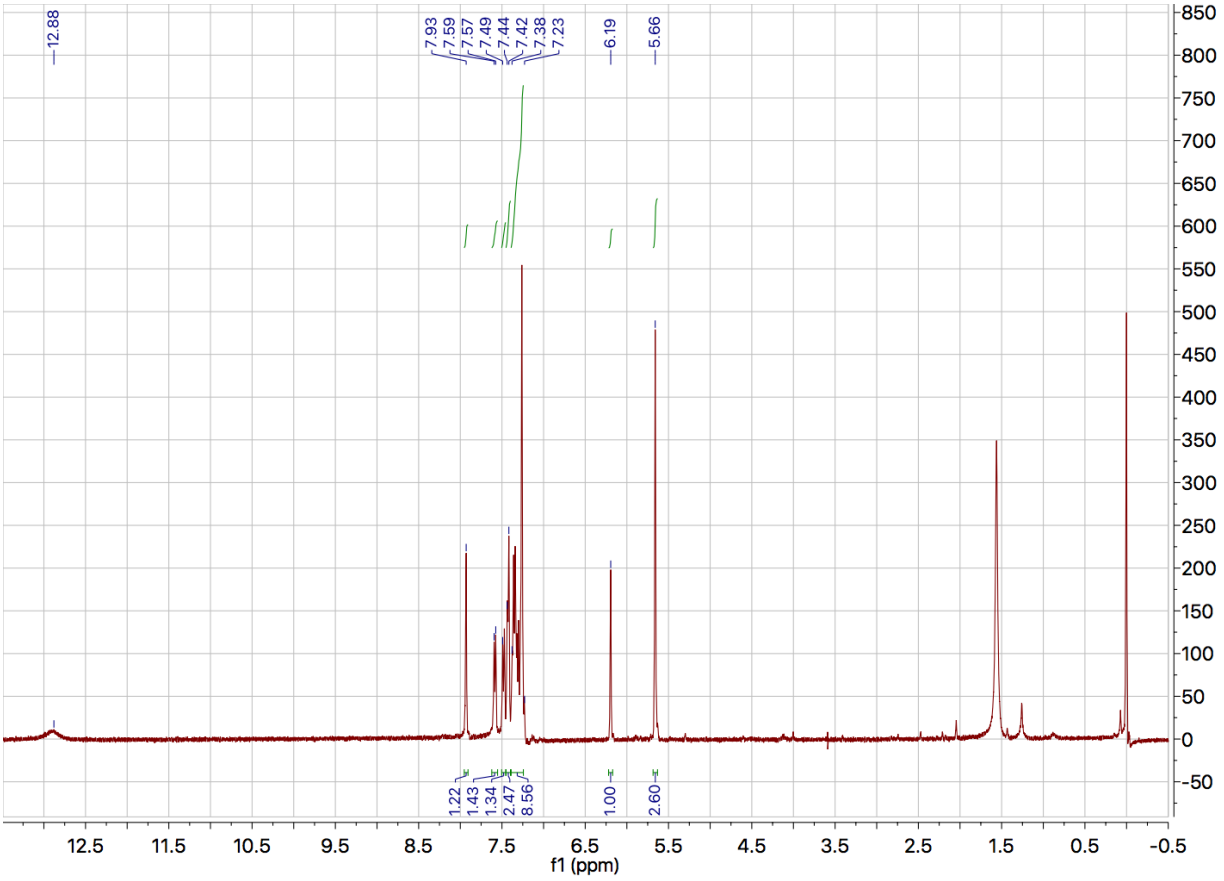

Figure AA-26. ^{13}C NMR spectrum for (*Z*)-2-((3-benzyl-3,6-dihydro-7*H*-[1,2,3]triazolo[4,5-*d*]pyrimidin-7-ylidene)methyl)benzo[*d*]oxazole (3')

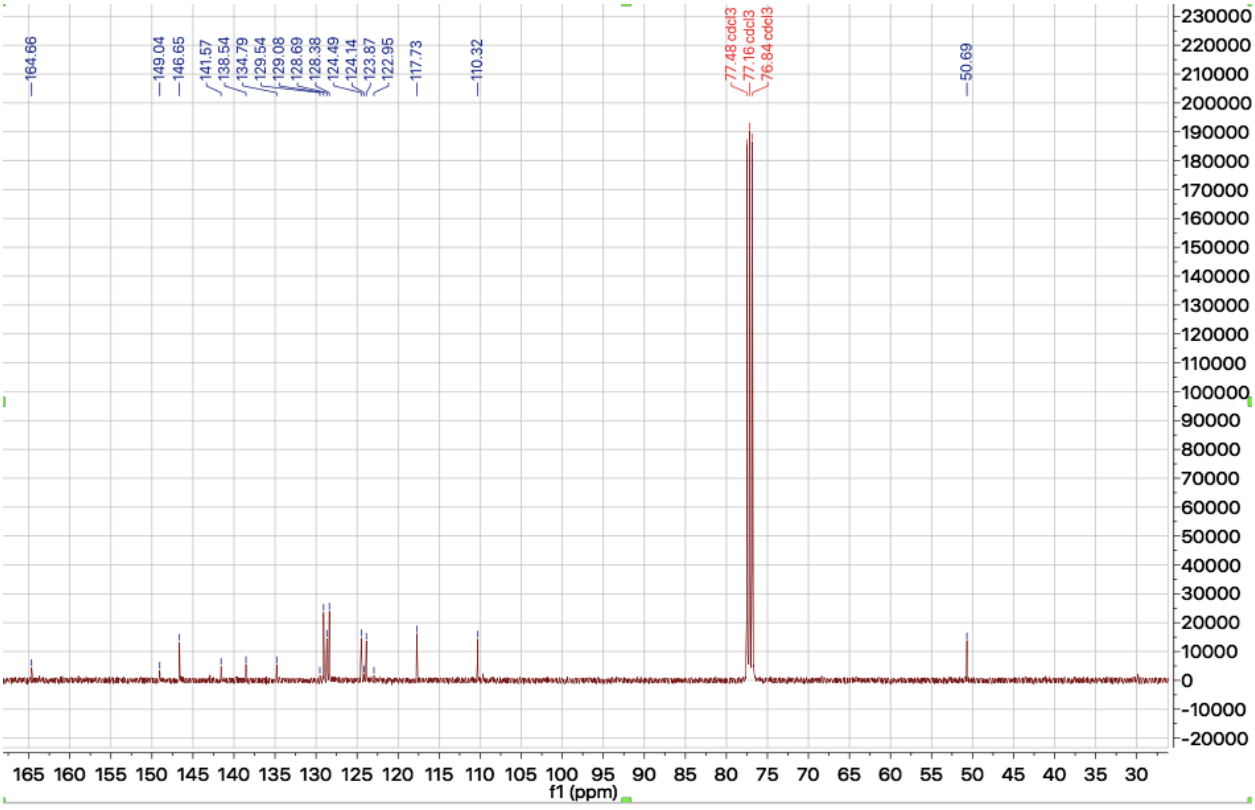

Figure AA-27. ^{1}H NMR spectrum for Ethyl trimethylsilylacetate (95)

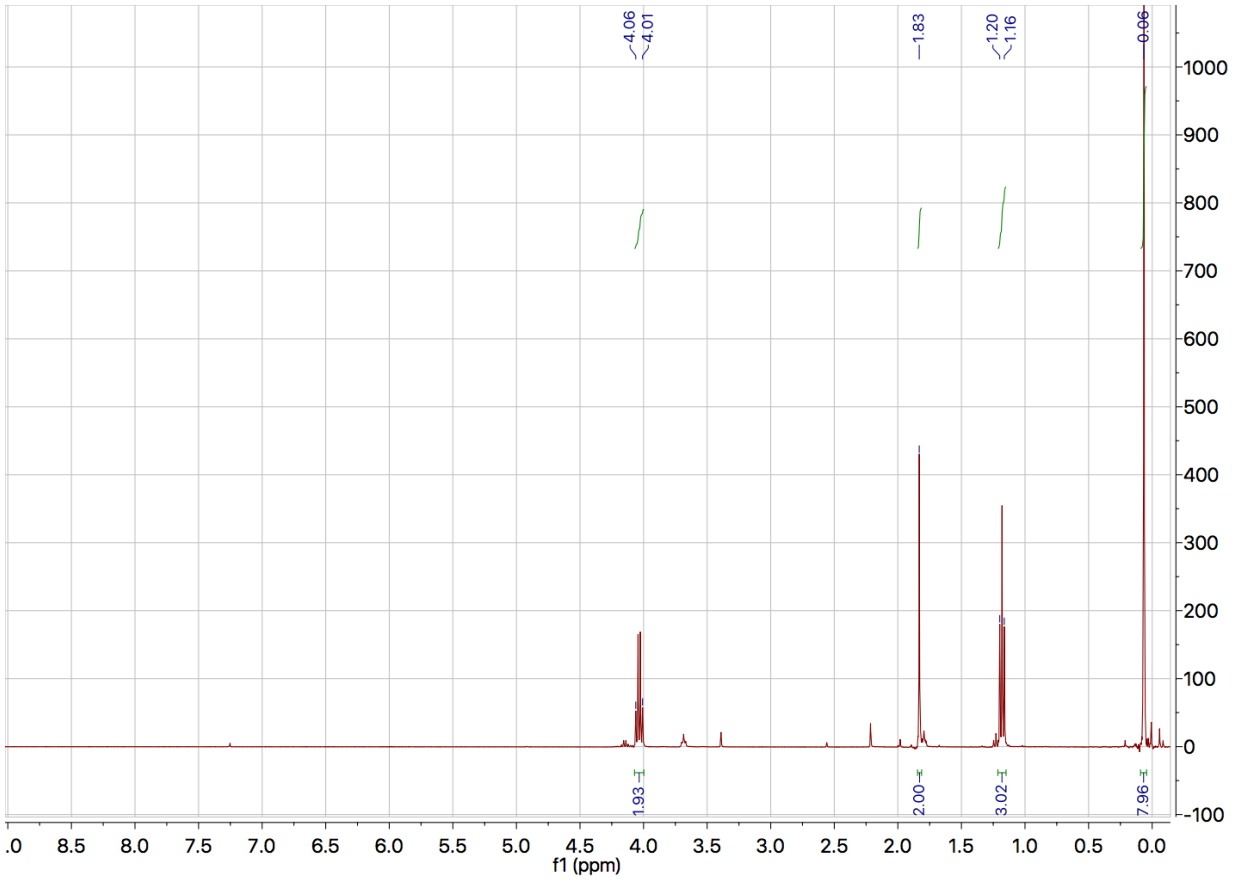

Figure AA-28. ^{1}H NMR spectrum for Phenyl Bromoacetate (107)

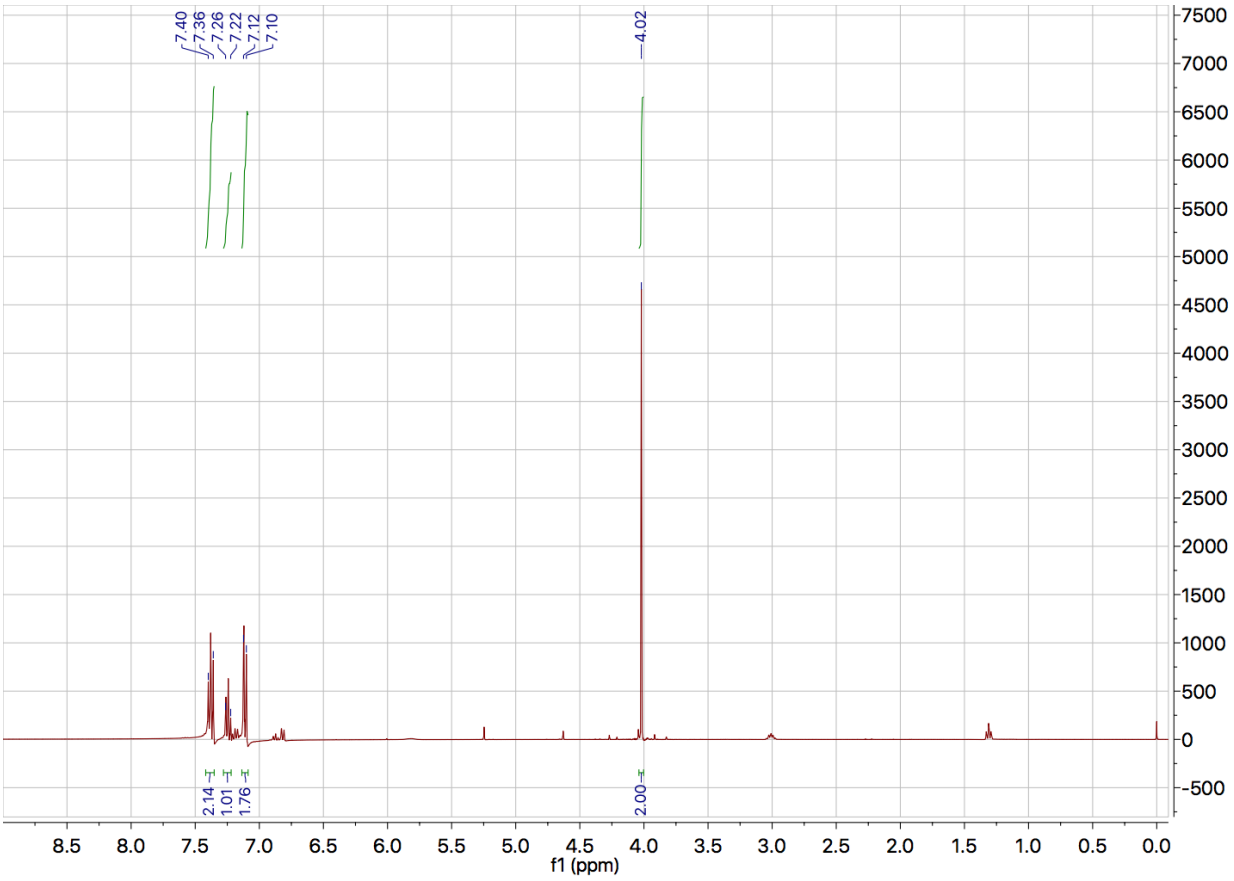

Figure AA-29. ^{1}H NMR spectrum for Phenyl trimethylsilylacetate (108)

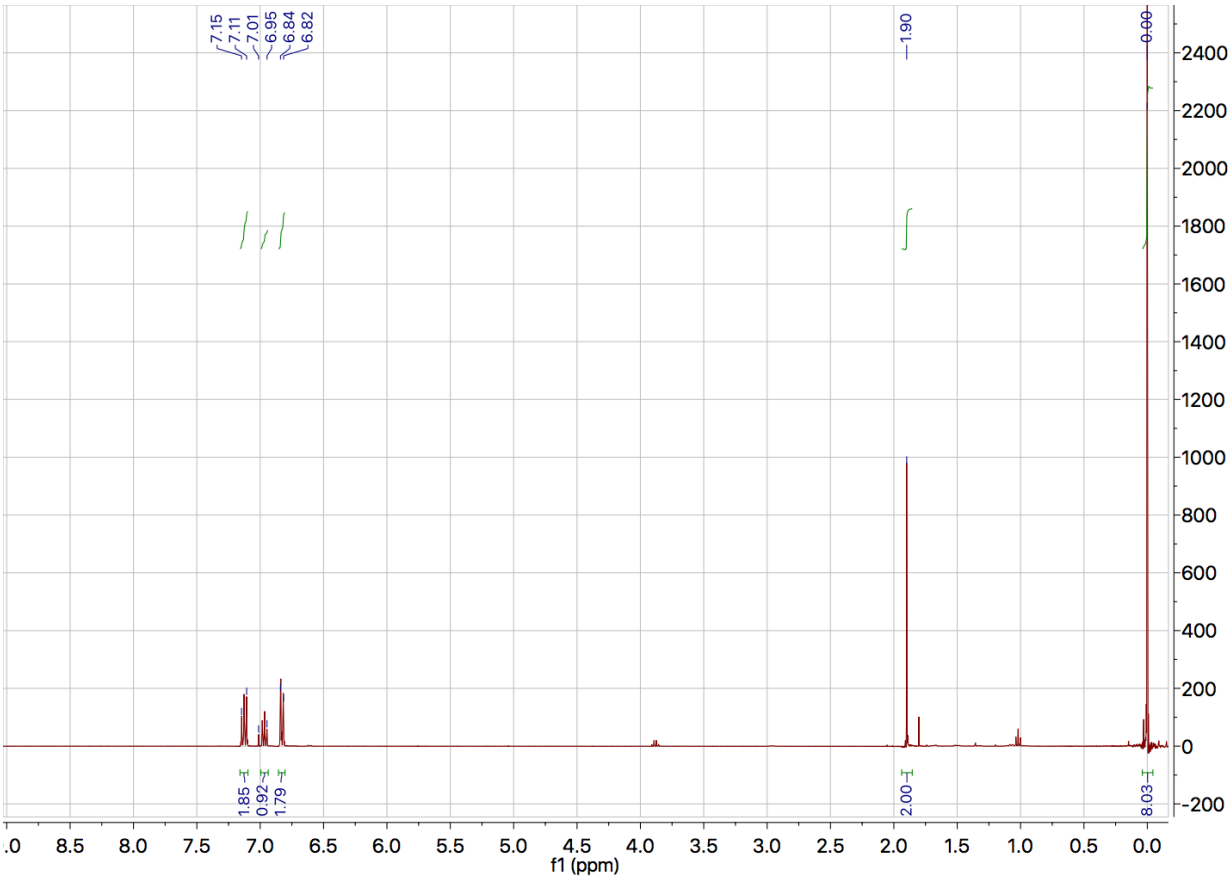

Figure AA-30. ^{13}C NMR spectrum for Phenyl trimethylsilylacetate (108)

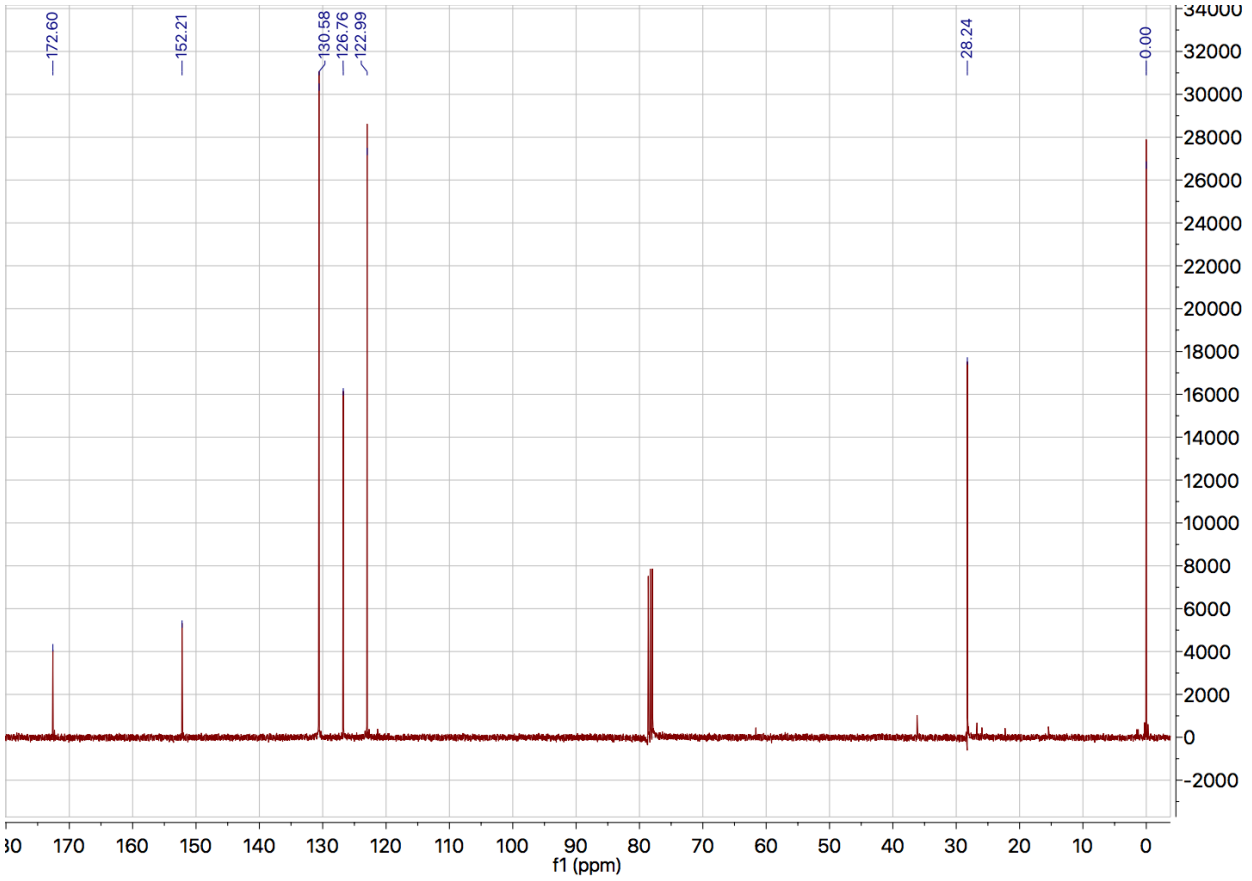

Figure AA-31. ^{1}H NMR spectrum for 2-(Trimethylsilyl) acetic acid (112)

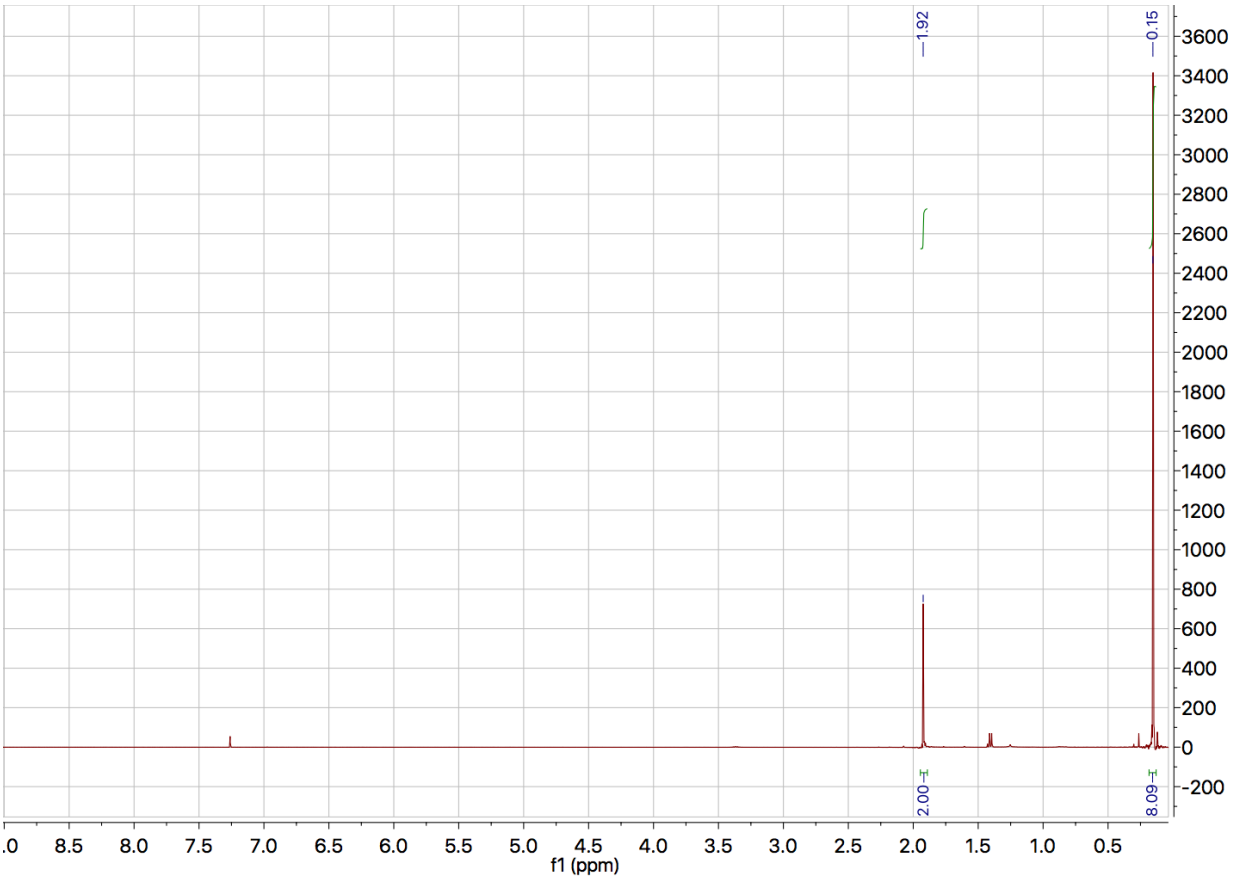

Appendix B BIOLOGICAL ASSAYS

B.1 Respiratory Burst Assay (Performed by Wyatt Slattery)

The respiratory burst response of neutrophils was measured using previously reported techniques with minor modifications [1]. HL-60 cells were cultured in Dulbecco's Modified Eagles' Medium (DMEM)/F12 containing 100 U/mL penicillin, 100 mg/mL streptomycin, and 10% Calf Bovine Serum (F10, all from Fisher Scientific, Ottawa, ON, Canada). HL-60 cells were differentiated into neutrophils following an incubation with 1.5% v/v DMSO in F10 for 5 days. Differentiated HL-60 cells were centrifuged for 7 min at 500 xg and the cell culture media was aspirated. Cells were resuspended in 2 mL phenol red-free DMEM/F12 containing 100 U/mL penicillin, 100 mg/mL streptomycin and 2% Calf Bovine Serum (F2, all from Fisher Scientific). The centrifugation step was repeated and differentiated HL-60 cells were resuspended in fresh F2 media to reach a density of $1x10^6$ cells/mL. Next, 250 μL of the cell suspension were plated in non-adjacent wells of a 96-well plate (Greiner Bio-One, Monroe, NC, USA) and stimulated with 0.5 mg/mL lipopolysaccharide (Sigma Aldrich, Oakville, ON, Canada) for a 24 h incubation. Cells were then treated with vehicle solution (0.1% DMSO) or 10 μM inhibitor compounds in DMSO for 20 min.

Prior to measuring respiratory burst, cell culture supernatants were aspirated to leave 85 μL remaining. Chemiluminescence was measured using a FLUOstar Omega microplate reader (BMG Labtech, Guelph, ON, Canada) and the following experimental parameters. Luminol sodium salt (Sigma Aldrich) was dissolved in PBS to reach a concentration of 10 mg/mL. N-Formyl-Met-Leu-Phe (Sigma Aldrich) was prepared as a 5 μM stock solution in PBS. Both solutions were warmed to 37 ^{O}C prior to injection. Luminol sodium salt solution was added to each well at a volume of 13 μL, followed by 8 μL N-Formyl-Met-Leu-Phe 5 min later. Chemiluminescent signal was calculated as total area under the curve for 15 min post-N-Formyl-Met-Leu-Phe injection. Chemiluminescent data are presented as a percent relative to cells incubated in F2 media only.

Cell viability Cytotoxic effects of inhibitor compounds were tested using the 3-(4,5-Dimethyl-2-thiazolyl)-2,5-diphenyl-2H-tetrazolium bromide (MTT) assay. Conversion of MTT to an insoluble purple formazan in live cells is readily quantifiable using spectrophotometry and highly correlated with cell viability [2, 3]. Differentiated HL-60 cells were prepared as outlined above with the following modifications. After incubation with vehicle solution (0.1% DMSO) or 10 μM inhibitor compounds in DMSO for 20 min, cell culture supernatants were aspirated to leave 40 μL remaining. 10 μL MTT

(Sigma Aldrich) solution in deionized water was added to cell cultures to reach a final concentration of 1 mg/mL. Differentiated HL-60 cells were then incubated for 1 h at 37 ^{o}C in humidity and 5% CO_2 atmosphere. Next, 20% sodium dodecyl sulfate/50% N,N-dimethylformamide (both from Fisher Scientific) solution in milliQ water (EMD Millipore) was added 1:1 with the cell culture volume in each well. Plates were incubated overnight at 37 °C in humidity and the absorbance of each well at 570 nm was measured using a FLUOstar Omega microplate reader (BMG Labtech). Cellular viability was calculated as a percent relative to fully viable cells incubated in cell culture media only.

B.2 Neuroprotective Assay (Performed by Aaron Johnstone)

Preparation, culture and immunocytochemical staining of DRG explants: Dorsal root ganglia (DRG) explant culture, fixation and immunostaining was performed on CD1 embryos (Charles River Laboratories) at 13.5 days post-fertilization as previously described except that here DRG explants were grown on 6-well plastic plates (Greiner bio-one).[106] All experimental procedures were approved by the Montreal Neurological Institute Animal Care Committee and University of British Columbia animal care committees and were in compliance with Canadian Council on Animal Care guidelines. DRG explants were seeded on 6-well plastic cell culture plates (Greiner bio-one) in media containing 12.5 ng/ml NGF (Alomone). After 60h of growth in NGF, cultures were either maintained in NGF or were deprived of NGF and exposed to anti-NGF antibody (2.8 ug/ml) in the presence of EGTA 6 mM (Alfa Aesar) for the 24 hour duration of NGF withdrawal.

Imaging and image pre-processing: DRG cultures fixed in 4% paraformaldehyde in PBS and immunostained with mouse anti-β-III tubulin (Millipore; 1:10 000) primary antibody and anti-mouse secondary conjugated to Alexa Fluor 488 (ThermoFisher; 1:5 000) were imaged at 5x magnification using a Zeiss Axioscope2 inverted epifluorescence microscope with an automated, motorized stage. Images were stitched automatically with Zen 2 software from Zeiss to produce a master image of all explants on the entire 6-well plate. From this master image, quarter-DRG fields were cropped using NIH ImageJ (FIJI build) to create an image set for quantification.

Quantification of axon area with Axoquant 2.0 in R Studio: R can be freely downloaded and installed from the R Project for Statistical Computing (**https://www.r-project.org/**). Additionally, users will download R Studio, a graphical interface for editing and running R packages freely available for download at **https://www.rstudio.com**. The Axoquant 2.0 script can be downloaded

at **https://github.com/BarkerLabUBC/Axoquant2.0** and opened in R Studio. Prior to analysis, images of DRG quarter-fields were organized in subfolders (one subfolder per well) named by embryo ID number, treatment name and repetition number within a single parent (experiment) folder. To analyze an experiment, the directory path to the experiment folder was entered in line 2 of the code designated "experiment.folder," and the code was executed through to the end of the script. As images are processed, the R Studio console displays an ascending image count to indicate progress. When finished with analysis, Axoquant 2.0 automatically exports a *.csv data file to the parent folder that can be opened in spreadsheet and in statistical analysis software. For statistical testing, the data was binned in 500 μm increments by averaging axon density within these bins. Data was imported into GraphPad Prism 6 for statistical analysis with two-factor ANOVA (repeated measures in the distance factor) followed by Dunnett's post hoc comparison with NGF-deprived controls.